Development and characterization of nano-micro structures as carrier for bioactive compounds

Boutrup Stephansen, Karen; Jessen, Flemming; Chronakis, Ioannis S.

Publication date:
2015

Document Version
Publisher's PDF, also known as Version of record

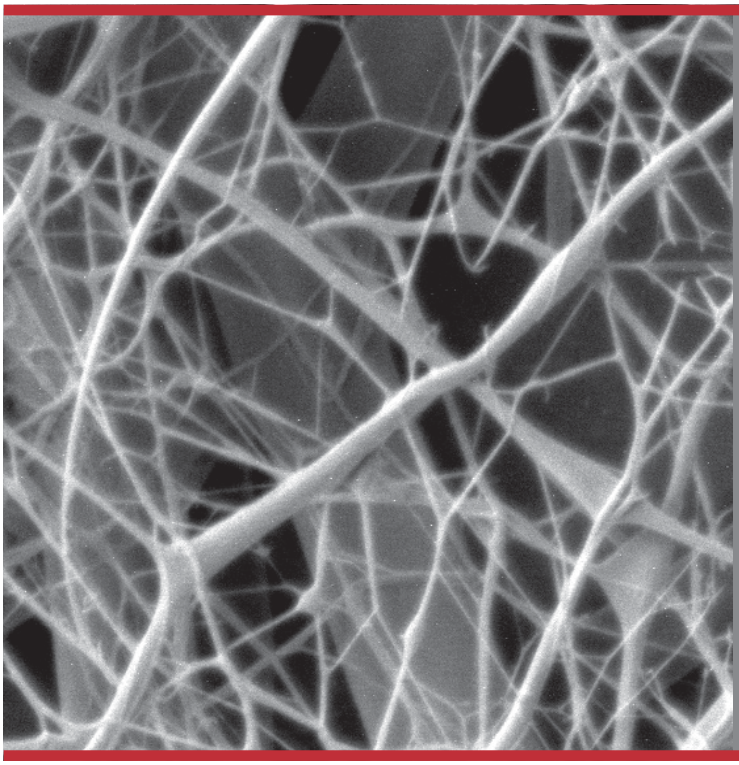

Development and characterization of nano-micro structures as carrier for bioactive compounds

Karen Stephansen
PhD Thesis May 2015

DTU Food
National Food Institute

Development and characterization of nano-micro structures as carrier for bioactive compounds

Submitted by

Karen Stephansen

PhD Thesis

Supervisors: Flemming Jessen and Ioannis S. Chronakis

National Food Institute, Technical University of Denmark

May 2015

Preface

This thesis entitled *"Development and characterization of nano-micro structures as carrier for bioactive compounds"* was submitted to fulfill the requirements to obtain the PhD degree at the National Food Institute, Technical University of Denmark. The PhD thesis is a part of the "Functional Electrospun Nano-Micro Structures" (FENAMI) project, funded by the Danish Research Counsel (DSF -10-93456, FENAMI Project). The experimental part of this project was carried out at the Technical University of Denmark and at the Faculty of Health and Medical Sciences, University of Copenhagen (FARMA, KU). The project was supervised by Senior Researcher Flemming Jessen, National Food Institute, Technical University of Denmark as main supervisor and Associate Professor Ioannis S. Chronakis, National Food Institute, Technical University of Denmark as co-supervisor.

First of all I would like to thank my supervisors; Flemming and Ioannis, for always having time for me, for all the fruitful discussions, and for showing me an enormous trust by allowing me to proceed in directions appealing to me. Moreover, a thank you to Ioannis for introducing me to electrospinning and to Flemming for sharing his large knowledge about fish proteins.

I would also like to thank Associate Professor Hanne Mørck Nielsen from FARMA, KU for allowing me to visit her research group, for supervising me during my stay there, and for introducing me to oral drug delivery. I enjoyed my stay at FARMA very much, which also brought a lot of interesting results. In continuation thereof I would like to thank Dr. María García-Díaz from FARMA, KU for introducing me to the laboratory facilities at the University of Copenhagen, for good collaboration, fruitful discussion, and good times.

Furthermore I would like to thank Professor Francisco M. Goycoolea from the Institute of Plant Biotechnology and Biology, University of Münster for a good collaboration and for introducing me to nanocomplexes.

Also a thank you to the entire Section for Biologics at the University of Copenhagen, and to the people in building 227 for good social activities and for contributing to a good research environment.

I would like to acknowledge the people who have provided practical assistance: Nis Korsgaard Andersen and Associate Professor Rafael Taboryski from DTU Nanotech for introduction and

access to the optical tensiometer, laboratory technician Karina Vissing from FARMA, KU for assistance with CMC determinations, Associate Professor Peter Waaben Thulstrup from the Department of Chemistry, University of Copenhagen for access to circular dichroism apparatus, DTU Environment for access to the Zetasizer, Thomas Andresen from DTU Nanotech for access to cell laboratory facilities, Senior Technician Maria L. Pedersen and Technician Thara Hussein from FARMA, KU for cell culturing, and to laboratory technician Lotte Svare Rasmussen (former DTU Food), for introducing me to the proteomics laboratory facilities. I would also like to thank the team at the Core Facility of Integrated Microscopy, especially Professor Klaus Qvortrup, for introduction to and assistance with electron and confocal microscopy.

Thank you to the Danish Strategic Research Counsel for funding this project, and to Otto Mønsteds foundation and the COST Action MP1206 for financially supporting my participation in conferences. I would also like to acknowledge contributions from the COMPACT partners (Innovative Medicines Initiative Joint Undertaking under grant agreement n°115363 resources).

A thank you to my sister, Anne Stephansen, for support and proof reading of the thesis, and thank you to my family and friends for supporting me during this study and accepting my absence in periods of time. And finally, a special thanks to my boyfriend and son, Kasper and Bertram, for never ending support, for cheering me up when needed, and for keeping my mind away from work once in a while.

Karen Stephansen, 2015

Abstract

New biopolymers are in high demand due to their excellent biocompatibility, biodegradability, and natural origin. In this PhD project, water soluble fish sarcoplasmic proteins (FSPs) from the North Atlantic cod (*Gadus morhua*) have been studied as a potential new biopolymer for development of nano-micro structures. Two kinds of nano-micro structures have been explored: electrospun fibers (Paper I, Paper II, and Paper III) and self-assembled nanocomplexes (NCXs) (Paper IV).

FSP was observed to be highly suitable for electrospinning. The fiber morphology varied significantly with FSP concentration, from beads to fibers. Moreover, the morphology within one FSP concentration was very diverse, as evident from the fiber diameter ranging from nanosized to micronsized (Paper I). The size distribution of the fiber diameter was decreased by removal of low molecular weight compounds (< 8 kDa). Despite the water-soluble nature of FSP, the fibers were insoluble in aquatic media (except at high sodium dodecyl sulfate concentrations) (Paper I, Paper II, and Paper III). Contact angle measurements indicated that the FSP fibers were hydrophobic, and incubation with the hydrophobic dye 8-anilino-1-naphthalenesulfonic acid (ANS), confirmed the presence of hydrophobic pockets inside or at the surface of the fibers (Paper III). Interestingly, the physical properties of the fibers significantly changed after incubation with surfactants as well as with the surfactant type; the FSP fibers were dense after incubation with cationic surfactant, whereas inner porosity of the fibers was observed after incubation with anionic or neutral surfactants. Moreover, the contact angle changed from being large for anionic surfactants, to being small for neutral and cationic surfactants. Lastly, the cationic and neutral surfactants decreased the amount of hydrophobic pockets available for dye interaction (Paper III). The inherent property of FSP as consumed food made the fibers degradable by proteolytic enzymes, and the degradation products were observed to inhibit the diabetes related enzyme dipeptidyl peptidase-4 (Paper I).

The FSP fibers showed potential as carrier system for delivery of drugs, bioactive agents, and nutraceuticals. The dipeptide Ala-Trp, rhodamine B, or insulin was encapsulated into the fibers, and the release was studied in biorelevant media (Paper I, Paper II, and Paper III). Release of Ala-Trp was slightly decreased in gastric environments compared to pH 6.8, whereas release of insulin was independent of pH. Instead, insulin release was affected by the presence of

biorelevant compounds, i.e. surfactants and proteins encountered in the intestinal system. Anionic surfactants increased the release of insulin from FSP fibers in a dose-dependent manner, neutral surfactants had no effect, and cationic surfactants decreased the insulin release to negligible amounts (Paper III). Encapsulation of insulin into the FSP fibers provided protection against chymotrypsin degradation, and interactions between the fibers and epithelial cells led to opening of the tight junction, which promoted an increased transepithelial transport of insulin without compromising cellular viability (Paper II).

The FSPs were also suitable for development of self-assembled NCXs. By gentle bulk mixing of FSP and alginate, stable NCXs were formed (Paper IV). The NCXs were 293 ± 3 nm and anionic (zeta potential was −42 ± 0.3 mV). The zeta potential as a function of pH revealed that the NCX surface was dominated by alginate. The NCXs were stable in biorelevant media, and at pH values from 2 to 9, except at pH 3 where the NCXs aggregated. Proteolytic enzymes were capable of degrading the NCXs. The viability of HeLa and U2OS cell lines was only decreased by high concentrations of NCXs (Paper IV).

It was concluded that FSP is highly suitable for the production of functional nano-micro structures for food and biomedical applications qua the ability of the FSPs to form electrospun fibers and self-assembled NCXs. The inherent properties of FSP of being biocompatible, biodegradable, and bioactive further promote the use of FSP as a biopolymer.

Resumé (Danish)

Nye biopolymerer er efterspurgte grundet deres biologiske kompatibilitet, nedbrydelighed samt naturlige oprindelse. Dette Ph.d-projekt har fokuseret på vandopløselige fiske sarkoplasmiske proteiner (FSP'er) fra den nordatlantiske torsks (*Gadus morhua*) potentiale som ny biopolymer til udvikling af nano-mikro strukturer. To typer af strukturer er blevet undersøgt; elektrospundne fibre (Paper I, Paper II og Paper III), og selvdannede nanokomplekser (NCX'er) (Paper IV).

FSP viste sig at være yderst velegnede til elektrospinning. Fibrenes morfologi varierede betydeligt, fra partikler til fibre, afhængigt af FSP koncentrationen. Desuden fandtes en stor diversitet i fibrenes morfologi inden for den samme FSP koncentration, idet størrelsen på fibrenes diameter varierede fra nanometer til micrometer (Paper I). Spredningen på størrelsen af fibrenes diameter kunne gøres mindre ved eliminering af stoffer med lav molekylvægt (< 8 kDa). Til trods for FSP'ernes vandopløselighed, var FSP fibrene uopløselige i vandige medier (med undtagelse af ved høje koncentrationer af natriumdodecylsulfat). Kontaktvinkelmålinger indikerede at FSP fibrene var hydrofobiske, og inkubation med den hydrofobe farve 8-anilino-1-naphthalensulfon syre (ANS) bekræftede tilstedeværelsen af hydrofobe lommer i eller på overfladen af fibrene (Paper III). Overraskende blev fibrenes fysiske egenskaber signifikant ændret efter at fibrene havde inkuberet med surfaktanter, og ændringerne var afhængig af surfaktanternes egenskaber; FSP fibrene var kompakte efter at have inkuberet med den kationiske surfaktant, hvorimod en indre porøsitet blev observeret efter inkubation med anioniske og neutrale surfaktanter. Derudover ændrede kontaktvinklen mellem buffer og FSP fibrene sig fra stor for de anioniske surfaktanter, til lille ved de kationiske og neutrale surfaktanter. Endelig sænkede de kationiske og neutrale surfaktanter antallet af tilgængelige hydrofobe lommer, som ANS kunne interagere med (Paper III). Eftersom FSP er en fødevare, blev fibrene nedbrudt af proteolytiske enzymer, og det blev observeret at nedbrydningsprodukterne inhiberede det diabetes relaterede enzym dipeptidyl peptidase - IV (Paper I).

FSP fibrene viste potentiale som indkapsuleringssystem for bioaktive stoffer, nutraceuticaler og lægemidler. Di-peptidet Ala-Trp, rhodamine B eller insulin blev hver især indkapsuleret i fibrene, og deres frigørelse fra fibrene i biologisk relevante medier blev undersøgt (Paper I, Paper II og Paper III). Frigørelse af Ala-Trp fra fibrene var marginalt mindre i et gastrisk miljø i

forhold til ved pH 6,8, hvorimod frigørelsen af insulin var uafhængig af pH. Til gengæld var frigivelsen af insulin påvirket af tilstedeværelsen af biologisk relevante stoffer, såsom surfaktanter og proteiner der findes i tarmsystemet. Anioniske surfaktanter forårsagede en dosisafhængig øget frigørelse af insulin fra FSP fibrene, neutrale surfaktanter havde ingen effekt, og kationiske surfaktanter bevirkede, at kun en forsvindende mængde insulin blev frigjort fra fibrene (Paper III). Indkapsulering af insulin i FSP fibrene beskyttede insulin mod enzymatisk nedbrydning med chymotrypsin, og vekselvirkninger mellem fibrene og epitelceller åbnede cellernes *tight junctions*, hvilket resulterede i øget transepitel transport af insulin uden at indvirke cellernes levedygtighed (Paper II).

FSP'erne var også anvendelige til udvikling af NCX'er. Ved at blande FSP med alginat blev stabile NCX'er dannet (Paper IV). NCX'erne var 293 ± 3 nm og anioniske (zeta potentialet var −42 ± 0,3 mV). Zeta potentialets variation som funktion af pH i mediet afslørede at NCXoverfladen var domineret af alginat. NCX'erne var stabile i biologisk relevante medier, samt ved pH værdier fra 2 til 9, med undtagelse af pH 3 hvor NCX'erne aggregerede. Proteolytiske enzymer kunne nedbryde NCX'erne. Levedygtigheden af HeLa og U2OS cellelinjer var kun nedsat ved høje koncentrationer af NCX (Paper IV).

Det blev konkluderet at FSP er højt egnede til produktion af funktionelle nano-mikro strukturer til fødevare og biomedicinske anvendelser qua FSP'ernes evne til at danne elektrospundne fibre og selvdannede NCX'er. De medfødte egenskaber som FSP besidder, såsom biologisk kompatibilitet, bionedbrydelighed og bioaktivitet gør FSP yderligere attraktivt til brug som biopolymer.

Table of contents

List of abbreviations

ADSCs	Adipose-derived stem cells
Alg	Alginate
ANS	8-anilino-1-naphthalenesulfonic acid
ATR-FTIR	Attenuated total reflectance - fourier transform infrared spectroscopy
AUC	Area under the curve
BC	Benzalkonium chloride
BSA	Bovine serum albumin
BZA	Benzoylacetone
CD	Circular dichroism
CMC	Critical micelle concentration
D-FSP	Dialyzed fish sarcoplasmic protein
DLS	Dynamic light scattering
DPP-IV	Dipeptidyl peptidase-4
FITC	Fluorescein isothiocyanate
FSPs	Fish sarcoplasmic proteine
GIP	Glucose-dependent insulinotropic polypeptide
GLP-1	Glucagon-like peptide-1
GC	Glycocholate
GDC	Glycodeoxycholate
GRAS	Generally Recognized As Save
HFIP	Hexafluoroisopropanol
HPMCP	Hydroxypropyl methyl cellulose phthalate
LMW	Low molecular weight
MTS	3-(4,5-dimethylthiazol-2-yl)-5-(3-carboxymethoxyphenyl)-2-(4-sulfophenyl)-2H-tetrazolium
NCX	Nanocomplex
MW	Molecular weight
P_{app}	Apparent permeability coefficient
PCL	Polycaprolactone
PDI	Poly dispersity index
PEO	Polyethylene oxide
PLGA	Poly(lactic-co-glycolic acid)
PLLA	Poly-l-lactide acid
PEO-PLLA	Poly(ethylene oxide)–poly(L-lactic acid)
PLLCL	Poly(L-lactic acid)-co-poly-(e-caprolactone)
PMS	Phenazine methosulfate
PVA	Polyvinylalcohol
RP-HPLC	Reversed – phase High pressure liquid chromatography
SDS	Sodium dodecyl sulfate
SDS-PAGE	Sodium dodecyl sulfate - polyacrylamide gel electrophoresis
SEM	Scanning electron microscopy
sPIN	Semi-interpenetration networks
SPI	Soy protein isolate
TC	Taurocholate
TDC	Taurodeoxycholate
TEER	Trans epithelial electrical resistance
TEM	Transmission electron microscopy
US-FDA	U.S. Food and Drug Administration
WPI	Whey protein isolate

List of publications

The findings in this PhD study have led to four papers. Throughout the thesis the papers will be referred to as Paper I, Paper II, Paper III, and Paper IV.

Paper I

Bioactive electrospun fish sarcoplasmic proteins as a drug delivery system

K. Stephansen, I.S. Chronakis, F Jessen

Colloids Surf. B. Biointerfaces. 122C (2014) 158–165

Paper II

Bioactive protein-based nanofibers promotes transepithelial permeation of intact therapeutic protein by interactions with biological components

K. Stephansen, M. García-Díaz, F. Jessen, I.S. Chronakis, H.M. Nielsen

Macromolecular Bioscience (in revision)

Paper III

Interactions between surfactants in solution and electrospun protein fibers - Effects on release behavior and fiber properties.

K. Stephansen, M. García-Díaz, F. Jessen, I.S. Chronakis, H.M. Nielsen

RSC Biomaterials Science (prepared for submission)

Paper IV

Design and characterization of self-assembled fish sarcoplasmic protein-alginate nanocomplexes

K. Stephansen, M. Mattebjerg, J. Wattjes, A. Milisavljevic, F. Jessen, K. Qvortrup, F. M. Goycoolea, I.S. Chronakis

International Journal of Biological Macromolecules 76 (2015) 146–152

International conference contributions

Poster	Controlled Release Society, 2015 (to be presented) *Edinburgh, Scotland*
Oral	Controlled Release Society Nordic, 2015 (to be presented) *Edinburgh, Scotland*
Oral	Composite, nanofabrication, food and pharma related application and packaging, controlled release, 2015 *Novi Sad, Serbia*
Poster	American Association pf Pharmaceutical Sciences Annual Meeting, 2014 *San Diego, USA*
Poster	3rd International Conference on Electrospinning, 2014 *San Francisco, USA*
Oral	Advanced Nano Materials – COST session, 2014 *Aveiro, Portugal*
Oral	Electrospinning, Principles, Possibilities and Practice, 2013 *London, UK*

1 Introduction

Functional nano-micro structures have gained widespread attention in a large range of research areas, and the continuous advancement in material properties causes the range of applications to expand equivalently. In the food and pharmaceutical industry nano-micro structures have become an essential active in optimizing drug bioavailability, increasing drug stability, minimization of side effects, sustainable materials, cost reduction etc.

Biopolymers are beneficial in the development of new nano-micro structures due to their excellent biocompatibility. Moreover, the use of biopolymers is appealing from an economical and world wealth point of view. The search for new biopolymers has therefore been reinforced.

1.1 Aim and outline

In this PhD project, the potential of using fish sarcoplasmic proteins (FSPs) from the Atlantic cod (*Gadus morhua*) as a new biopolymer for development of nano-micro structures has been explored. Since FSP is a food product, special focus has been on evaluating the nano-micro structures for oral drug delivery, an administration form that is appealing due to patient convenience, compliance, and cost.

An overview of the PhD projected is illustrated in Figure 1. The flexibility of the FSPs were explored by studying two types of nano-micro structures; electrospun FSP fibers and nanocomplexes (NCXs) made from electrostatic self-assembly of FSPs and alginate (also a biopolymer), but with special focus on the fibers.

The main results obtained during this PhD project are presented through four papers. In Paper I the development and characterization of FSP fibers including morphology, stability, encapsulation, and drug release were described. FSP fibers as a drug delivery system was further studied in Paper II. A growing amount of new drugs are biopharmaceuticals, which has intensified the search for new delivery systems for these biological macromolecules. For that reason, insulin was chosen as a model drug in Paper II, and the release of insulin from insulin loaded FSP fibers (FSP-Ins fibers) in bio-relevant buffers was studied in addition to the ability of the fibers to protect insulin from proteolytic degradation. Moreover, the effect of the FSP

fibers on the transepithelial permeation of insulin was studied *in vitro*. In Paper II, insulin release was found to be affected by the presence of bio-relevant compounds. This observation led to the study presented in Paper III, where interactions between FSP-Ins fibers and surfactants were the main focus; the effect of surfactants on insulin release, porosity, contact angle, and surface hydrophobicity were explored.

In the last paper, Paper IV, the development of NCXs made from electrostatic self-assembly of FSP and alginate was described. The NCXs were characterized with respect to size, poly dispersity index, zeta potential, stability, and toxicity investigations.

The four papers provided an insight to how FSP can be used as a biopolymer to develop nano-micro structures in the food and pharmaceutical industry. The following sections introduce the electrospinning process, the NCXs, and lastly the FSPs.

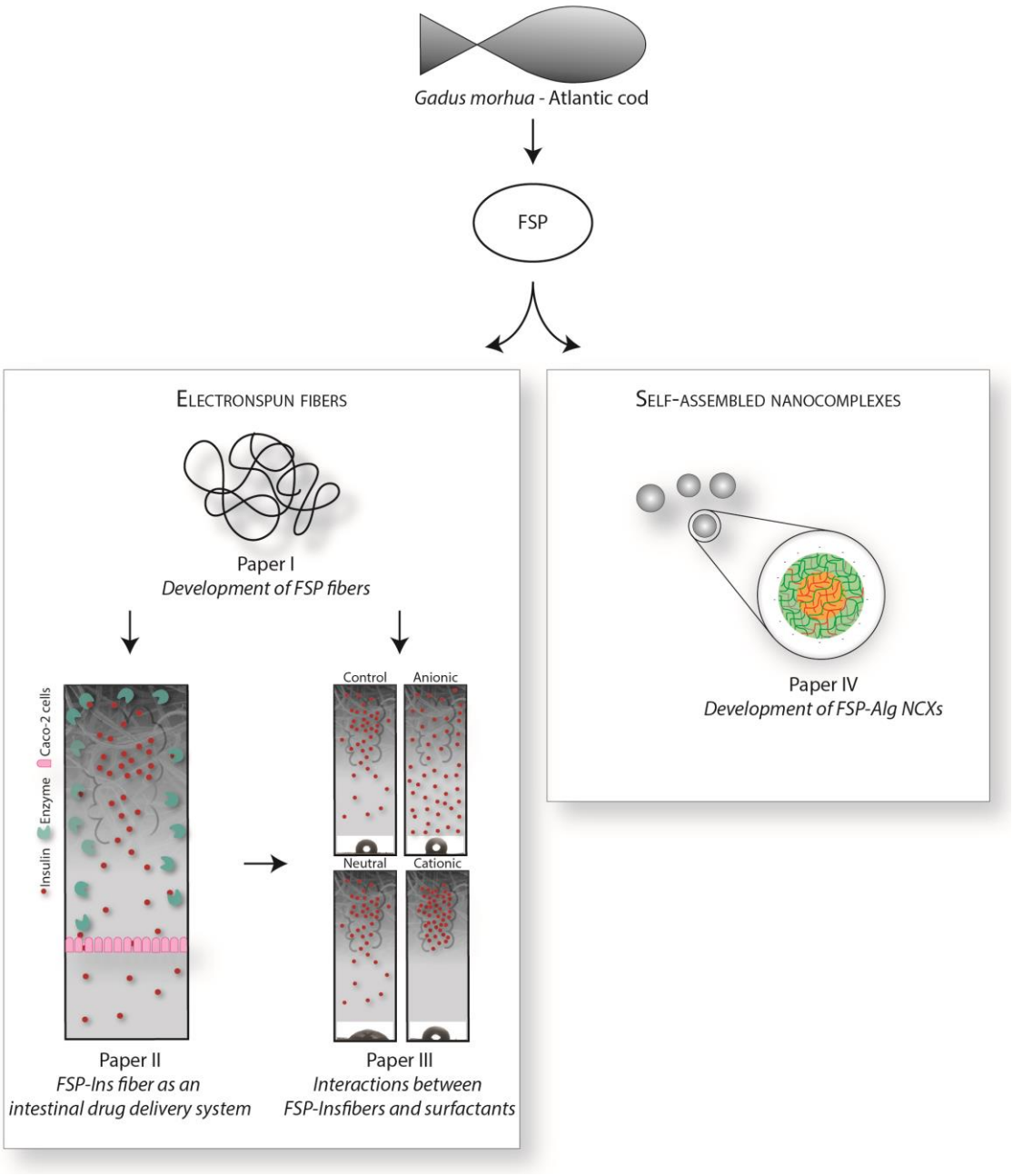

Figure 1. Overview of the thesis outline. With point of view in FSPs, two types of nano-micro structures were explored; electrospun fibers and NCXs. In Paper I the development of FSP fibers was described, and the potential of using the FSP fibers for intestinal delivery of biopharmaceuticals was explored in Paper II. In Paper III interactions between FSP-Ins fibers and bio-relevant compounds (surfactants) was studied. The potential of using FSPs together with alginate in a self-assembling system to develop NCXs was presented in Paper IV.

1.2 Electrospinning

Electrospinning was first discovered by Rayleigh in 1897, and electrospray was studied in detail in 1914 by Zeleny [1]. Formhals patented the technique in 1934 [2] and published patents describing the technique that led to the production of polymer fibers, in the years after. In 1969, Taylor studied the electrically driven jet [3], which formed the groundwork for electrospinning. In the following decades, only few researchers studied and used electrospinning, but in the beginning of the 21th century the technique started to gain widespread interest in the research community.

Electrospinning is suitable for production of continuous and functional nano-micro structures from a wide range of (bio)polymers [4–6]. A generalized electrospinning setup is shown in Figure 2. A high-voltage electrostatic field is used to charge the surface of a polymer solution droplet (the Taylor cone), thereby inducing ejection of a liquid jet through a spinneret. On the way to the collector, the jet will be subjected to forces that allow the jet to stretch immensely. Simultaneously, the jet will solidify through solvent evaporation, and electrically charged nano-micro fibers will remain, directed by electrical forces towards the collector.

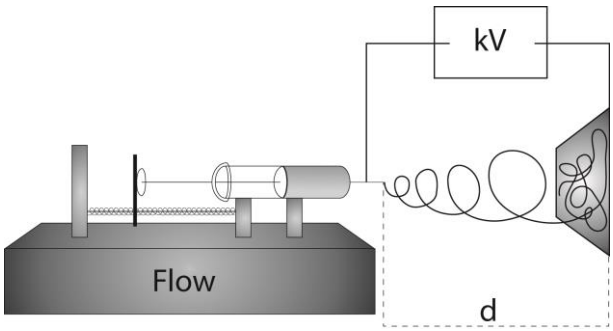

Figure 2. Schematic illustration of the electrospinning setup. The fiber morphology may be controlled by for instance the feed rate of the polymer solution (flow), the distance between the needle and the collector plate (d), and the voltage applied between the needle and the collector plate.

Several parameters in the electrospinning process can affect fiber morphology such as processing parameters (distance between needle and collector, flowrate, applied voltage, etc.), solution parameters (concentration, viscosity, etc.), and ambient parameters (humidity and temperature). The effect on the fiber morphology caused by each parameter depends on the polymer. For instance, by increasing the humidity, pores on the fiber surface can be created (Figure 3 A and B) [7], and by increasing the distance between needle and collector plate, the

fiber diameter can be decreased (Figure 3 C and D) [8]. Generalized effects of the main processing parameters on fiber morphology are listed in Table 1. The choice of collector determines the fiber pattern; a solid collector can provide randomly oriented fibers (Figure 3 D) or aligned fibers [9], and in wet electrospinning a liquid is used as a collector [10,11].

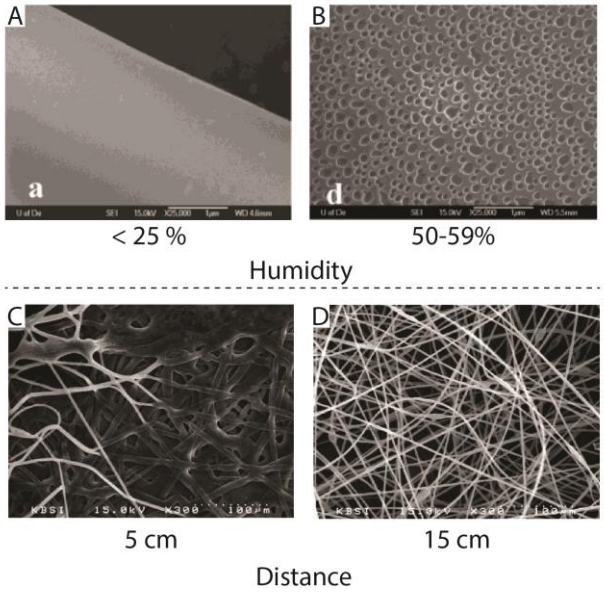

Figure 3. SEM images illustrating how processing parameters can affect fiber morphology. The top images show electrospun polystyrene fibers at two different humidities; A) > 25% and B) 50-59% (modified from [7]), and the bottom images show electrospun polystyrene fibers made using two different syringe-collector distances (d); C) 5 cm and D) 15 cm (modified from [8]).

Table 1. Overview of parameters that can affect the fiber morphology [4].

Parameter	Change
Solution parameters	
Increased viscosity	Decrease in bead generation, increased fiber diameter
Increased polymer concentration	Increased fiber diameter
Increased polymer molecular weight	Decreased bead generation
Increased conductivity	Decreased fiber diameter
Increased surface tension	Stability of the jet
Processing parameters	
Increased applied voltage	Decreased fiber diameter
Increased distance	There is a minimum distance required. Above/below this distance causes bead generation, increased distance may also decrease fiber diameter.
Increased flowrate	Increased fiber diameter, however bead generation if the flow rate becomes too large.
Ambient parameters	
Increased humidity	Increase in circular pores on the fibers
Increased temperature	Decreased fiber diameter

A large variety of polymers have been electrospun, and many reviews have focused on the properties of polymeric fibers, for instance references [6,12–14]. However, many synthetic polymers lack the biocompatibility and degradability needed for applications in biological systems - properties that characterize many biopolymers. For that reason electrospinning of proteins have been explored [15], and electrospun protein fibers will be discussed in the following section.

1.2.1 Electrospinning of proteins

Dror *et al.* have investigated some of the underlying mechanisms behind protein electrospinning, and how the properties of protein fibers can be controlled. The authors studied electrospinning of bovine serum albumin (BSA), and found that the electrospinnability and the mechanical properties of the produced nano-micro fibers could be controlled by manipulating protein conformation, protein aggregation, and intra/inter-molecular disulfide bonds [16]. Woerdemann *et al.* also considered some of the mechanisms behind electrospinning of proteins. The authors studied wheat gluten proteins and found that the highest molecular weight (MW)

proteins were responsible for the lower threshold concentration for fiber formation. Moreover, the authors found that fiber formation was a result of chain entanglements and reversible junctions in the proteins, the breaking and reforming of disulfide bonds in particular [17] – which was in agreement with the findings of Dror *et al.* [16]. In general, proteins must be more or less unfolded in order to be electrospinnable - and dependent on the protein of interest - there are several ways to fulfill this requirement; choice of solvent, addition of denaturing agents, heat etc. Gelatin has shown to be a promising material for tissue engineering, and Sajkiewicz and Kolbuk described in a review which solvents and associated ambient parameters that can be used for electrospinning of gelatin [18]. Formation of a triple-helix is connected to gelation of gelatin, which prevents electrospinnability. Accordingly, combinations of solvents and ambient parameters that destabilize triple-helix formation are favorable. Moreover the authors speculated if a change in molecular conformation can have an effect on the cellular response [18].

The morphology of protein fibers can vary similarly to polymer fibers, for which reason each biopolymer must be characterized individually. Figure 4 shows examples of electrospun protein fibers. Soy protein isolate (SPI)/polyvinyl alcohol (PVA) fibers had bead-like structures (Figure 4 A). At 11 wt% SPI/PVA the amount of beads were decreased, and by adding Triton X-100 to the electrospinning solution the beads were eliminated [19]. Electrospinning of 15 % gelatin provided homogenous fibers (Figure 4 B) [20], and fibers of 10 % BSA or 20% hemoglobin resulted in fibers with a ribbon like structure (Figure 4 C and D) [16,21]. In Figure 4 E - G the morphology of whey protein isolate (WPI)/poly(ethylene oxide) (PEO) fibers from solutions with different pH values are shown, exemplifying how much solution properties can affect fiber morphology; from bead-like structures to homogenous fibers [22].

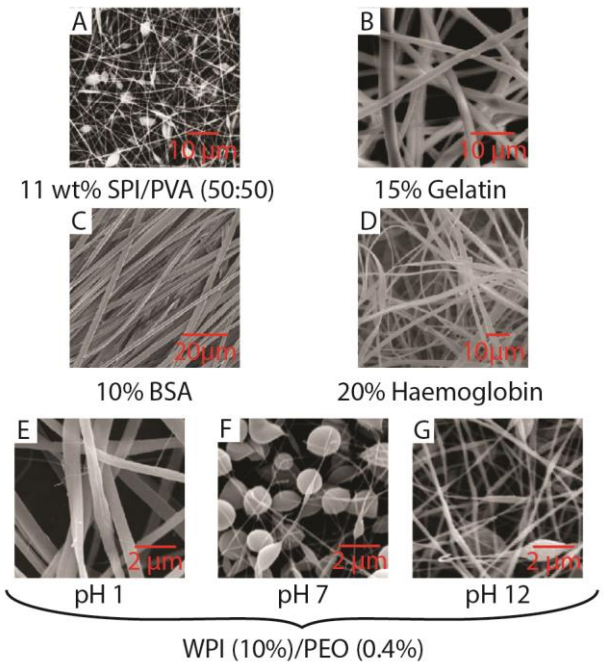

Figure 4. SEM images of electrospun fibers with different morphologies. A) 11 wt% SPI/PVA (modified from [19]), B) 15 % gelatin (modified from [20]), C) 10% BSA (modified from [16]), D) 20 % hemoglobin (modified from [21]), and (E-G) WPI/PEO (10%/0.4%) at pH 1, 7 and 12 (modified from [22]).

The challenges met during the development of specific protein fibers depends on the application of the fibers. Frequent obstacles are related to fiber stability in aqueous media and sufficient mechanical strength. The mechanical strength can be improved by crosslinking or by addition of polymers to the fiber matrix, and the stability can be improved by crosslinking. An example is electrospun gelatin fibers (Figure 5 A), which were degraded upon exposure to water (Figure 5 B) [23]. To increase the stability of the gelatin fibers in aqueous media, the fibers were crosslinked. As evident from Figure 5 C and D, crosslinking resulted in increased fiber diameter and smearing of the fiber structure, but the stability was improved [23]. Another example is crosslinking of PEO/casein fibers, but in contrast to the gelatin fibers, no large change in morphology was observed upon crosslinking (Figure 5 E-F) [24]. In general, electrospun fibers made from biopolymers are degradable [15], which is also one of the benefits of these materials. The rate by which the fibers degrade (either because of solvent or enzymatic degradation) depends on the material and post processing procedures such as crosslinking. For the PEO/casein fibers minor degradation was observed after exposure to enzymes (Figure 5 G) [24], and for gelatin fibers the stability can vary from a couple of hours [25] to 24 hours [26] or longer periods of time [27].

Drawbacks of crosslinking are among others the toxicity related to many crosslinking agents, such as glutaraldehyde [28], which is not beneficial especially when the fibers are intended for biomedical applications. In fact, the toxicity of some fibers have been proposed to originate from residues of unreacted crosslinking agents if the fibers were not rinsed thoroughly enough [23]. Alternative non-toxic crosslinking procedures have been pursued. For instance, Erdogan *et al.* recently showed that oleuropein, a major component of olive leaf extract, can be used as a natural crosslinker for zein fibers [29]. Noszczyk *et al.* found that albumin/PEO fibers spontaneously crosslinked during 21 days at 37 °C, after which excessive PEO could be washed away [30]. The study did not reveal which chemical bonds that were responsible for the hardening of the albumin fiber mat. The stability of the fibers depended on the thickness of the fiber sheet, however the albumin mats used in the study by Noszczyk *et al.* were completely resorbable within six days after subcutaneous implantation in mice [30].

Despite the gentler crosslinking methods discovered, the need for crosslinking is a drawback of many proteins fibers. Gentle methods are often either expensive or nonexistent, and moreover post processing steps may compromise fiber properties such as the 3D structure (Figure 6), and increase cost. For that reason, protein fibers that are stable in aquatic media without crosslinking are highly appealing such as the laminin fibers developed by Neal *et al.* [31] or the FSP fibers developed in Paper I.

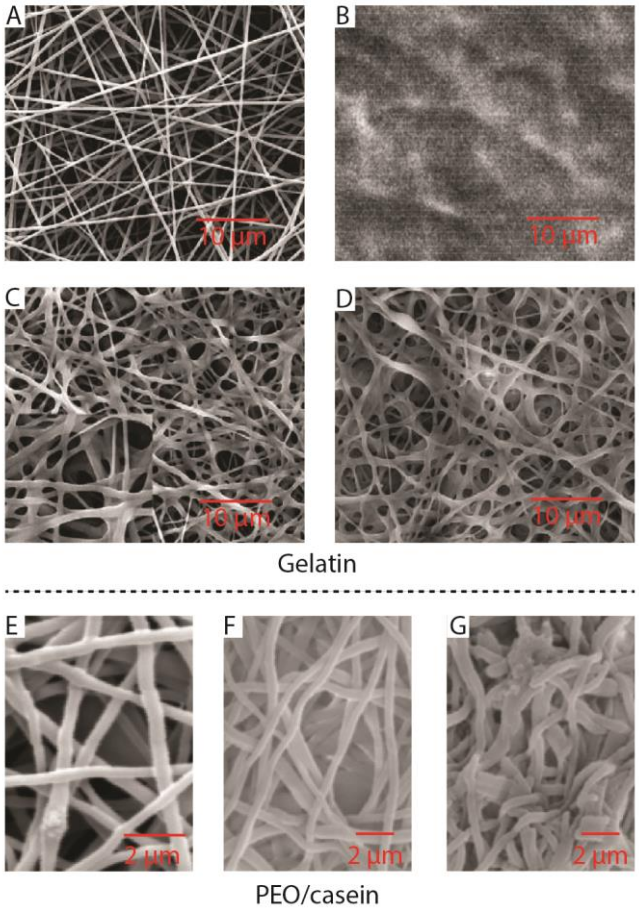

Figure 5. SEM images showing the effect of crosslinking of gelatin (modified from [23]) and PEO/casein (modified from [24]). A) 10% gelatin, B) 10% gelatin after adding a drop of water, C) crosslinked 10% gelatin, D) crosslinked 10% gelatin after being immersed in 37 °C water for 6 days, E) PEO/Casein fibers, F) crosslinked PEO/Casein fibers, and G) crosslinked PEO/Casein fibers after α-chymotrypsin degradation for 25 h.

Electrospun protein fibers have a large potential for biomedical, biosensing, and food related applications. The following paragraph will provide a review of some of the applications that have been studied for electrospun protein fibers.

Gelatin has been widely studied alone and in combination with synthetic polymers for tissue engineering, but also for other applications [20,25,26,32–38]. A series of studies presenting semi-interpenetration networks (sIPN) were recently published [25,26,37], where gelatin was electrospun and subsequently mixed with a photo-reactive crosslinking agent. Crosslinking of the gelatin fibers increased the stability of the gelatin scaffold in aqueous solutions, but the morphology of the fibers was interfered after incubation in simulated saliva fluid (Figure 6) [37]. The gelatin sPIN were evaluated for wound dressing purposes and transbuccal delivery of

insulin. In the latter study, the sPIN promoted increased transbuccal permeability of intact insulin *in vitro*, most likely due to a sustained release and localization of insulin close to the buccal mucosal site [25]. Pant *et al.* studied gelatin/nylon-6 fibers for hard tissue engineering; nylon-6 provided good mechanical properties, and the gelatin increased cellular compatibility [32]. Similarly, Kuppan *et al.* studied gelatin/polycaprolactone (PCL) fibers for esophageal tissue engineering, and found that cell proliferation on the gelatin/PCL nanofibrous scaffold was significantly higher than on the PCL nanofibrous scaffold [35]. Other structural proteins such as collagen [39,40] and elastin [41] have also been electrospun into nanofibers for biomedical application. For instance, in a study by Wang *et al.* low molecular weight (LMW) fish scale collagen peptides were electrospun together with chito-oligosaccharides, to develop an antibacterial wound dressing material. The authors found that the fiber scaffold supported proliferation of human skin fibroblast [39].

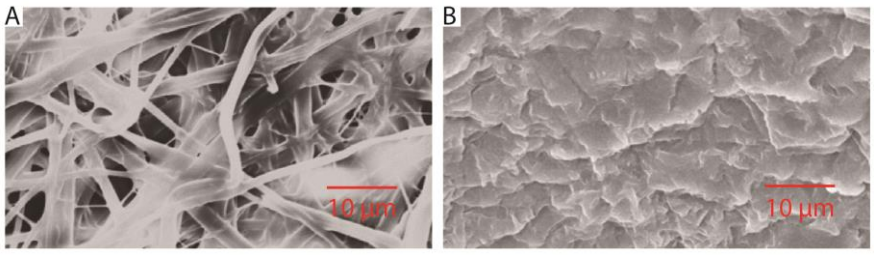

Figure 6. SEM images of A) sPIN and B) sPIN after 24 h incubation in simulated saliva fluid (12 mM KH_2PO_4, 40 mM NaCl, 1.5 mM $CaCl_2$, with NaOH adjusted to pH 6.2). Modified from [37].

Electrospinning of silk proteins has also been widely studied [42–48]. The excellent biocompatibility of silk fibers makes them appealing for biomedical applications, though sericin has to be removed from the protein solution, since sericin has a negative effect on the biocompatibility [49]. For instance, Dinis *et al.* applied silk fibers to promote nerve reconstruction. The silk fibers were further functionalized by incorporation of nerve growth factor and ciliary neurotrophic factor into the fibers, and the functionalized fibers led to a 3-fold increase in neurite length [47]. Soy proteins have also gained widespread interest in an electrospinning context [19,50–53]. The popularity of soy proteins is among others caused by its use in health food products, and the fact that soy proteins are one of the cheapest and most widely grown vegetable products with a wide range of uses. Unfortunately soy proteins cannot be electrospun alone, but need a carrier polymer in order to engage in electrospun fiber networks. PEO have been explored as a carrier polymer for SPI by Thirugnanaselvam *et al.*,

who studied PEO/SPI fibers for wound healing applications. The fibers showed positive results with respect to antimicrobial activity and growth of new epithelium *in vivo* [51]. Zein, gliadin, and hordein, prolamine proteins originating from corn, wheat, and barley, respectively, have also been electrospun for drug delivery and tissue engineering applications among others [54–57]. For instance, Brahatheeswaran *et al.* developed curcumin loaded zein fibers for soft tissue engineering. The authors found that curcumin was released in a sustained manner and maintained its free radical scavenging ability. The zein fibers also provided an attractive structure for attachment and growth of fibroblast *in vitro* [55]. Moreover, zein fibers have also been used to provide oxidative stability of fish oils [58,59]. Moomand *et al.* showed that omega-3 fatty acids were less oxidized when encapsulated into zein fibers, compared to nonencapsulated omega-3 fatty acids. In a study by Wang *et al.*, hordein and gliadin fibers were compared to zein fibers, and the authors found that hordein fibers showed lower cytotoxicity than gliadin and zein fibers [56]. Amaranth protein isolates also originate from plants. These proteins have been electrospun together with pullulan, to create an encapsulation system that maintained the antioxidative properties of quercetin and ferulic acid. Quercetin and ferulic acid were released in a sustained manner, and the antioxidative properties were preserved to a greater extent than the non-encapsulated compounds [60]. Xie *et al.* studied PVA and casein/PEO fibers with immobilized lipase enzymes. The catalytic activity of lipase was higher in the PVA/lipase fibers compared to in the PEO/casein/lipase fibers, and lipase was 6 times more active in the PVA/lipase fibers than in the cast membrane from the same solution, most likely due to the larger surface area of the fibers, allowing for more lipase enzymes to be accessible [24]. Hemoglobin and myoglobin have also been electrospun into bioactive fiber sheets. The idea was to utilize the physiological properties of hemoglobin and myoglobin to create a biological construct for oxygen delivery in wound healing [21]. The authors characterized the morphology, porosity, and mechanical properties, whereas proof of concept was not provided. Another bioactive fiber sheet was developed by electrospinning the basement membrane protein laminin I, for tissue engineering applications. The fibers maintained their geometry for at least two days in culture, without chemical crosslinking, and the authors found that PC12 neuronal cells extended their neurites on the fiber scaffolds *in vitro* without nerve growth factor stimulation [31]. The human albumin fibers that were previously described were intended for anti-adhesive wound dressings. The fibers were found to have a positive effect on the wound healing, by suppressing cell migration, while only provoking limited local inflammatory response [30].

1.2.2 Electrospun fibers in drug delivery

Electrospun fibers have a broad range of biomedical applications, one being drug delivery. There exist multiple ways by which a drug can be encapsulated into electrospun fibers. Blending the drug into the polymer solution before electrospinning will provide a homogenous distribution of the drug throughout the fibers (see Paper I and Paper II), and adsorption of the drug on to the fiber surface, will deposit the drug on the surface of the fiber [61]. By using coaxial electrospinning the drug can be placed in the core or the shell of the fiber [61], and lastly, the fibers can be combined with particulate systems, where the drug is encapsulated in the particles [61]. Drug delivery is used in many different applications, and some of them are presented in the following sections.

1.2.2.1 Local drug delivery

Localized drug delivery is beneficial in for instance tissue engineering and regenerative medicine, but also for delivery of chemotherapeutics [61,62]. In cancer therapy a high, local concentration of the administered drug is desired in order to treat cancer cells effectively. Systematic administration is challenging, among others since many of the therapeutic agents suffer from instability in the biological environment, have poor solubility, and cause undesired side effects in healthy tissue [63,64]. Several strategies have been investigated to circumvent those obstacles, using for instance liposomes, micelles, or hydrogels [65], but despite of impressive achievements, the problems have still not been overcome. Drug loaded electrospun nanofibers have been proposed as a solution. For solid tumors, the normal strategy to reduce the risk of reappearance is a combination between surgical operations to remove the tumor, and postsurgical chemotherapy or radiation therapy. In that context, electrospun fibers can deliver the anti-cancer drugs locally, as the fibers are easily inserted at the tumor site in connection with the tumor removal. The electrospun fibers will subsequently provide a controlled and sustained release of multiple drug combinations. Benefits of local delivery are high bioavailability, minimization of side effects, and a reduction in the need for frequent administrations, which will improve life quality of the patient. The strategy was among others explored by Liu *et al.*, who developed doxorubicin-loaded poly-L-lactide (PLLA) electrospun nanofiber for local chemotherapy against secondary hepatic carcinoma. The doxorubicin was released from the fibers to the fiber-mat-covered area of tissue during the first 24 h *in vivo*, which resulted in inhibition of tumor growth and increased survival time of the mice [66]. Xu *et al.* developed a dual drug delivery system that enabled concomitant delivery of a hydrophobic drug (paclitaxel)

and a hydrophilic drug (doxorubicin), by using W/O emulsion electrospinning of the amphiphillic PEO–PLLA diblock copolymer. The aqueous phase contained doxorubicin, and the oily phase was a chloroform solution of PEO–PLLA and paclitaxel [67]. The authors found that the dual drug delivery system showed a higher inhibition and apoptosis against rat glioma C6 cells *in vitro*, compared to when the drugs were in separate drug delivery systems [67].

1.2.2.2 Wound dressing

For severe wounds, such as burns, split-skin graft-donor sites, or diabetic ulcers, a combination of wound protection, adjustment of wound moisture, air supply for cell respirations, and antibiotics to prevent infections is optimal and necessary for accelerating the wound healing process. Bioactive wound dressings such as foams, hydrogels, and films have been developed [68], but they do not possess all of the required properties listed above. Electrospun fibers have shown great potential for wound healing applications [69]. The fibers can be applied directly to the wounded area, where the porosity of the fiber network allows for air supply to the wound, and in the same time the small pore size can preserve the wound from bacterial infections. The high surface area enables adjustment of moisture, as the fibers easily can absorb exudates. Lastly the fibers offer easy incorporation of antibiotics to prevent infections. The antibiotics can either be released fast or in a long and sustained manner. Kataria *et al*. studied PVA/alginate fibers loaded with the antibiotic drug ciprofloxacin. The drug loaded fibers were applied to a wounded rabbit, and promoted faster wound healing compared to a market product [70]. Thakur *et al.* developed a dual drug delivery system, consisting of PLLA fibers with an anesthetic drug (lidocaine) and an antibiotic drug (mupirocin). The authors found that the release kinetics of mupirocin was altered by the presence of lidocaine in the same polymer matrix. By using a dual spinneret the release profile of mupirocin was optimized, and the dual spinneret technique was found to provide the best fiber scaffold for wound healing purposes *in vitro* [71]. Eriksen *et al.* studied PCL fibers loaded with an antimicrobial peptide, and the drug release and antimicrobial activity were compared to tetracycline loaded PCL fibers. Antimicrobial peptides are appealing since they have a broad spectrum of antimicrobial activity, in addition to being biocompatible which reduces the risk of side-effects. The antimicrobial peptides were most likely affected during processing since the peptide loaded fibers did not exhibit sufficient antimicrobial effects to prevent bacterial growth, however the potential of using the antimicrobial peptides were apparent from the drug release studies: The release of tetracycline from the PCL fibers followed an exponentially release profile, whereas the peptides were released linearly. The sustained and

prolonged release observed for the peptide is beneficial for long term drug delivery systems, for instance in relation with implants [72].

1.2.2.3 Tissue engineering

The morphology of electrospun fibers has similarities to the extra cellular matrix. For that reason the fibers can provide directed cell growth [73–75], and addition of for instance growth factors or DNA will make the fiber scaffold even more effective [74,75]. This makes electrospun fibers ideal for tissue engineering applications.

Electrospun fibers for regenerative medicine or tissue engineering are the sub-categories within electrospinning, where encapsulation of biopharmaceuticals has been studied the most [75–78], among others since the majority of cell-growth-promoting drugs are biological macromolecules. Figure 7 illustrates the effect of encapsulating insulin and epidermal growth factor into gelatin/poly(L-lactic acid)-co-poly-(e-caprolactone) (PLLCL) fibers. The images show immunocytochemical staining of Ker 10 – a protein specific to epidermal differentiation, and the increased expression of Ker 10 in Figure 7 A (expression of Ker 10 on gelatin/PLLCL fibers with encapsulated growth factors) compared to Figure 7 B (expression of Ker 10 on gelatin/PLLCL fibers) indicated an increased differentiation of ADSCs on fibers with added growth factors [78].

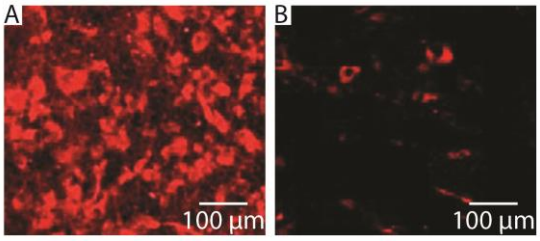

Figure 7. Immunocytochemical analysis of the expression of Ker 10 on A) gelatin/PLLCL fibers with encapsulated growth factors and B) gelatin/PLLCL fibers. Modified from [78].

1.2.2.4 Oral drug delivery

Oral drug delivery is the most patient convenient administration form, and drug delivery systems that enable oral administration have a huge effect on life quality of patients with high needs of medicine. In this PhD project oral drug delivery was the main application studied. Accordingly, the introduction to electrospun fibers in oral drug delivery will be more elaborated, with a special emphasis on intestinal drug delivery as the foremost target area.

The oral cavity

A large surface area is a key property of electrospun fibers. The large surface are can be utilized in obtaining increased dissolution of a compound, which is useful in fast-dissolving drug delivery systems, where the target area is the oral cavity. The benefits of using electrospun fibers are rapid disintegration, without the need of water. The oral mucosa is an appealing delivery site since it is permeable and vascularized. The release and uptake of a drug in the mouth will thus enhance bioavailability and provide a fast response [79]. A potential drawback of the oral cavity as a target area is the risk of involuntary swallowing of saliva which will wash away the active compound before it is absorbed (though omission of water reduces this risk). Drug absorption is also challenged by the small surface area of the sublingual mucosa, and it may be affected by tongue movements [80,81]. Furthermore, human senses such as taste and touch, may affect patient convenience. Delivery through the oral cavity is nevertheless appealing for patients with swallowing difficulties such as children [82].

Drugs that have been incorporated into fast-dissolving drug delivery systems are for instance paracetamol [83] and caffeine [83,84]. Encapsulation into electrospun fibers caused the drugs to dissolve faster than the pure drugs *in vitro*. The oral cavity (buccal and sublingual) has also been target area for delivery of biopharmaceuticals; insulin [25,85] and nystatin [37]. The mucoadhesive properties of the fibers (gelatin and alginate/PVA) were explored [37,85], since mucoadhesiveness may favor drug absorption by prolonging the retention time, and release the drug in the proximity of the membrane. The gelatin fibers and the alginate/PVA fibers were both found to be mucoadhesive; however the effect of the mucoadhesive properties on drug absorption was not studied [37,85]. Benefits of mucoadhesive properties in general have been explored in several studies [86–90].

The intestine

The small intestine is an obvious target for drug delivery. It is more permeable than the gut and the colon, and it is the site for absorption of nutrients as dictated by nature [91]. An increasing amount of new drugs are either poorly soluble or biopharmaceuticals, but for these compounds intestinal drug delivery are challenging.

Low solubility of a drug limits drug absorption in the gastrointestinal tract. Different strategies such as encapsulation and micronization have been suggested as a way to increase solubility and transepithelial permeation [92–94]. As an alternative, the large surface-to-volume ratio of

electrospun fibers can aid the dissolution of poorly soluble drugs [95]. This has been explored for oral administration of itraconazole [96], quercetin [97], and diosmin [98], and all compounds gained increased solubility upon encapsulation into electrospun fibers. For instance, incorporation of diosmin into hydroxypropyl cellulose/PVA/PEO fibers provided approximately 70% dissolution of diosmin compared to negligible amounts of dissolved diosmin from powder and tablet forms (Figure 8) [98]. The increased solubility was first of all due to the increased surface-to-volume ration as previously mentioned, but additionally it was the non-crystalline form of diosmin that was present inside the fibers. The increased dissolution led to higher initial plasma levels, increased maxima plasma concentrations, and increased cumulative absorption *in vivo* [98].

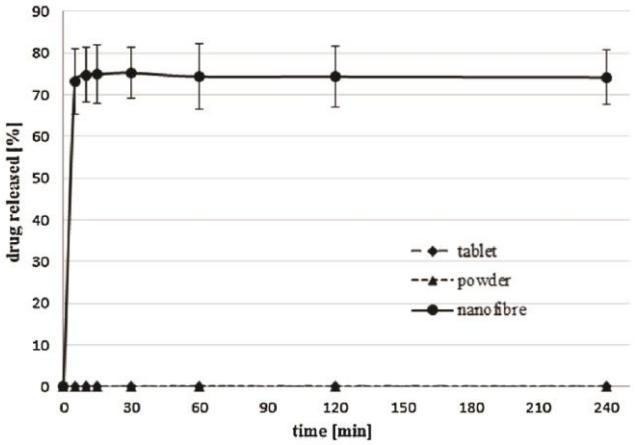

Figure 8. Comparison of *in vitro* diosmin dissolution from powdered drug, micronized form, and electrospun fibers of hydroxypropyl cellulose/PVA/PEO in the ratio of 45:47.5:7.5 [98].

Intestinal delivery using electrospun fibers has also been explored for delivery of antibiotics. Delivery of antibiotics through the intestine entails obstacles such as permeation through the epithelial layer and maintained stability when it passes the low pH in the stomach. To deliver the drug in its active form, a carrier material that is stable in the stomach, but releases the cargo in the small intestine can be used [99–103]. For instance, Wang *et al.* encapsulated erythromycin into electrospun hydroxypropyl methyl cellulose phthalate (HPMCP) for intestinal delivery. The authors found that the release of erythromycin from HPMCP fibers went from a slow release in gastric juice to almost 1st order kinetics in intestinal juice [104]. Similarly, electrospun eudragit fibers have been studied for intestinal delivery of mebeverine hydrochloride [105] and aceclofenac/pantoprazole [106]. In the latter case, aceclofenac loaded

zein fibers were electrospun concomitant with pantoprazole loaded eudragit fibers, to develop a dual delivery system, where one drug (pantoprazole) minimized the side effects (gastrointestinal toxicity) caused by the other drug (aceclofenac). Pantoprazole is unstable in acidic environments and accordingly needs protection through the stomach. This was provided by eudragit, and the simultaneous administration of aceclofenac and pantoprazole, using zein and eudragit fibers, reduced the ulcer inducing tendency of aceclofenac *in vivo* [106]. Eudragit fibers have also been studied for colon targeted drug delivery of diclofenac [101,107] and budesonide [108]. For instance, the release of budesonide from ethylcellulose/eudragit S100 core/shell fibers at pH values < 7.4 was minimal, but when the pH of the release medium was increased to 7.4 (pH in the colon), budesonide was released exponentially due to dissolution of the eudragit S100 shell (Figure 9) [108]. For the ethylcellulose/eudragit S100 blend fibers the release of budesonide was initiated at pH 6.8 (Figure 9). The *in vivo* release behavior of budesonide was studied by analyzing budesonide concentration in the stomach, the intestine, and the colon, which showed similar results as the *in vitro* experiments. The core-shell fibers reached 3 fold higher budesonide concentrations in the colon compared to the blend fibers [108].

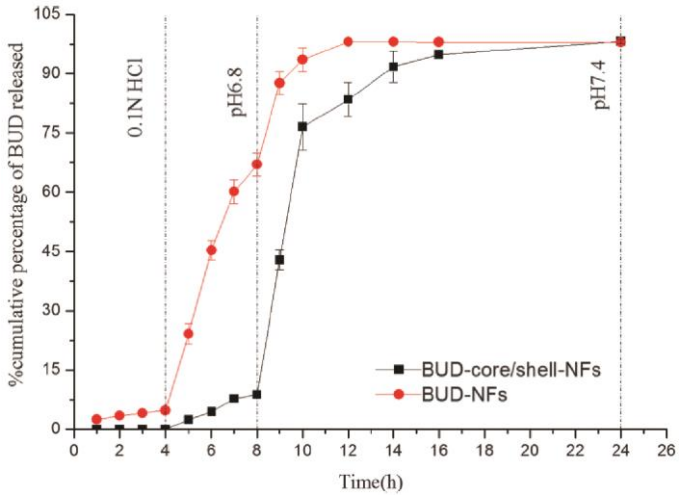

Figure 9. *In vitro* release of budesonide from core/shell fibers (black) and bend fibers (red) at varying pH values [108].

Therapeutic proteins and peptides are being increasingly used for treatments of numerous diseases, due to their high selectivity and effective drug action among other beneficial effects. The biopharmaceuticals deviate from small molecules especially with regards to their larger size

and poor enzymatic stability [109], which make it extremely challenging to obtain a therapeutic effect, unless the drugs are injected. Some of the challenges associated with oral drug delivery of biopharmaceuticals are to ensure sufficient structural and chemical stability, by protection against the harsh acidic environment in the stomach and the proteolytic enzymes in the gastrointestinal tract. Furthermore, permeation through the mucosa and permeation through the intestinal epithelium may be hindered by the size and chemical properties of the biopharmaceuticals [110–113]. Several strategies have been proposed to overcome obstacles related to delivery of biological macromolecules through the small intestine [112,114–123]; examples are hydrogels [124], lipid-based carriers [125], permeation enhancers [123], and bioadhesive microspheres [126]. Despite the many promising attempts to develop new oral formulations for biopharmaceuticals, none has so far succeeded, and new approaches are needed.

The potential of using electrospun fibers for intestinal delivery of biopharmaceutics has not been studied extensively. This matter was therefore explored and evaluated in Paper II, where especially obstacles related to small intestinal enzymes (chymotrypsin) and transepithelial permeation was addressed.

The intestine contains a range of physiological compounds such as bile salts, lipids, and enzymes, and their interactions with food are crucial in the digestion of a meal. In general, physiological compounds are found all over the human body and engage in interactions [127]. The physiological compounds may also interact with drug delivery systems and affect e.g. their stability and drug release properties, though this is rarely considered when a drug delivery system is evaluated [33,42,55,70,105,128–140]. Some studies have taken biorelevant compounds into account, and have observed an effect on the drug release from the electrospun fibers. Alborzi *et al.* studied the release of folic acid from alginate/pectin/PEO fibers, and found that the *in vitro* release of folic acid was affected by the presence of a bile extract [99]. Sofokleous *et al.* studied release of amoxicillin from poly(D,L-lactide-co-glycolide) (PLGA) for wound healing purposes, and found the drug release from the PLGA fibers to vary between the release media (water, simulated body fluid, and phosphate buffered saline) [141]. Moreover, Maretschek *et al.* found that release of cytochrome C from PLLA fibers was increased when Tween 20 was present in the release medium [142], and in Paper II insulin release was increased

in simulated intestinal fluid (with physiological compounds), compared to release in a buffer without physiological compounds.

The understanding of the interactions between biorelevant compounds and electrospun fibers are still inadequate, for which reason the interactions were systematically investigated in Paper III.

1.3 Nanocomplexes

Interactions between biomacromolecules (DNA, proteins, polysaccharides etc.) are inherent in nature and a prerequisite for life. Proteins and polysaccharides perform key functions such as providing physical structure, conferring protection against pathogens, performing enzymatic reactions, and signaling, in addition to many further specialized functions. Moreover, interactions between proteins and polysaccharides can be utilized in technological applications to form self-assembled NCXs.

When oppositely charged compounds interact, they may self-assemble into supramolecular organized systems. These ionic complexes are attractive for their simplicity, and since their self-assembly is dependent on pH and ionic strength, the complexes can be made sensitive to stimuli such as pH, heat, and light [143,144]. In many cases, this response can be utilized as an activating effect, where the NCXs respond to stimulation *in vivo*. When developing stable NCXs based on electrostatic self-assembly, it is crucial to assess the conditions in which the components are oppositely charged. The physicochemical properties of the constituent molecules will subsequently influence the properties of the resulting nano-assembly and the supramolecular architecture [145]. The optimal conditions, where aggregation and precipitation of the NCXs are avoided, often lie within a narrow range of composition, or external conditions [146].

Polysaccharides have been widely explored for the development of particulate systems [147,148]. Interactions between polysaccharides and mucus [149–151] make polysaccharide-based particles interesting for mucosal delivery, one example being alginate and chitosan based carrier systems [152]. Goycoolea *et al.* developed insulin loaded nanoparticles by ionic gelation of chitosan using tripolyphosphate and concomitant complexation of alginate, for transmucosal, nasal delivery of insulin. The chitosan-tripolyphosphate-alginate complexes promoted increased

systemic absorption of insulin *in vivo* [153]. In another study Sarmento *et al*. studied insulin loaded nanoparticles made from ionotropic pre-gelation of alginate and subsequent complexation with chitosan for oral administration. The particles were found to be mucoadhesive, since the particles could be detected in the intestinal mucosa, and the alginate-chitosan particles increased the bioavailability of insulin *in vivo* [154].

Polysaccharides may also engage in colloidal polyelectrolyte complexes together with proteins, by spontaneous electrostatic interactions in aqueous medium [146,148,155,156]. The protein-polysaccharide complexes have been explored for development of biocompatible drug delivery carriers or as self-assembled gelling complexes. Combinations such as gelatin/casein [157], alginate/casein [158,159], alginate/BSA [160–162], BSA/fucoidan [163], alginate/lysozyme [146,162,164], lactoferrin/gum arabic [165], soybean protein isolate/chitosan [166], alginate/WPI [167,168], lysozyme/low methoxyl pectin [169], hyaluronic acid/lysozyme [170,171], and β-lactoglobulin/alginate [162,172] have been explored. As an example, Fioramonti *et al*. studied alginate/WPI NCXs [168]. The WPI were heated in order to create soluble protein aggregates, and subsequently alginate was deposited onto the surface of the protein aggregates. Thermal treatment of WPI at 85 ºC caused a greater exposure of hydrophobic patches, which was beneficial since the WPI/alginate NCXs were intended for protection of lipophilic bioactive agents [168]. Electrostatic complexation between alginate and casein into hydrogel particles has also been studied [158]. The particles remained intact from pH 4 to 5, but aggregated or dissociated at lower or higher pH, as indicated by the protein being on particle form (pH 5), in solution (pH 7), or aggregated (pH 3) (Figure 10). The authors also found that lipid droplets encapsulated in the particles were released in simulated oral conditions, which made the particles applicable for oral delivery of lipophilic active ingredients [158].

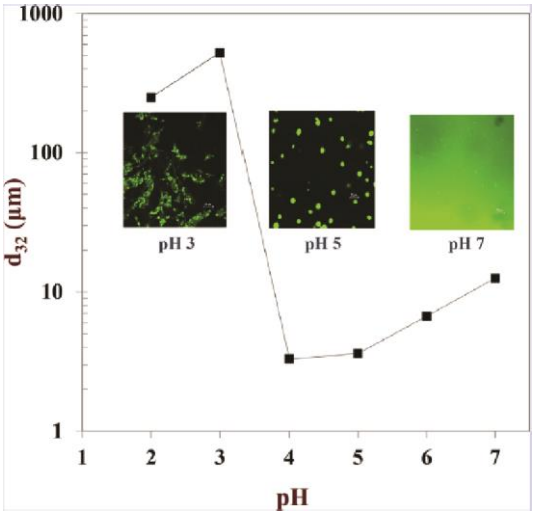

Figure 10. Influence of pH on the mean particle diameter (d_{32}) of hydrogel particles. Confocal micrographs show the hydrogel particles at pH 3, 5, and 7 with the protein phase stained green using FITC [158].

Particle based systems are being increasingly applied in delivery of nutrients [173,174]. One example is delivery of folate, an essential nutrient, which is challenged by the insolubility of the oxidized version, folic acid, in acidic environments. To overcome the limited absorption due to insolubility, Ding *et al.* developed folic acid-loaded soy protein/soy polysaccharide nanogels that stabilized folic acid under acidic conditions and released it rapidly at neutral pH [175].

Self-assembled particle systems can also be used for protection of proteins. For instance, Water *et al.* used complexation between hyaluronic acid and lysozyme, a model protein, to increase the stability of lysozyme [171]. A similar study was performed by Zhao *et al.*, who studied BSA and alginate complexation, and the authors found that the majority of BSA was recovered with maintained secondary structure and conformational properties, after dissociation of the protein–alginate complexes [160].

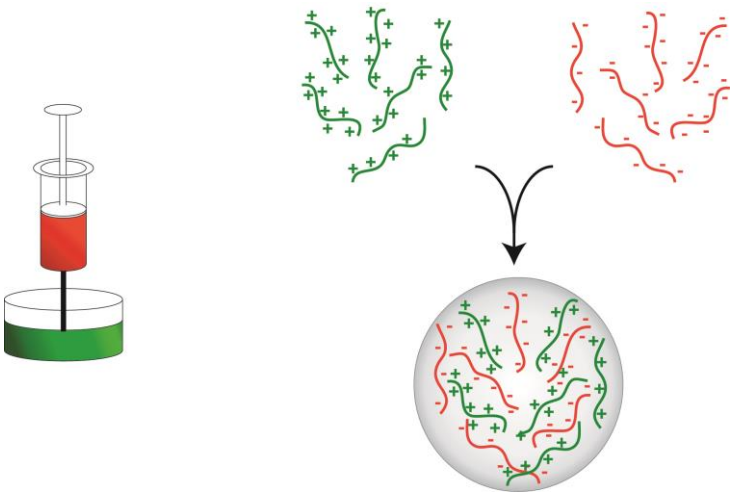

Figure 11. Schematic illustration of NCX formation. The FSPs and alginate were gently mixed, after which NCXs were formed spontaneously due to electrostatic self-assembly.

As indicated by the above and the extensive literature, there is a large interest in exploring NCXs made from electrostatic self-assembly between proteins and polysaccharides. The ability of FSP to self-assemble with alginate was therefore explored in Paper IV. A schematic illustration of the particle processing procedure is shown in Figure 11. Alginate was chosen, due to its cyto-compatibility, biocompatibility, and biodegradation [176]. Moreover, the U.S. Food and Drug Administration (US-FDA) has recognized alginate as being a "Generally Recognized As Save" (GRAS) material. From a commercial point of view, this approval makes alginate even more appealing. With the current large emphasis on sustainable research, and since biopolymers in general are considered beneficial and sustainable, alginate's origin from brown algae makes it further attracting [177].

Alginate is a linear co-polymer composed of homopolymeric (1→4)-linked poly–L– α guluronate (poly–G) and poly–D– β mannuronate (poly–M), the chemical structures are shown in Figure 12. The physical-chemical, functional, and bioactive properties of alginate are mainly determined by the MW and the molar ratio of D–mannuroate to L–guluronate residues (M/G ratio). Moreover, the negatively charged glucuronic side chains of alginate have been shown to interact with mucin [178], one of the major components in mucus, which gives alginate mucoadhesive properties [178,179]. Particle systems with mucoadhesive properties have been subject to a lot of interest in drug delivery aspects [180]. As previously mentioned, mucoadhesive properties can prolong the retention time in the mucus, and thus extend the time for drug absorption. In addition to mucoadhesive properties, alginate has been shown to affect

tight junctions in a Caco-2 cell monolayer [181,182], which can lead to increased drug permeation and accordingly increased bioavailability.

The feasibility of using alginate in protein-polysaccharide complexes have already been mentioned, and together with the benefits of FSPs described in section 1.4, NCXs composed of FSPs and alginate may be highly potential for oral drug delivery purposes.

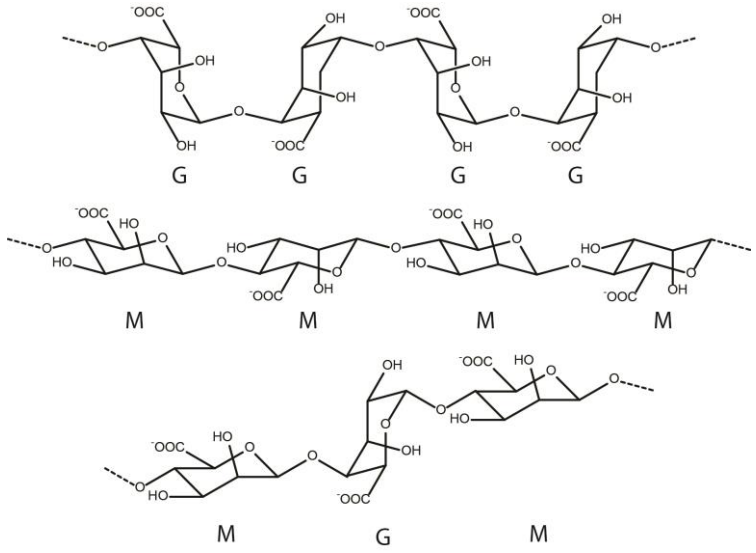

Figure 12. Chemical structures of alginate showing the homopolymeric (1→4)-linked poly–L– α guluronate (poly–G) (top), poly–D– β mannuronate (poly–M) (middle), and the mixed polymer (bottom).

1.4 Fish sarcoplasmic proteins

FSPs are water soluble sarcoplasmic fish proteins from the Atlantic cod (*Gadus morhua*). A one-dimensional gel electrophoresis of the FSPs can be found in Paper I, and a two-dimensional gel electrophoresis of the water soluble proteins from a cod muscle is seen Figure 13. The FSPs account for 25-30 % of the fish muscle proteins, they are easily accessible, and comprise peptides and proteins of up to ~200 kDa in MW. The numerous health benefits and bioactive properties of fish make FSPs appealing to use in an oral drug formulation [183–187]. An example is inhibitory effects against dipeptidyl peptidase-4 (DPP-IV) [188], an enzyme with an essential role in glucose metabolism and linked to type 2 diabetes, and DPP-IV inhibitors have been proposed as a potential new treatment for this disease [189,190]. Moreover, dietary cod proteins have been shown to improve insulin sensitivity in insulin-resistant subjects [191,192]. From an economical and sustainable point of view, FSPs are beneficial since many of the

proteins that constitute the FSP mixture also are found in the waste water from the fish industry [193–195]. The wastewater originating from the fish industry could thus provide a large and cheap source for FSPs. Utilization of wastewater from the fish industry have previously been studied [196]. Ferraro *et al.* characterized the wastewater from salting of codfish, and found that the wastewater contained compounds such as free amino acids, peptides, and proteins [195]. The intestinal permeability of salt-containing mixtures of amino acids extracted from this wastewater was investigated, and the authors found that the amino acids were transported across the epithelial cell layer *in vitro*, and have thus potential in food, feed, cosmetics, and pharmaceutical formulations [197].

FSPs have not been studied for development of nano-micro structures previously. The health benefits and economical perspectives make FSPs a very interesting material to explore, for which reason it was chosen for this PhD project.

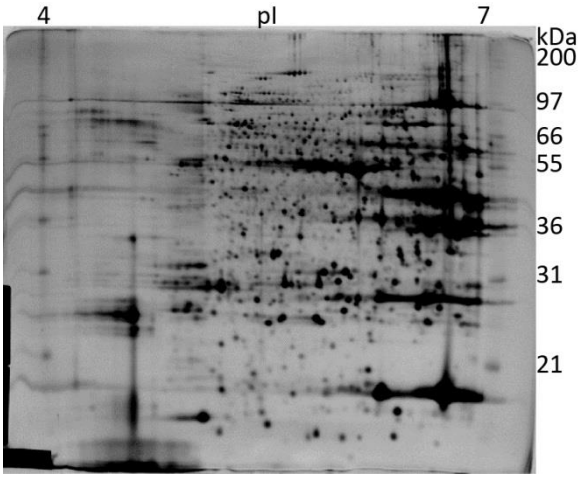

Figure 13. Two-dimensional gel electrophoresis of the water soluble proteins from cod muscle. Immobiline Drystrips (GE Healthcare, 18 cm, pI 4-7) were used for the first dimensional protein separation and the second dimensional SDS-PAGE was run in a 12 % acrylamide gel. The gel was silver stained (unpublished results, Flemming Jessen).

2 Introduction to the methods used

This section will give a brief introduction to the main methods used in the PhD project. A short statement introducing how and in which papers (Paper I, Paper II, Paper III, and Paper IV) the given methods have been used is provided. The included methods are; scanning and transmission electron microscopy (SEM and TEM), confocal microscopy, assessment of hydrophobic surfaces using fluorescence from 8-anilino-1-naphthalenesulfonic acid (ANS), attenuated total reflectance - fourier transform infrared spectroscopy (ATR-FTIR), circular dichroism (CD), sodium dodecyl sulfate - polyacrylamide gel electrophoresis (SDS-PAGE), DPP-IV bioactivity assay, reversed phase – high pressure liquid chromatography (RP-HPLC), cell based assays, dynamic light scattering (DLS), contact angle measurements, and critical micelle concentration (CMC) determinations.

2.1 Electron microscopy

Two types of electron microscopy were used in this PhD project; SEM and TEM. Both are widely used to investigate inner and outer structures of electrospun fibers and particles in general.

The electron microscope consists of an electron gun, a system of condenser lenses, a specimen holder, and a detector. For both SEM and TEM an electron gun sends electrons towards the specimen, and lenses ensure that the beam is focused onto the sample. In TEM another lens system is placed after the sample, to collect the beam into the detector. Details about the electron gun and lens systems will not be discussed here; instead this section will focus on the interactions between sample and electrons. For further information about electron microscopy, see references [198,199].

The general principle behind electron microscopy is illustrated in Figure 14. Primary electrons enter the sample and interact in scattering events, and the same and/or different electrons leave the sample to create an image. If the sample and the primary electrons interact elastically, the energy of the electron is not changed detectably, whereas in inelastic scattering the electrons will transfer some of the energy to the interacting atom.

In TEM, where the electron beam passes through a thin specimen, elastic scattering is important. When the electron beam hits the specimen, the electrons are scattered through the sample, and the spatial distribution of the scattered electrons, the electron diffraction pattern, will contain information about the spacious orientation of atoms in the sample. From the diffraction pattern, the TEM image can be created. Contrast arises because of interference between electrons from different angles, however, for many samples the inherent contrast is poor (the NCXs in Paper IV), and in these situations the sample may benefit from negative staining. In negative staining, a staining agent is added (often a heavy metal salt, since these compounds interact readily with the electrons), which will surround the sample and thus increase deflection of the electron beam. The high energy (40-120 kV) of the electrons gives TEM microscopes a high resolution (for some TEM instruments sub-50-pm resolution can be obtained [200]), and TEM can therefore be used to study very small objects. TEM was utilized in Paper IV to study shape and size of the NCXs.

In SEM the electron beam scans the surface of a sample, and an image is created by monitoring the intensity of selected electrons - the secondary or backscattered electrons. Secondary electrons are generated when primary electrons interacts inelastically with an atom in the sample, thereby causing emission of an electron, whereas backscattered electrons are reflected by the sample after elastic scattering events. As both types of electrons originate from the surface of the sample, the field of depth is high in SEM, compared to TEM, which makes SEM excellent for morphology studies. SEM was therefore used to study the morphology of electrospun fibers in Paper I and Paper II, and it was used to study the fiber porosity in Paper III. SEM has a range of other applications such as elementary analysis, but those applications will not be discussed here, since they were not utilized in this project.

When studying biological samples by using SEM, such as protein fibers in Paper I, Paper II, and Paper III, the sample must be coated with a metal that reflects the electrons. The coating also helps to avoid charging of the surface. In Paper III the porosity of the fibers, was studied by freezing fracture the fibers with or without the buffer. In order to obtain a surface structure, the sample was sublimated before coating with a metal. The sublimation made the fibers stand out from the ice block, thereby enabling porosity analysis.

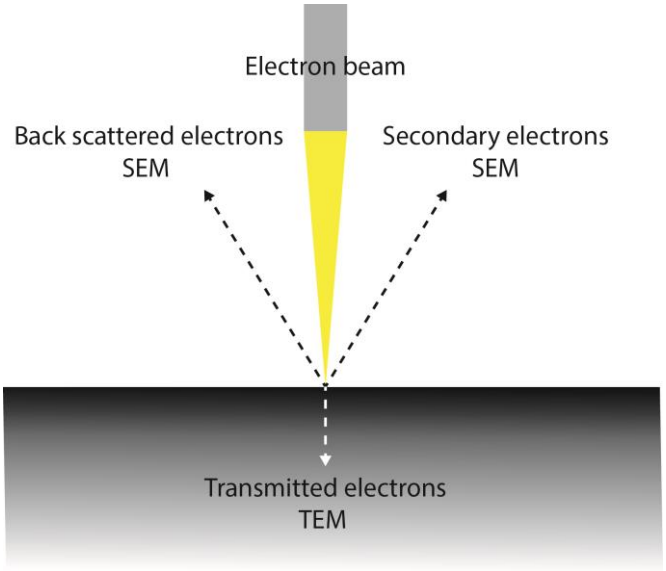

Figure 14. Schematic illustration of electron microscopy. In SEM backscattered and secondary electrons are used to create an image of the surface, whereas TEM utilizes transmitted electrons which allows for investigation of the inner structure.

2.2 Confocal microscopy

In confocal microscopy the property of fluorophores to emit light upon irradiation and the microscope's ability to select between many focal planes are utilized to localize fluorophores in a sample. A schematic illustration of a confocal microscope is shown in Figure 15, and a detailed introduction to confocal microscopy is found in [201,202].

In Paper I the fluorescent molecule rhodamine B was encapsulated into FSP fibers. By studying the fibers in the confocal microscope, knowledge about the distribution of rhodamine B inside the fibers was obtained. Similar studies were conducted for insulin in Paper II. However, since insulin is not intrinsically fluorescent, insulin was labelled with fluorescein isothiocyanate (FITC), a well-known fluorescent probe which enabled evaluation of the insulin distribution inside the fibers.

In Paper II, confocal microscopy was also used to study the tight junctions in a Caco-2 cell monolayer. As described in section 2.9.1, tight junctions are composed of interacting proteins that ensure good connectivity of the monolayer. As with insulin, the tight junction proteins are not intrinsically fluorescent, and thus not detectable in a confocal microscope. A labeling procedure similar to the one used for insulin was not possible, since the tight junction proteins

are attached to the cells. Instead, fluorescent labeled antibodies were used. Antibodies are proteins that interact with specific proteins with high selectivity. By incubating the fluorophore-labelled antibody with the cells, it was possible to visualize the tight junctions in the confocal microscope through fluorescence from the antibody. Lastly, confocal microscopy was utilized in Paper III, to study fluorescence from ANS. This will be further elaborated in section 2.3.

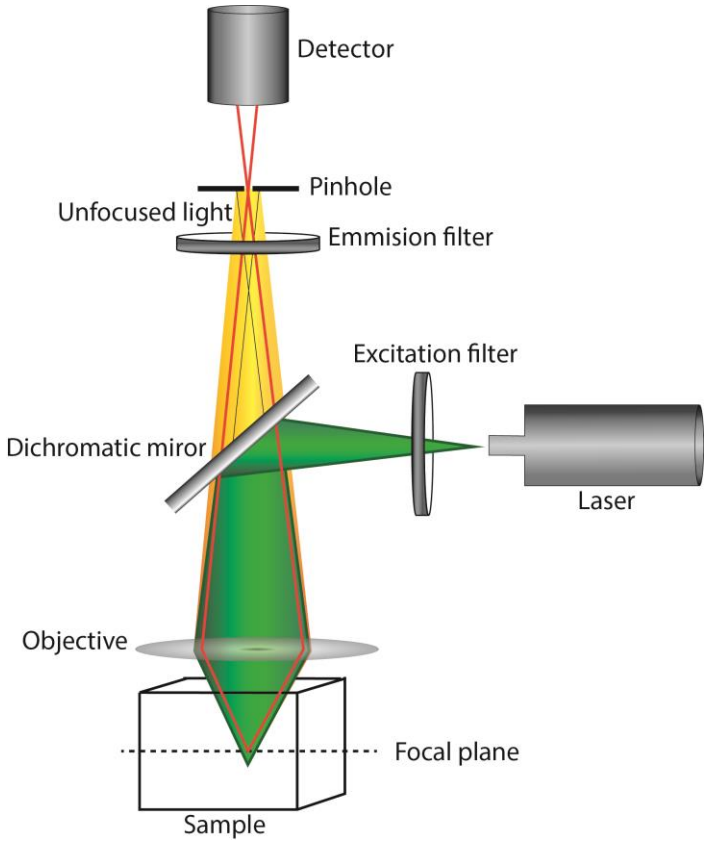

Figure 15. Schematic illustration of confocal microscopy.

2.3 Assessment of hydrophobic regions on the FSP-Ins fibers using ANS fluorescence

In Paper III the hydrophobic nature of the FSP-Ins fibers was investigated using ANS fluorescence. When ANS interacts with hydrophobic moieties (for instance hydrophobic regions on the FSP-Ins fibers), the fluorescence exhibits a strong blue shift and a significant increased fluorescence quantum yield, compared to when ANS is in a hydrophilic environment, where it barely fluoresce [203,204]. Accordingly, any fluorescence from ANS after incubation of with

the FSP-Ins fibers will reveal the presence of hydrophobic pockets on the fibers (Figure 16). The samples were studied by using confocal microscopy.

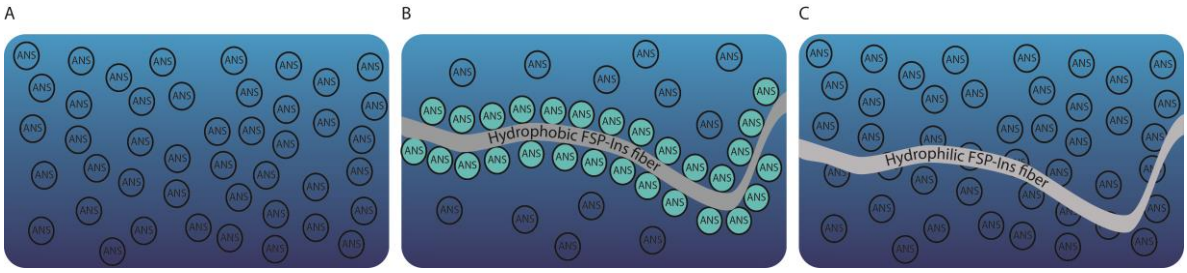

Figure 16. A) Schematic illustration of how ANS was used to investigate hydrophobic regions on electrospun fibers. A) The ANS solution before addition of fibers is not fluorescent. B) When adding a hydrophobic fiber, the ANS molecules will adhere to the fiber surface, and the change in the surrounding chemical environment will cause an increase in quantum yield and a blue shift of the ANS fluorescence, making the fibers visual in a confocal microscope. C) When adding a hydrophilic fiber to the ANS solution, nothing visual happens.

2.4 ATR-FTIR

Energetically, molecular vibrations are in the IR-range (e.g. 200 – 4000 cm^{-1}), and can thus be studied with IR spectroscopy. IR-absorption of side chains in a protein may deviate from absorption of side chains in a dipeptide, for instance as a result of the surrounding environment [205]. This was utilized in Paper I, where ATR-FTIR was used to study the encapsulation of a dipeptide into FSP fibers.

ATR is a sampling technique that can be used together with FTIR to study solid or liquid samples without sample preparation. ATR is highly suitable to study electrospun fibers, since alternative sample preparations such as dissolution or crushing will destroy the fibers.

The principle behind ATR-FTIR is illustrated in Figure 17. Briefly, in ATR-FTIR the beam travels through the ATR crystal until it hits the surface between sample and crystal with an angle of incidence (θ_i). Depending on the size of this angle, a part of the beam will be refracted, with an angle of refraction (θ_R), through the sample, and the rest of the beam will be reflected, with an angle of reflectance (θ_r). When the angle of refraction reaches 90° all light is reflected. The critical angle (θ_c) is the minimum angle of incidence, causing total reflectance and angles above θ_c, will also cause total reflectance. When the beam hits the surface between sample and crystal with an angle of incidence that is larger than the critical angle ($\theta_i > \theta_c$), an evanescent wave is created which will extend into the sample, where the light can be absorbed. Subsequently the beam travels towards the detector. In FTIR an interferometer enables

simultaneous measurements of all frequencies, which results in extremely fast measurements compared to the old fashion dispersive instruments. For further introduction to FTIR-ATR see references [206,207].

The FTIR spectra of FSP fibers were complex due to the mixture of proteins in the fibers. The peaks in FTIR spectra are a combination of absorption bands from all compounds in the sample, and the presence of many different compounds in one sample will thus decrease the fine structure. Furthermore, the signal is sensitive to changes in the immediate environment surrounding the vibration; such changes can lead to altered bond polarity, which affects the band intensity. In Paper I, the FTIR spectra were therefore only compared, in order to detect differences originating from the encapsulated dipeptide.

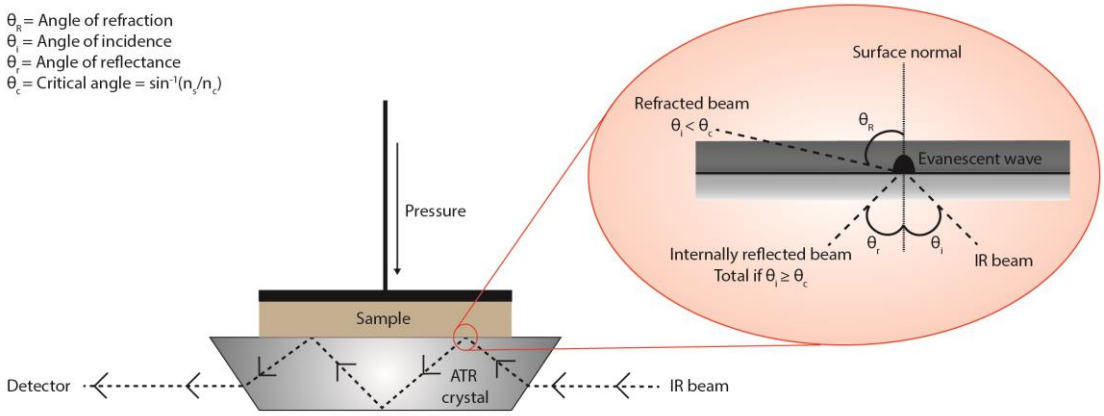

Figure 17. Illustration of the principles behind ATR-FTIR. When the IR beam hits the surface between the ATR crystal and the sample, with an angle larger than the critical angle, an evanescent wave is created, which will extend into the sample where the light can be absorbed. Subsequently the beam is send towards the detector.

2.5 SDS-PAGE

SDS-PAGE was performed according to the method of Laemmli [208], to analyze the protein composition of FSP in Paper I, and to study the degradation of FSP fibers and FSP-Alg NCXs in Paper IV.

The mobility of a protein in a polyacrylamide gel is dependent on MW, charge, and shape. Addition of SDS will unfold the protein and create a rod-like protein micellar-structure which, together with an excess of negative charge, causes the shape and charge of the protein to have no influence on the migration in the gel. Accordingly, the mobility of the proteins is solely

determined by the MW. This is utilized in SDS-PAGE, where protein migration in a polyacrylamide gel is used for separation of proteins according to their MW. By applying an electrical field to the gels, the proteins will migrate through the gel, and by comparing the corresponding band pattern with known standards, information about protein MW can be obtained.

2.6 Circular dichroism

Circularly polarized light arises as a result of two polarized, electrical waves being perpendicular to each other and separated with a specific phase shift (Figure 18). The phase shift determines if the light is left or right handed. Optically active molecules interact differently with right and left handed circular polarized light; this difference is reflected in the extinction coefficient, ε, and accordingly in the absorbance, A, according to Lambert Beer's law. In CD the difference in absorbance between right (R) and left (L) handed light is measured, from which structural information can be obtained:

$$\Delta\varepsilon = \varepsilon_L - \varepsilon_R$$

$$\Delta A = A_L - A_R$$

Proteins are optically active (for a deeper introduction to the optical activity of biopolymers, the reader may refer to [209]), and CD spectroscopy can therefore be used to analyze the secondary and tertiary structures of proteins. In far-UV CD (200 – 250 nm) light is absorbed by the protein backbone, and especially secondary structure (e.g. α-helix, β-sheet, random coil) can be analyzed in this region. In near-UV CD (> 250 nm) the signal is affected by the dipole orientation, or the local environment of tyrosine, cysteine, tryptophan, and phenylalanine groups. Near-UV CD can therefore be used to analyze changes in the tertiary structure of a protein.

In Paper II the near-UV spectrum of released insulin was compared to the spectrum of unprocessed insulin to verify that the tertiary structure of insulin was intact after release from the FSP-Ins fibers. Low molecular weight (LMW) compounds were released from the fibers simultaneously with insulin, which resulted in noisy far-UV CD spectra. Since the released LMW FSPs were mainly small peptides, the amount of tertiary structure was limited, for which

reason the near-UV spectrum contained less noise from the LMW compounds, and therefore more suited for the investigation.

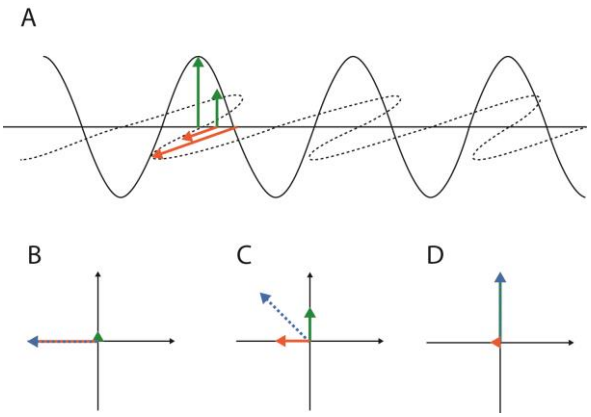

Figure 18. A) Two electromagnetic waves propagating according to time. B-D) Graphical illustration of the electrical field of two electromagnetic waves. The light in this figure will be right handed (clockwise).

2.7 RP-HPLC

RP-HPLC is a fast and reliable technique for quantitative analysis of both small and large compounds. In Paper II and Paper III RP-HPLC was used for quantification of insulin in release and transport experiments.

In RP-HPLC, the sample is injected into a column, and the time it takes the compound to travel through the column (the retention time) is analyzed. The column in RP-HPLC is packed with nonpolar, small, and uniformly sized particles ($\leq$ 10 μm), and interactions between nonpolar groups in the sample and the stationary phase will affect the retention time, and separate the compounds according to their physical-chemical properties.

The area under the curve (AUC) of a peak in a RP-HPLC chromatogram can be related to the amount of analyte in the sample, which allows for quantitative determinations.

2.8 Dynamic light scattering and zeta potential measurements

DLS was used in Paper IV to obtain information about the size distribution and homogeneity of the NCXs, both key elements in the development of particulate systems.

The experimental setup is illustrated in Figure 19 A. Briefly, DLS utilizes the scattering events that take place after a monochromatic beam of laser light has impinged on a sample, to calculate the size distribution of particles in a sample (Figure 19 B) [210].

In addition to the mean particle diameter the PDI can be investigated. The PDI is a measure of the homogeneity of the sample, and can thus also provide information about the stability of the particles.

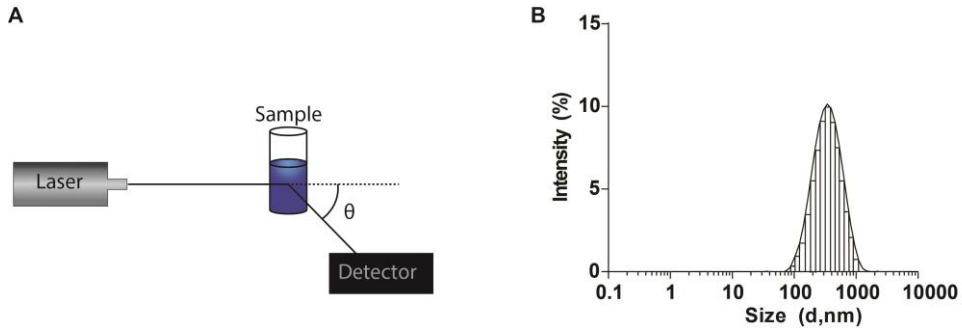

Figure 19. A) Schematic illustration of a DLS experiment. B) Example of a particle size distribution diagram.

The zeta potential is a physical measure of the charge of a compound. In solution, charged particles are surrounded by oppositely charged ions, the inner part being strongly attached to the particle, and the outer layer being more diffuse. The zeta potential is defined as the potential at the slipping plane, see Figure 20.

Zeta potential measurements had several applications in Paper IV. Firstly, the optimal pH for electrostatic self-assembly of positively charged FSP and negatively charged alginate was investigated using zeta potential measurements. The average pI of FSPs and pKa of alginate were determined as the pH at which the net charge of the solution was zero. The optimal pH for self-assembly was in between those pH values. Secondly, the zeta potential of the particles was used for evaluating the stability of the NCXs. Particles with a positive or negative net charge of 30 mV is considered a stable system, since repulsive forces between the particles will prevent the particles from aggregating [211]. When the net charge of the particles approaches 0 mV, the particles will have a greater ability to aggregate [211]. Lastly, the zeta potential measurements were used to speculate about the architecture of the NCXs. Since the charges of the two constituents in the NCXs were known (alginate was negatively charged and FSPs was positively

charged), the zeta potential could be used to hypothesize about the distribution of the two compounds inside the NCXs.

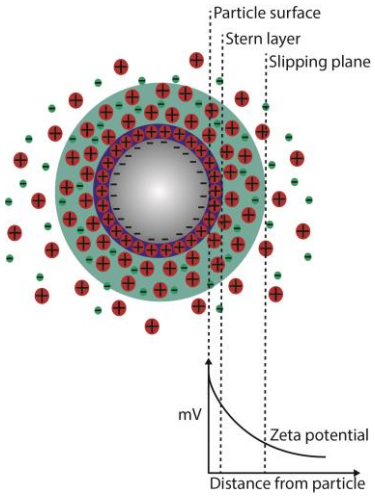

Figure 20. Illustration of a charged particle (grey) in solution, surrounded by a layer of strongly attached oppositely charged ions (dark blue), and an outer layer being more diffuse (light blue). The zeta potential is defined as the potential at the slipping plane.

2.9 Cell models

2.9.1 Caco-2 cell model – the oral route

The intestinal epithelium consists of a monolayer of cells, mainly absorptive enterocytes, but also goblet cells, M-cells, and endocrine cells are present [212]. The cells are polarized, which refers to the asymmetric orientation of different aspects of the cells, e.g. the surface of the cells. The apical side denotes the surface of the cells, and the basolateral side is opposite to the apical side (see Figure 21). Epithelial cells are connected through junctions on the lateral side of the cells: tight junctions, desmosomes, and adherent junctions. Tight junctions are multi protein complexes placed close to the apical side, and they ensure close contact between two cells, and serve as an absorption barrier for molecules. Drugs and nutraceuticals can be absorbed across the epithelia through the cells (transcellular pathway (Figure 21)) by passive diffusion or via receptor-mediated internalization pathways followed by transcytosis [213–215]. Alternatively, drugs and nutraceuticals can be absorbed between two cells (paracellular pathway (Figure 21)) by passive diffusion, however, paracellular transport may also involve signaling pathways, regulation of proteins, and alternations in cytoskeletal organization, which result in opening of the junctions and allows for permeation of the respective molecule [216,217].

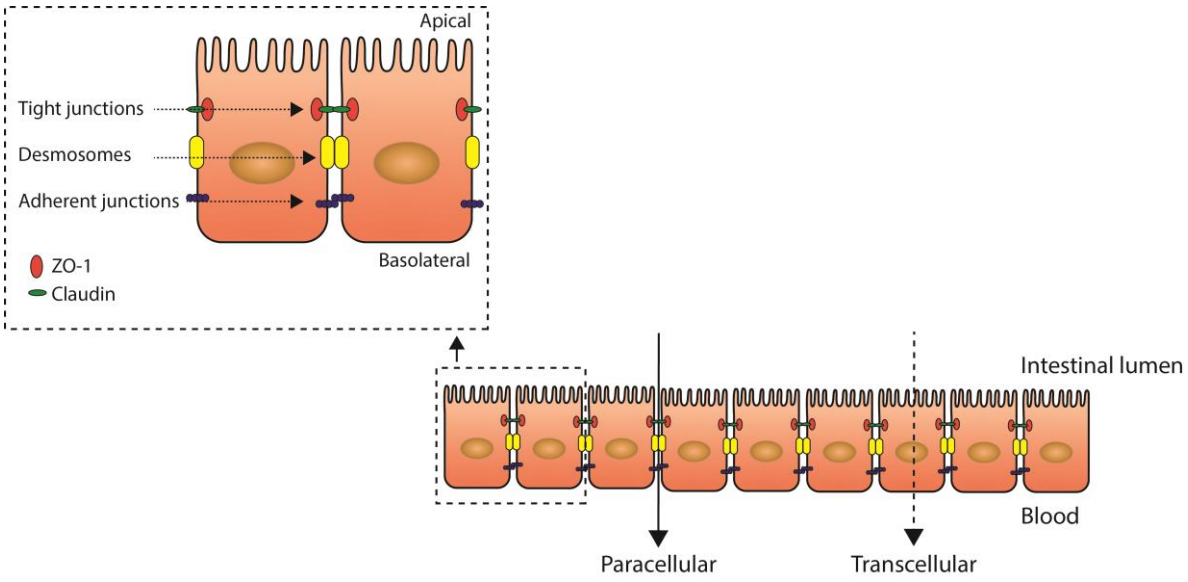

Figure 21. Illustration the intestinal epithelium and the paracellular and transcellular route of permeation. The tight junctions, desmosomes, and adherent junctions are highlighted, in addition to the ZO-1 and claudin proteins.

The Caco-2 cell model is frequently used to mimic the epithelial layer in the small intestine *in vitro*, to study intestinal permeability [218]. The Caco-2 cells originate from a colon cell line, but when cultured under specific conditions, the Caco-2 cells can polarize and express receptors that resemble the adsorptive enterocyte cells found in the small intestine [219]. Figure 22 shows an illustration of the setup employed for the cell-based experiments in Paper II, where transepithelial permeation of insulin was studied. From the accumulated amount of transported insulin, the apparent permeability coefficient (P_{app}) can be calculated and used as a measure for the permeability of the monolayer:

$$P_{app} = \frac{dQ}{dt} \cdot \frac{1}{AC_0}$$

Where dQ/dt is the linear rate of appearance of the compound on the basolateral side of the monolayer, A denotes the surface area of the monolayer (1.12 cm^2), and C_0 is the initial concentration on the apical side of the monolayer.

Changes in the integrity of the monolayer may originate from modulations of tight junctions or cell death. The integrity can be investigated by studying the transepithelial electrical resistance (TEER), which is a measure of the flux of ions across the monolayer. Variations in TEER during an experiment can thus provide information about the mechanism by which a molecule is

transported; a decreased TEER often indicates paracellular transport facilitated by opening of the tight junctions - provided that the cell viability is not compromised. In Paper II TEER investigations were employed to explore the mechanism behind the transepithelial permeation of insulin.

Tight junction protein complexes are composed of proteins such as claudins, which are associated with cytoplasmic proteins like ZO-1 [212] (see zoom in in Figure 21). In Paper II claudin-4 and ZO-1 were stained by using fluorophore-labelled antibodies (cf. section 2.2), to study the structural state of the tight junctions after incubation with FSP-Ins fibers.

The viability of the Caco-2 cells can be investigated by measuring the relative metabolism of treated cells, in relation to untreated cells. In Paper II, this was done by the MTS/PMS (3-(4,5-dimethylthiazol-2-yl)-5-(3-carboxymethoxyphenyl)-2-(4-sulfophenyl)-2H-tetrazolium/phenazine methosulfate) assay [220]. The MTS/PMS assay is a colorimetric assay, where the cell viability is assessed by monitoring a reduction of MTS, to a colored formazan product using absorbance spectroscopy. The reduction of MTS is only possible by viable cells, and the relative viability can therefore be quantified by comparison to a positive control.

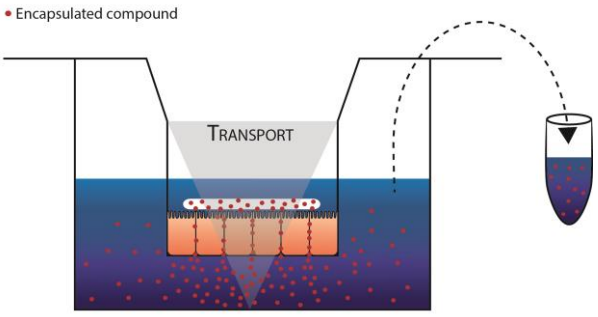

Figure 22. Illustration of a Transwell® setup with seeded Caco-2 cells. A sheet of fiber with an encapsulated compound was placed on top of the cells. The compound was released and permeated the monolayer. The accumulated amount of permeated compounds was determined by taking out samples from the basolateral side and analyzing them using RP-HPLC.

The Caco-2 cell model does not take the mucus layer into account. Mucus is a viscoelastic non-Newtonian gel that covers the epithelial layer and thus serves as a protection barrier for the cells [221,222]. The major components of mucus are water and mucins, but small amounts of proteins, lipids, DNA, and electrolytes are also present [223]. Mucins are large, glycosylated proteins produced by goblet cells found in the epithelial layer [224], and disulfide bonds and numerous of non-covalent bonds build up the highly entangled network of mucus [224]. Co-

culture cell models comprising Caco-2 cells and mucus-secreting cells have been developed to obtain an *in vitro* cell model that resembles the intestine more than the Caco-2 cell model [225–228]. Alternatively, Boegh *et al.* have developed a biosimilar mucus that resembles the properties of the native mucus without being toxic (native mucus exerts a cytotoxic effect on the cells and can therefore not be applied), thus allowing for investigations of the steric and interactive barriers of the mucus layer [223,229]. Investigation of the performance of the FSP-Ins fibers in mucus containing cell models was beyond the scope of this PhD project.

2.9.2 HeLa and U2OS cell lines

In Paper IV, the toxicity of the NCXs was studied in HeLa and U2OS cell lines. The cell viability after incubation with the NCXs, FSPs, or alginate was monitored using the MTS/PMS assay, as described above.

2.10 Contact angle measurements

In Paper III, interactions between surfactants and FSP-Ins fibers were investigated by using contact angle measurements. Absorption of a liquid by electrospun fibers is also referred to as wetting, and the contact angle can be used as a quantitative measure for this process [230]. The contact angle also provides information about the strength of the solid/liquid interactions; a small contact angle indicates strong interactions, exemplified by the contact angle between water and a hydrophilic surface. A change in the contact angle can thus be regarded as a change in interactions between the solid and the liquid. In Paper III, changes in contact angles were used as an indication of interactions between surfactants in a buffer and electrospun fibers. In specific, any difference between the contact angle for buffer A (with surfactants) and the contact angle for buffer B (without surfactants), when deposited on FSP-Ins fibers, was ascribed to interactions between surfactants and the fibers.

To determine the contact angle between the buffer and the FSP-Ins fibers, a static mode was used where a single drop of buffer was deposited on the fiber surface, and a high speed camera subsequently monitored the absorption of the liquid. The contact angle was deduced from the resulting images (Figure 23 A), and the Young/Laplace fitting procedure was used to determine the contact angles [231,232]. The average value between the left and the right contact angle was used.

Immediately after deposition of the drop on the fiber surface the drop was unstable. To account for this instability, the first linear part of the (time, contact angle)-graph is extrapolated, and the intersection with the y-axis was used as the measure for the contact angle (Figure 23 B).

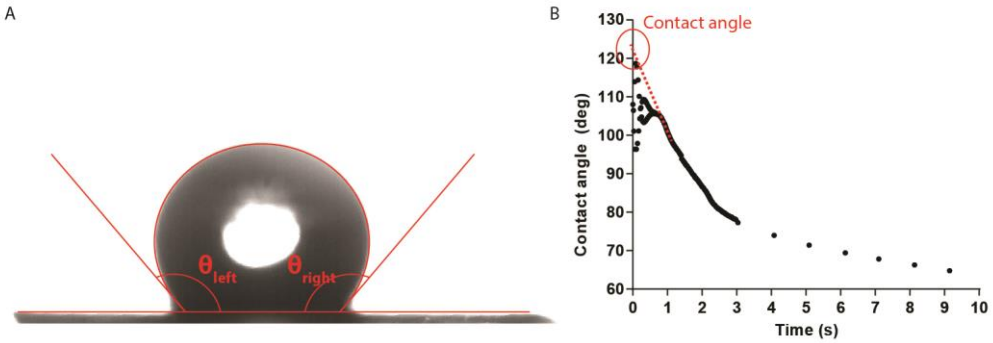

Figure 23. A) Example of an image recorded with the high speed camera in a contact angle experiment. The image shows a drop of buffer on the fiber surface, and the contact angle is highlighted with red. B) Contact angle plotted as a function of time. Due to instabilities in the drop immediately after deposition, the contact angle will fluctuate. In order to find the initial contact angle, the first linear part of the graph is therefore extrapolated, and the intersection with the y-axis is defined as the contact angle.

2.11 Critical micelle concentration determinations

Surfactants in solution will at a given surfactant concentration start to form micellar structures (Figure 24 B); this concentration is known as the CMC. In Paper III, the CMC of the surfactants was determined to investigate if there was any relation between the CMC and the observations made from fiber-surfactant interactions.

A colorimetric assay that utilizes the tautomerism of benzoylacetone (BZA) was used to study the CMC of the surfactants [233]. BZA exists in two tautomeric forms: the ketone and the enol form (Figure 24 A). The cis-enolic form is more stable in nonpolar environments, where intermolecular hydrogen bonds with the solvent are less pronounced. Formation of micelles will provide a less polar environment for BZA, and the enolic BZA will accordingly engage in the micellar network (Figure 24 B), and the concentration of enolic BZA will increase with increasing amounts of micelles. Enolic BZA absorbs light at 312 nm, which allows for quantification by monitoring the increase in absorbance using UV-VIS spectroscopy.

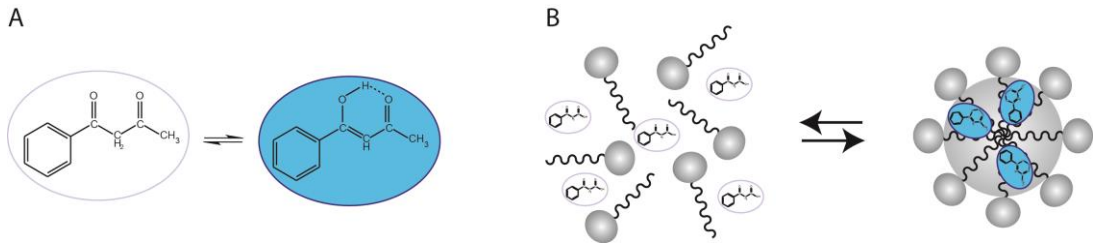

Figure 24. A) The two tautomeric forms of BZA; ketone (left) and enol (right). B) Illustration of formation of a micelle. The enolic form of BZA will engage in the micellar network and become detectable by using UV absorption spectroscopy.

2.12 DPP-IV assay

DPP-IV is a peptidase that selectively removes N-terminal dipeptides from oligopeptides, with a strong preference for proline > alanine > serine as the penultimate amino acid [234]. DPP-IV degrades glucose-dependent insulinotropic polypeptide (GIP) and glucagon-like peptide-1 (GLP-1) [235], enzymes that stimulate insulin-secretion [236]. Degradation of GIP and GLP-1 will therefore result in a decreased insulin secretion, for which reason DPP-IV inhibitors are interesting materials in diabetes treatments [190,237]. The ability if the FSP degradation products to inhibit DDP-IV was investigated in Paper I by using the DPP-IV assay. The DPP-IV assay is a colorimetric assay, where Gly-Pro-ρ-nitroanilide is cleaved into a chromophore by

DPP-IV (Figure 25), and the DPP-IV activity is quantified by monitoring the increase in absorbance over time [188,238]. The potency of an inhibitor can be deduced from a dose-response curve which is constructed by plotting the DPP-IV activity as a function of inhibitor concentrations.

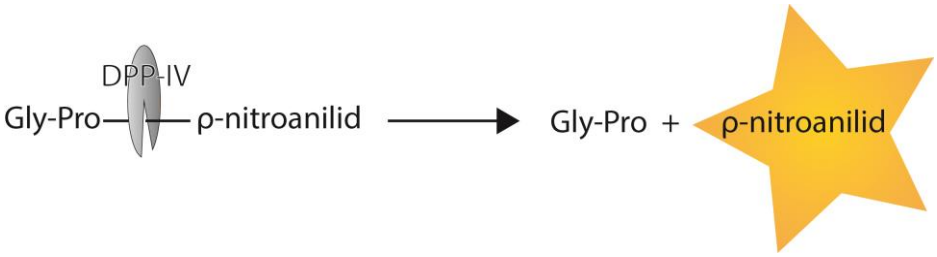

Figure 25. The principle behind the DPP-IV assay. When DPP-IV cleaves the bond between proline and ρ-nitroanilid, ρ-nitroanilid can absorb light and the concentration can thus be determined with absorption spectroscopy.

3 Results and discussion

This section has been divided into two parts; part A concerns electrospinning of FSP, and is composed of three subsections constituted by Paper I, Paper II, and Paper III. Part B concerns the self-assembly of FSP and alginate into NCXs, and is composed of one subsection constituted by Paper IV.

The results and discussions will thus be presented throughout the subsections, which each are composed of the abstract from the given paper (for the full papers see Appendix I-IV), a comments section that describes observations and challenges related to the project, and future work.

Part A and part B are each ended with concluding remarks about the feasibility of using the given preparation technique for preparation of FSP nano-micro structures.

3.1 Part A - electrospinning

3.1.1 Development of protein nanofibers

3.1.1.1 Paper I

Abstract from the paper:

Nano-microfibers were made from cod (Gadus morhua) sarcoplasmic proteins (FSPs) (Mw < 200 kDa) using the electrospinning technique. The FSP fibers were studied by scanning electron microscopy, and the fiber morphology was found to be strongly dependent on FSP concentration. Interestingly, the FSP fibers were insoluble in water. However, when exposed to proteolytic enzymes, the fibers were degraded. The degradation products of the FSP fibers proved to be inhibitors of the diabetes-related enzyme DPP-IV. The FSP fibers may have biomedical applications, among others as a delivery system. To demonstrate this, a dipeptide (Ala-Trp) was encapsulated into the FSP fibers, and the release properties were investigated in gastric buffer and in intestinal buffer. The release profile showed an initial burst release, where 30% of the compound was released within the first minute, after which an additional 40% was released (still exponential) within the next 30 min (gastric buffer) or 15 min (intestinal buffer). The remaining 30% was not released in the timespan of the experiment.

For the full paper “Bioactive electrospun fish sarcoplasmic proteins as a drug delivery system”, see Appendix I.

3.1.1.2 Comments to the study

Paper I concerns the development of electrospun FSP fibers. The proteins were extracted from centrifuged tissue fluid without further purification, and consequently compounds such as salts and nucleotides were also present in the final material. Despite the complexity of the FSP mixture, no variation in electrospinning, fiber morphology, or fiber properties were observed throughout the PhD study, where FSP from three different cods was used arbitrarily. Instead difficulties occurred due to ambient parameters; temperature and humidity, with humidity being the more influential factor (low humidity was preferred). It was unfortunately not possible to explore the influence of the ambient parameters with the setup available, nor was it possible to optimize the process accordingly.

One of the benefits of using FSP is the very few processing steps it takes to obtain the material. However, purification is possible, and this was briefly touched upon in preliminary studies, where the effect of LMW proteins, salts, etc., on electrospinning of FSP was investigated by dialyzing the centrifuged tissue fluid prior to freeze drying (D-FSPs). The dialysis removed compounds with MW up to 8 kDa. The viscosity of the D-FSPs was increased compared to the same concentration of FSP, and as expected the diameter of the resulting electrospun fibers was also increased (Figure 26). The morphology of the D-FSP fibers was more homogenous than the FSP fibers with negligible amounts of bead-like structures. The increased viscosity of the D-FSP solution may result from i) removal of charged LMW compounds that have an effect on the molecular interactions in the solution, or ii) by removing the LMW compounds the concentration of high MW proteins was increased, and this led to an increased degree of chain entanglements and thus an increased viscosity. Purification or selection of specific protein fractions of the FSPs were not explored further in this thesis.

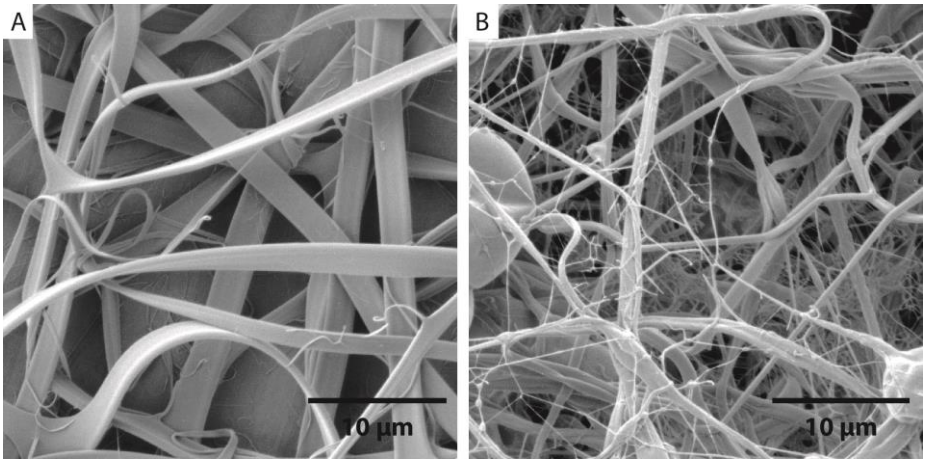

Figure 26. SEM images of A) dialyzed-FSP-Ins fibers ([FSP] = 100 mg/ml and [insulin] = 20 mg/ml), and B) regular FSP-Ins fibers ([FSP] = 125 mg/ml and [insulin] = 20 mg/ml) (Paper II).

3.1.1.3 Future work

Electrospinning of FSPs has shown promising results. Further exploring the electrospinnability of different protein fractions with different MW ranges, and investigating the morphology and properties of the fibers, will provide a detailed knowledge about electrospinning of fish proteins. It will also elucidate which proteins that enable electrospinning, and which proteins that has an effect on the morphology of the fibers. Special emphasis on proteins that are found in the wastewater from the fish industry will make the FSP fibers further appealing for industrial applications.

In this PhD project hexafluoro-2-propanol (HFIP) was used to facilitate electrospinning of FSP. HFIP is a well-known solvent for electrospinning, since its ionic strength can facilitate electrospinning of troublesome materials. Drawbacks of HFIP are the cost and organic origin, which encourage the search for alternative GRAS solvents. Exploring the electrospinnability of the FSPs as described in the above paragraph will also enable solvent optimization, which should focus on GRAS solvents.

3.1.2 FSP-Ins fibers as an intestinal drug delivery system

3.1.2.1 Paper II

Abstract from the paper:

In the present study the potential of using bioactive electrospun fish proteins (FSPs) as a carrier matrix for small therapeutic proteins was demonstrated especially focusing on the challenges with oral delivery. The inherent structural and chemical properties of FSPs as a biopolymer facilitated interactions with cells and enzymes found in the gastrointestinal tract and displayed excellent biocompatibility. More specifically, insulin was efficiently encapsulated into FSP fibers maintaining its conformation, and subsequent controlled release was obtained in simulated intestinal fluid. The encapsulation of insulin into FSP fibers provided protection against chymotrypsin degradation, and resulted in an increase in insulin transport to around 12% without compromising the cellular viability. This increased transport was driven by interactions upon contact between the nanofibers and the Caco-2 cell monolayer leading to the opening of the tight junction proteins. Overall, electrospun FSPs may constitute a novel material for oral delivery of biopharmaceuticals.

For the full paper "Bioactive protein-based nanofibers promote transepithelial permeation of intact therapeutic protein by interactions with biological components", see Appendix II.

3.1.2.2 Comments to the study

In Paper II the potential of using FSP fibers for oral delivery of biopharmaceuticals was explored. The nature of FSP as consumed food together with the benefits of oral delivery provided the rationale for studying this route of administration. *Biopharmaceuticals* is a hot topic, and much attention has been drawn towards the development of new approaches for delivery of these biological macromolecules. The central role of insulin in diabetes has motivated extensive studies of this compound, and as a result, *in vitro* methods for accurate and effective evaluation and quantification of insulin have been optimized, which makes insulin an ideal model compound. *In vivo*, insulin is easily monitored via blood glucose, and the bioavailability can be assessed quantitatively by determination of insulin concentrations in the blood. For those reasons insulin was chosen as model drug in Paper II.

In Paper II the potential of using FSP-Ins fibers for delivery on insulin via the intestine was explored by using *in vitro* methods. The performance of the fibers *in vivo* was studied in rats (unpublished data), however these studies entailed challenges. For the fibers to have an effect *in vivo* they must reach the intestine in a controllable manner, and for that reason the fibers were added to a capsule which subsequently was coated with eudragit. However the capsules were too large to exit the stomach of the rat, and accordingly the capsules were degraded in the stomach, and the fate of the FSP-Ins fibers were unknown. In Paper I it was found that the FSP fibers were degraded in pepsin, but dependent on the degradation time, the fibers may be able to reach the intestine and tricker a response. Such studies were, however, out of scope for this thesis.

3.1.2.3 Future work

Insulin permeation was promoted by interactions between the FSP-Ins fibers and the Caco-2 cells. Since mucus covers the intestinal epithelium, it would be interesting to explore the effect of mucus on the interactions beteen FSP-Ins and the Caco-2 cells, by using an *in vitro* model that takes the mucus into account. It will also be valuable to perform additional *in vivo* studies with an animal model applicable for intestinal evaluation such as a rat where the stomach is bypassed. Alternatively the FSP-Ins fibers must be further characterized and developed, or formulated, to ensure that the fibers reach the small intestine.

The benefits of mucoadhesiveness have previously been described, and due to the nature of FSP as a complex protein mixture, it could be interesting to explore the mucoadhesive properties of the FSP fibers. The fiber properties may be optimized by addition of mucoadhesive compounds, or by addition of compounds that alter the protein network inside the fibers and thus creates new properties. In continuation, hybrid delivery systems could be developed, where mucus penetrating particles are combined with mucoadhesive fibers. Furthermore compounds such as permeation enhancers and mucolytics may be added to further increase drug absorption.

3.1.3 Interactions between surfactants and FSP fibers

3.1.3.1 Paper III

Abstract from the paper:

Interactions between compounds found in the human body such as proteins, bile salts, etc. and electrospun compounds has hitherto been an unstudied phenomena, despite the exposure of fibers to such biorelevant compounds in many biomedical applications such as tissue engineering, wound healing and drug delivery. In this study we present a systematic investigation of how surfactants and proteins, as physiological relevant components, interact with insulin loaded fish sarcoplasmic protein (FSP) electrospun fibers (FSP-Ins fibers) and thereby affect fiber properties such as hydrophilicity, stability and release characteristics of an encapsulated drug. Interactions between insulin-loaded protein fibers and five anionic surfactants (the bile salts sodium taurocholate, sodium taurodeoxycholate, sodium glycocholate and sodium glycodeoxycholate, and sodium dodecyl sulfate), a cationic surfactant (benzalkonium chloride) and a neutral surfactant (Triton X-100) were studied. The anionic surfactants increased the insulin release in a concentration-dependent manner, whereas the neutral surfactant did not have a significant effect on the release. Interestingly, almost no insulin was released from the fibers when benzalkonium chloride was present. The FSP-Ins fibers were dense after incubation with this cationic surfactant, whereas high fiber porosity was observed after incubation with anionic or neutral surfactants. Contact angle measurements and staining with the hydrophobic dye 8-anilino-1-naphthalenesulfonic acid indicated that the FSP-Ins fibers where hydrophobic, and showed that the fiber surface properties were affected differently by the surfactants. Bovine serum albumin also affected insulin release in vitro, indicating that also proteins can affect the fiber performance.

For the full paper “Interactions between surfactants in solution and electrospun protein fibers - Effects on release behavior and fiber properties”, see Appendix III.

3.1.3.2 Comments to the study

The release studies presented in Paper II revealed that biorelevant compounds can affect fiber properties which thereby motivated the study presented in Paper III. Physiologically relevant compounds are rarely taken into account when investigating fiber properties, but as demonstrated in Paper III, the presence of such compounds can have a huge influence on the

behavior of the fibers. The surfactants included in Paper III were chosen because of physiological relevance (taurocholate (TC), taurodeoxycholate (TDC), glycocholate (GC), glycodeoxycholate (GDC), and BSA) or to cover a broad spectrum of surfactants; anionic (SDS), cationic (benzalkonium chloride (BC)), and neutral (Triton X-100). This range of different surfactants enabled a thorough investigation of interactions between fibers and surfactants.

A theoretical investigation of the release mechanism behind release of a drug from electrospun fibers is not trivial. Srikar *et al.* developed a model that described the release of water-soluble compounds from nondegradable fibers [129]. This model was used by Khansari *et al*. to describe the release of rhodamine B and riboflavin from soy-protein-containing hydrophilic and hydrophobic fibers. Khansari *et al.* furthermore studied the effect of porogens on the release profile, however since the proteins and porogens were soluble materials, the fibers were no longer completely nondegradable, which caused Srikar's model to deviate from the experimental data [128]. In Paper III, the variations in insulin release from the fibers, and the variations in inner porosity of the fibers, were both dependent on which surfactant that was present in the buffer. This indicated that i) the FSP-Ins fibers were partly degradable, as evident from the porosity, ii) the degradability was affected by the presence of surfactants, and iii) the release of insulin was strongly affected by the presence of surfactants. Accordingly, in order to perform a theoretical analysis of the mechanism behind insulin release from FSP-Ins fibers in the absence and presence of surfactants, a mathematical model that takes the above mentioned observations into account must be developed. Development of such a model was beyond the scope of this PhD project.

Release of rhodamine B from rhodamine B loaded FSP fibers was studied in a similar manner as insulin (0 mM, 3 mM and 6 mM surfactant concentrations) to investigate if the effects of the surfactants were similar on other drug delivery systems (unpublished data). Encapsulation of rhodamine B into FSP fibers was briefly touched upon in Paper I, where the encapsulation and distribution was analyzed. Rhodamine B release from the fibers in MES-HBSS in the presence and absence of surfactants are shown in Figure 27. From these data it was evident that the release of rhodamine B was different from the release of insulin; release of rhodamine B in MES-HBSS reached 70 % within 3 h, compared to approximately 50 % for insulin. Release of rhodamine B was increased in 6 mM TC, whereas no significant change was observed in 3 mM

TC. The trend of rhodamine B release in the presence of SDS was similar to that of TC, except that the effect in 6 mM SDS was more pronounced compared 6 mM TC. BC had no effect on rhodamine B release, compared to almost no release of insulin when BC was added to the release media. The presence of Triton X-100 only caused minor effects on rhodmine B release, which was similar to the effects observed for insulin release.

The release data presented in Figure 27 clearly indicated that the rhodamine B release was affected by the surfactants, however differently compared to their effects on the insulin release. Variations in the way the surfactants affected the drug delivery systems may be due to different release behaviors of insulin and rhodamine B, or due to the fiber properties being modified by encapsulation of the respective compound. The high maximum release for rhodamine B in MES-HBSS made it difficult to make similar concentration-dependency analysis for rhodamine B, as for insulin, where maximum release was lower and thus, where the span between maximum release and 100% release was larger. For that reason, the study presented in Paper III was limited to insulin.

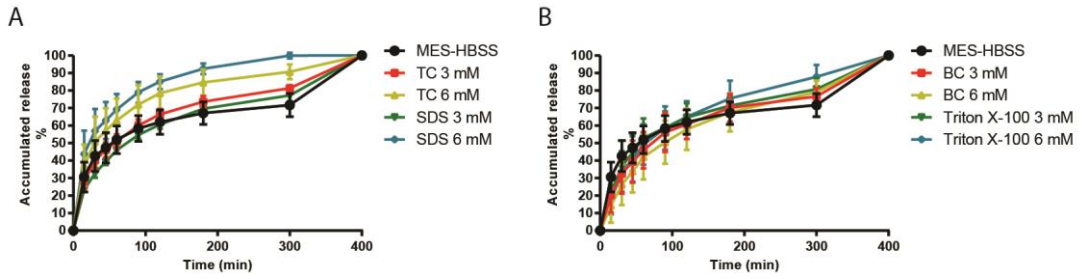

Figure 27. *In vitro* rhodamine B release from FSP fibers in MES-HBSS with varying concentrations of surfactants. A) MES-HBSS (black), 3 mM TC (red), 6 mM TC (yellow), 3 mM SDS (green) and 6 mM SDS (blue). B) MES-HBSS (black), 3 mM BC (red), 6 mM BC (yellow), 3 mM Triton (green) and 6 mM Triton X-100 (blue). Data represent mean ± SD, $n \geq 3$. After 300 min trypsin was added to the solution which allowed for quantification. Unpublished data.

3.1.3.3 Future work

The study in Paper III included seven surfactants, and BSA was briefly touched upon. In order to further explore the mechanism behind surfactant-fiber interactions, for instance by a structure-activity analysis, more surfactants should be included in the study. Moreover, the effect of other physiological compounds such as protein, mucin, DNA etc. should also be explored. In continuation, inclusion of other electrospun fibers and other cargo will also be highly relevant.

The investigations presented in Paper III were all indirect and qualitative indications of the interactions that take place between surfactants and FSP-Ins fibers in solution. Direct and quantitative measurements of the surfactant-fiber interaction would also contribute to elucidate and understand the mechanisms behind the interactions.

3.1.4 Conclusion and outlook

The studies presented in Paper I, Paper II, and Paper III showed that the FSPs were highly suitable for the production of electrospun fibers:

Electrospinning of FSPs were found to be stable, since no variation in electrospinning or fiber properties were observed throughout the three studies (Paper I, Paper II, and Paper III), where FSPs from three different cods were used arbitrarily.

The morphology of the FSP fibers was diverse, as evident from the fiber diameter ranging from nanometer to micrometer scale, dependent on both FSP concentration and FSP composition (Paper I). The adjustable morphology of the fibers allows for optimization of the fibers according to the application.

LMW compounds were released from the FSP fibers upon contact with aquatic media, however the FSP fibers remained insoluble (Paper I), except at high SDS concentrations (Paper II and Paper III). Most fibers made from biopolymers are water soluble and need crosslinking in order to become insoluble. The inherent stability of the FSP fibers makes them appealing cf. section 1.2.

The FSP fibers were degraded into small peptides by proteolytic enzymes (Paper I). The residual degradation products were shown to inhibit the diabetes related DPP-IV (Paper I), which can be considered an added advantage when selecting appropriate carrier matrices, depending on the target.

The carrier potential of the FSP fibers was explored by encapsulating Ala-Trp (Paper I), rhodamine B (Paper I and Paper III), or insulin (Paper II and Paper III) into the fibers. The compounds were uniformly distributed throughout the fibers (Paper I and Paper II). Encapsulation of insulin did not have a significant effect on fiber morphology, and high loading capacities with high loading efficiency was successfully obtained (Paper II). High loading

capacity and high loading efficiency are both key properties for drug delivery systems in order to increase the amount of drug available for absorption into the bloodstream.

Encapsulation of insulin into the FSP fibers caused insulin to be detectable in α-chymotrypsin-containing buffer for up to 8 h as compared to 1 h when insulin was not embedded in the fibers (Paper II). The protective effects of the FSP fibers are beneficial for oral drug delivery of biopharmaceuticals, where enzymatic degradation of the drug is a major challenge.

The release of insulin from FSP-Ins fibers was increased in the presence of anionic surfactants. The neutral surfactant did not have an effect on the release, and the cationic surfactant limited the release to negligible amounts (Paper III). Cryo-SEM images of the FSP-Ins fibers after incubation with the surfactants showed a correlation between release of cargo and increased porosity; when insulin was released, porosity was observed (Paper III).

Contact angle measurements revealed that the surfactants had a significant influence on wetting of the fibers; for anionic surfactants large contact angles were observed, whereas the presence of the cationic surfactant and especially the neutral surfactant decreased the contact angle considerably (Paper III).

Interactions between fibers and surfactants were further illustrated with ANS fluorescence, where a decrease in the fluorescence was observed after incubation with neutral or cationic surfactants compared to incubation with anionic or no surfactants (Paper III).

The FSP fibers interacted with intestinal Caco-2 cells and caused an effect on the tight junctions, demonstrated by a decrease in integrity, which promoted increased transepithelial permeation of insulin without compromising cellular viability (Paper II). The interactions between electrospun fibers and the epithelial cells may be used to promote increased uptake of biopharmaceuticals in general.

3.2 Part B - Nanocomplexes

3.2.1 Nano-microstructures as nanocomplexes made from electrostatic self-assembly

3.2.1.1 Paper IV

Abstract from the paper:

Macrostructures based on natural polymers are subject to large attention, as the application range is wide within the food and pharmaceutical industries. In this study we present nanocomplexes (NCXs) made from electrostatic self-assembly between negatively charged alginate and positively charged fish sarcoplasmic proteins (FSPs), prepared by bulk mixing. A concentration screening revealed that there was a range of alginate and FSP concentrations where stable NCXs with similar properties were formed, rather than two exact concentrations. The size of the NCXs was 293 ± 3 nm, and the zeta potential was −42 ± 0.3 mV. The NCXs were stable in water, gastric buffer, intestinal buffer and HEPES buffered glycose, and at all pH values from 2 to 9 except pH 3, where they aggregated. When proteolytic enzymes were present in the buffer, the NCXs were degraded. Only at high concentrations the NCXs caused a decreased viability in HeLa and U2OS cell lines. The simple processing procedure and the high stability of the NCXs, makes them excellent candidates for use in the food and pharmaceutical industry

For the full paper "Design and characterization of self-assembled fish sarcoplasmic protein-alginate nanocomplexes", see Appendix IV.

3.2.1.2 Comments to the study

In Paper IV NCXs made from self-assembly of FSP and alginate were described. Throughout the NCX studies, FSP originating from three cods was used arbitrarily, and despite the very complex protein mixture, the properties of NCXs did not exhibit large variations.

3.2.1.3 Future work

NCXs composed of alginate and FSP have potential as drug carriers, and accordingly the next step will be to encapsulate an active ingredient and study the ability of the NCXs to act as a drug carrier. The FSP fibers protected insulin against proteolytic degradation, and the NCXs could have similar properties. Alginate has been shown to be mucoadhesive, for which reason the mucoadhesive properties of the NCXs should be explored, in order to obtain full benefit from the NCXs. Moreover, alginate has been shown to affect tight junction permeability. Modulations of the tight junctions can facilitate increased bioavailability of a drug; hence the ability of the NCXs to increase transepithelial permeation must be studied, and potentially utilized to transport active ingredients across the epithelial layer.

From a particle development point of view, it would be interesting to explore selected FSP fractions as counter material to alginate. This may increase the homogeneity of the NCXs and also provide further details about the NCXs such as the structural network.

3.2.2 Conclusion and outlook

The NCXs developed from electrostatic self-assembly of alginate and FSP were easily formed by bulk mixing of the two constituents. Combining different concentrations of alginate and FSPs revealed optimal processing conditions, however it also showed that formation of NCXs is flexible in terms of processing concentrations since small changes in alginate or FSP concentrations did not alter NCX properties.

The NCXs were stable in water, in biorelevant media, and at different pH values, except at pH 3 where the NCXs aggregated. The zeta potential of the NCXs at the processing conditions was -42 ± 0.3 mV, which indicated that the shell of the NCXs was dominated by alginate. Changes in the zeta potential of the NCXs as a function of pH revealed that the electrostatic interactions holding the particles together varied with pH.

As separate compounds alginate and FSPs did not reduce cell viability, and only at high concentrations of NCXs was the cell viability in HeLa and U2OS cell lines affected.

4 Conclusion

The potential of using FSP as a new biopolymer for development of nano-micro structures using either electrospinning or electrostatic self-assembly was evaluated in Paper I, Paper II, Paper III, and Paper IV. Overall the four studies showed that FSP is highly applicable as a biopolymer, since the FSPs accommodate many of the properties that are sought for in such components. These properties were shown to also be present in the fabricated nano-micro structures:

One of the benefits of the majority of biopolymers is their inherent biocompatibility. The biocompatibility of FSP was illustrated by cell based studies, where no decrease in viability was observed in Caco-2 cells, HeLa cells, or U2OS cells, except at high NCX concentrations, where minor toxicity was introduced in HeLa and U2OS cells.

Another advantage of using biopolymers is their natural ability to interact with biological systems. The FSP fibers interacted with enzymes and were degraded, and they interacted with Caco-2 cells and promoted increased transepithelial permeation of insulin. Moreover, the fibers interacted with biorelevant compounds, which affected the physical properties of the fibers. Interactions between the FSPs and alginate led to stable NCXs, and interactions between the FSPs in the electrospun fiber matrix caused the FSP fibers to be stable in aquatic media, despite the water soluble nature of the FSPs.

Nano-micro structures are often developed from pure materials. One of the benefits of using a complex mixture of proteins was the diverse morphology observed for the FSP fibers. However, the fiber morphology could also be made more homogenous by using selected protein fractions, as evident from the morphology of the electrospun D-FSPs.

The findings in this PhD study illustrate that FSP shows great potential as a novel biopolymer. The inherent compatible nature of the FSPs and their versatility in applications emphasize the prospects of this natural material. Excitingly, many applications and possibilities are yet to be explored.

5 References

[1] J. Zeleny, The electrical discharge from liquid points, and a hydrostatic method of measuring the electric intensity at their surfaces, Phys. Rev. 3 (1914) 69–91. doi:10.1103/PhysRev.3.69.

[2] A. Formhals, U.S. Patent Number: 1975504, 1934.

[3] G. Taylor, Electrically Driven Jets, Proc. R. Soc. A Math. Phys. Eng. Sci. 313 (1969) 453–475. doi:10.1098/rspa.1969.0205.

[4] N. Bhardwaj, S.C. Kundu, Electrospinning: A fascinating fiber fabrication technique, Biotechnol. Adv. 28 (2010) 325–347. doi:10.1016/j.biotechadv.2010.01.004.

[5] S. Viju, Applications of polymeric nanofibers, Man-Made Text. India. 49 (2006) 253–256. doi:10.1007/978-3-642-27148-9.

[6] A. Frenot, I.S. Chronakis, Polymer nanofibers assembled by electrospinning, Curr. Opin. Colloid Interface Sci. 8 (2003) 64–75. doi:10.1016/S1359-0294(03)00004-9.

[7] C.L. Casper, J.S. Stephens, N.G. Tassi, D.B. Chase, J.F. Rabolt, Controlling surface morphology of electrospun polystyrene fibers: Effect of humidity and molecular weight in the electrospinning process, Macromolecules. 37 (2004) 573–578. doi:10.1021/ma0351975.

[8] G.-T. Kim, Y.-J. Hwang, Y.-C. Ahn, H.-S. Shin, J.-K. Lee, C.-M. Sung, The morphology of electrospun polystyrene fibers, Korean J. Chem. Eng. 22 (2005) 147–153. doi:10.1007/BF02701477.

[9] W.-E. Teo, R. Inai, S. Ramakrishna, Technological advances in electrospinning of nanofibers, Sci. Technol. Adv. Mater. 12 (2011) 013002. doi:10.1088/1468-6996/12/1/013002.

[10] G. Viswanathan, S. Murugesan, V. Pushparaj, O. Nalamasu, P.M. Ajayan, R.J. Linhardt, Preparation of biopolymer fibers by electrospinning from room temperature ionic liquids, Biomacromolecules. 7 (2006) 415–418. doi:10.1021/bm050837s.

[11] S. Zhu, H. Yu, Y. Chen, M. Zhu, Study on the morphologies and formational mechanism of Poly(hydroxybutyrate-co-hydroxyvalerate) ultrafine fibers by dry-jet-wet-electrospinning, J. Nanomater. 2012 (2012). doi:10.1155/2012/525419.

[12] A. Arinstein, E. Zussman, Electrospun polymer nanofibers: Mechanical and thermodynamic perspectives, J. Polym. Sci. Part B Polym. Phys. 49 (2011) 691–707. doi:10.1002/polb.22247.

[13] Z.M. Huang, Y.Z. Zhang, M. Kotaki, S. Ramakrishna, A review on polymer nanofibers by electrospinning and their applications in nanocomposites, Compos. Sci. Technol. 63 (2003) 2223–2253. doi:10.1016/S0266-3538(03)00178-7.

[14] V. Leung, F. Ko, Biomedical applications of nanofibers, Polym. Adv. Technol. 22 (2011) 350–365. doi:10.1002/pat.1813.

[15] D.B. Khadka, D.T. Haynie, Protein- and peptide-based electrospun nanofibers in medical biomaterials, Nanomedicine Nanotechnology, Biol. Med. 8 (2012) 1242–1262. doi:10.1016/j.nano.2012.02.013.

[16] Y. Dror, T. Ziv, V. Makarov, H. Wolf, A. Admon, E. Zussman, Nanofibers made of globular proteins, Biomacromolecules. 9 (2008) 2749–2754. doi:10.1021/bm8005243.

[17] D.L. Woerdeman, S. Shenoy, D. Breger, Role of Chain Entanglements in the Electrospinning of Wheat Protein-Poly(Vinyl Alcohol) Blends, J. Adhes. 83 (2007) 785–798. doi:10.1080/00218460701588398.

[18] P. Sajkiewicz, D. Kołbuk, Electrospinning of gelatin for tissue engineering – molecular conformation as one of the overlooked problems, J. Biomater. Sci. Polym. Ed. 25 (2014) 2009–2022. doi:10.1080/09205063.2014.975392.

[19] D. Cho, O. Nnadi, A. Netravali, Y.L. Joo, Electrospun hybrid soy protein/PVA fibers, Macromol. Mater. Eng. 295 (2010) 763–773. doi:10.1002/mame.201000161.

[20] Z.M. Huang, Y.Z. Zhang, S. Ramakrishna, C.T. Lim, Electrospinning and mechanical characterization of gelatin nanofibers, Polymer (Guildf). 45 (2004) 5361–5368. doi:10.1016/j.polymer.2004.04.005.

[21] C.P. Barnes, M.J. Smith, G.L. Bowlin, S.A. Sell, J.A. Matthews, D.G. Simpson, et al., Feasibility of Electrospinning the Globular Proteins Hemoglobin and Myoglobin, J. Eng. Fiber. Fabr. 1 (2006) 16–29.

[22] A.C. Vega-Lugo, L.T. Lim, Effects of poly(ethylene oxide) and pH on the electrospinning of whey protein isolate, J. Polym. Sci. Part B Polym. Phys. 50 (2012) 1188–1197. doi:10.1002/polb.23106.

[23] Y.Z. Zhang, J. Venugopal, Z.M. Huang, C.T. Lim, S. Ramakrishna, Crosslinking of the electrospun gelatin nanofibers, Polymer (Guildf). 47 (2006) 2911–2917. doi:10.1016/j.polymer.2006.02.046.

[24] J. Xie, Y. Lo Hsieh, Ultra-high surface fibrous membranes from electrospinning of natural proteins: Casein and lipase enzyme, in: J. Mater. Sci., Springer Netherlands, 2003: pp. 2125–2133. doi:10.1023/A:1023763727747.

[25] L. Xu, N. Sheybani, S. Ren, G.L. Bowlin, W.A. Yeudall, H. Yang, Semi-Interpenetrating Network (sIPN) Co-Electrospun Gelatin/Insulin Fiber Formulation for Transbuccal Insulin Delivery, Pharm. Res. 32 (2014) 275–285. doi:10.1007/s11095-014-1461-9.

[26] A.A. Dongargaonkar, G.L. Bowlin, H. Yang, Electrospun blends of gelatin and gelatin-dendrimer conjugates as a wound-dressing and drug-delivery platform, Biomacromolecules. 14 (2013) 4038–4045. doi:10.1021/bm401143p.

[27] S.R. Gomes, G. Rodrigues, G.G. Martins, M.A. Roberto, M. Mafra, C.M.R. Henriques, et al., In vitro and in vivo evaluation of electrospun nanofibers of PCL, chitosan and gelatin: A comparative study, Mater. Sci. Eng. C. 46 (2015) 348–358. doi:10.1016/j.msec.2014.10.051.

[28] A. Jayakrishnan, S.R. Jameela, Glutaraldehyde as a fixative in bioprostheses and drug delivery matrices, Biomaterials. 17 (1996) 471–484. doi:10.1016/0142-9612(96)82721-9.

[29] I. Erdogan, M. Demir, O. Bayraktar, Olive leaf extract as a crosslinking agent for the preparation of electrospun zein fibers, J. Appl. Polym. Sci. 132 (2015) 41338. doi:10.1002/app.41338.

[30] B.H. Noszczyk, T. Kowalczyk, M. Łyżniak, K. Zembrzycki, G. Mikułowski, J. Wysocki, et al., Biocompatibility of electrospun human albumin: a pilot study, Biofabrication. 7 (2015) 015011. doi:10.1088/1758-5090/7/1/015011.

[31] R.A. Neal, S.G. McClugage, M.C. Link, L.S. Sefcik, R.C. Ogle, E.A. Botchwey, Laminin nanofiber meshes that mimic morphological properties and bioactivity of basement membranes, Tissue Eng. Part C. Methods. 15 (2009) 11–21. doi:10.1089/ten.tec.2007.0366.

[32] H.R. Pant, C.S. Kim, Electrospun gelatin/nylon-6 composite nanofibers for biomedical applications, Polym. Int. 62 (2013) 1008–1013. doi:10.1002/pi.4380.

[33] J. Hu, J. Wei, W. Liu, Y. Chen, Preparation and characterization of electrospun PLGA/gelatin nanofibers as a drug delivery system by emulsion electrospinning, J. Biomater. Sci. Polym. Ed. 24 (2012) 1–14. doi:10.1080/09205063.2012.728193.

[34] G. Iucci, F. Ghezzo, R. Danesin, M. Modesti, M. Dettin, Biomimetic peptide-enriched electrospun polymers: A photoelectron and infrared spectroscopy study, in: J. Appl. Polym. Sci., 2011: pp. 3574–3582. doi:10.1002/app.34768.

[35] P. Kuppan, S. Sethuraman, U.M. Krishnan, PCL and PCL-gelatin nanofibers as esophageal tissue scaffolds: Optimization, characterization and cell-matrix interactions, J. Biomed. Nanotechnol. 9 (2013) 1540–1555. doi:10.1166/jbn.2013.1653.

[36] M. Li, M.J. Mondrinos, M.R. Gandhi, F.K. Ko, A.S. Weiss, P.I. Lelkes, Electrospun protein fibers as matrices for tissue engineering, Biomaterials. 26 (2005) 5999–6008. doi:10.1016/j.biomaterials.2005.03.030.

[37] D.C. Aduba, J.A. Hammer, Q. Yuan, A.W. Yeudall, G.L. Bowlin, H. Yang, Semi-interpenetrating network (sIPN) gelatin nanofiber scaffolds for oral mucosal drug delivery, Acta Biomater. 9 (2013) 6576–6584. doi:10.1016/j.actbio.2013.02.006.

[38] M. Li, Y. Guo, Y. Wei, A.G. MacDiarmid, P.I. Lelkes, Electrospinning polyaniline-contained gelatin nanofibers for tissue engineering applications, Biomaterials. 27 (2006) 2705–2715. doi:10.1016/j.biomaterials.2005.11.037.

[39] Y. Wang, C. Zhang, Q. Zhang, P. Li, Composite electrospun nanomembranes of fish scale collagen peptides/chito-oligosaccharides: antibacterial properties and potential for wound dressing., Int. J. Nanomedicine. 6 (2011) 667–676. doi:10.2147/IJN.S17547.

[40] J.A. Matthews, G.E. Wnek, D.G. Simpson, G.L. Bowlin, Electrospinning of collagen nanofibers, Biomacromolecules. 3 (2002) 232–238. doi:10.1021/bm015533u.

[41] D.B. Khadka, M.I. Niesen, J. Devkota, P. Koria, D.T. Haynie, Unique electrospun fiber properties obtained by blending elastin-like peptides and highly-ionized peptides, Polymer (Guildf). 55 (2014) 2163–2169. doi:10.1016/j.polymer.2014.03.012.

[42] T. Elakkiya, G. Malarvizhi, S. Rajiv, T.S. Natarajan, Curcumin loaded electrospun Bombyx mori silk nanofibers for drug delivery, Polym. Int. 63 (2014) 100–105. doi:10.1002/pi.4499.

[43] F. Zhang, B. Zuo, Z. Fan, Z. Xie, Q. Lu, X. Zhang, et al., Mechanisms and control of silk-based electrospinning, Biomacromolecules. 13 (2012) 798–804. doi:10.1021/bm201719s.

[44] J. Chutipakdeevong, U.R. Ruktanonchai, P. Supaphol, Process optimization of electrospun silk fibroin fiber mat for accelerated wound healing, J. Appl. Polym. Sci. 130 (2013) 3634–3644. doi:10.1002/app.39611.

[45] S. Shahverdi, M. Hajimiri, M.A. Esfandiari, B. Larijani, F. Atyabi, A. Rajabiani, et al., Fabrication and structure analysis of poly(lactide-co-glycolic acid)/silk fibroin hybrid scaffold for wound dressing applications, Int. J. Pharm. 473 (2014) 345–355. doi:10.1016/j.ijpharm.2014.07.021.

[46] R. Machado, A. da Costa, V. Sencadas, C. Garcia-Arévalo, C.M. Costa, J. Padrão, et al., Electrospun silk-elastin-like fibre mats for tissue engineering applications, Biomed. Mater. 8 (2013) 065009. doi:10.1088/1748-6041/8/6/065009.

[47] T.M. Dinis, G. Vidal, R.R. Jose, P. Vigneron, D. Bresson, V. Fitzpatrick, et al., Complementary Effects of Two Growth Factors in Multifunctionalized Silk Nanofibers for Nerve Reconstruction, PLoS One. 9 (2014) e109770. doi:10.1371/journal.pone.0109770.

[48] T.M. Dinis, R. Elia, G. Vidal, A. Auffret, D.L. Kaplan, C. Egles, Method to Form a Fiber/Growth Factor Dual-Gradient along Electrospun Silk for Nerve Regeneration., ACS Appl. Mater. Interfaces. 6 (2014) 16817–16826. doi:10.1021/am504159j.

[49] W. Zhong, M.M.Q. Xing, H.I. Maibach, Nanofibrous materials for wound care, Cutan. Ocul. Toxicol. 29 (2010) 143–152. doi:10.3109/15569527.2010.489307.

[50] F. Song, D.L. Tang, X.L. Wang, Y.Z. Wang, Biodegradable soy protein isolate-based materials: A review, Biomacromolecules. 12 (2011) 3369–3380. doi:10.1021/bm200904x.

[51] M. Thirugnanaselvam, N. Gobi, S. Arun Karthick, SPI/PEO blended electrospun martrix for wound healing, Fibers Polym. 14 (2013) 965–969. doi:10.1007/s12221-013-0965-y.

[52] X. Xu, L. Jiang, Z. Zhou, X. Wu, Y. Wang, Preparation and properties of electrospun soy protein isolate/polyethylene oxide nanofiber membranes, ACS Appl. Mater. Interfaces. 4 (2012) 4331–4337. doi:10.1021/am300991e.

[53] D. Cho, A.N. Netravali, Y.L. Joo, Mechanical properties and biodegradability of electrospun soy protein Isolate/PVA hybrid nanofibers, Polym. Degrad. Stab. 97 (2012) 747–754. doi:10.1016/j.polymdegradstab.2012.02.007.

[54] Q. Jiang, Y. Yang, Water-Stable Electrospun Zein Fibers for Potential Drug Delivery, J. Biomater. Sci. Polym. Ed. 22 (2011) 1393–1408. doi:10.1163/092050610X508437.

[55] D. Brahatheeswaran, A. Mathew, R.G. Aswathy, Y. Nagaoka, K. Venugopal, Y. Yoshida, et al., Hybrid fluorescent curcumin loaded zein electrospun nanofibrous scaffold for biomedical applications, Biomed. Mater. 7 (2012) 045001. doi:10.1088/1748-6041/7/4/045001.

[56] Y. Wang, L. Chen, Electrospinning of prolamin proteins in acetic acid: The effects of protein conformation and aggregation in solution, Macromol. Mater. Eng. 297 (2012) 902–913. doi:10.1002/mame.201100410.

[57] Y. Wang, L. Chen, Fabrication and characterization of novel assembled prolamin protein nanofabrics with improved stability, mechanical property and release profiles, J. Mater. Chem. 22 (2012) 21592–21601. doi:10.1039/c2jm34611g.

[58] K. Moomand, L.-T. Lim, Properties of Encapsulated Fish Oil in Electrospun Zein Fibres Under Simulated In Vitro Conditions, Food Bioprocess Technol. (2014) 431–444. doi:10.1007/s11947-014-1414-7.

[59] K. Moomand, L.T. Lim, Oxidative stability of encapsulated fish oil in electrospun zein fibres, Food Res. Int. 62 (2014) 523–532. doi:10.1016/j.foodres.2014.03.054.

[60] M. Aceituno-Medina, S. Mendoza, B.A. Rodríguez, J.M. Lagaron, A. López-Rubio, Improved antioxidant capacity of quercetin and ferulic acid during in-vitro digestion through encapsulation within food-grade electrospun fibers, J. Funct. Foods. 12 (2015) 332–341. doi:10.1016/j.jff.2014.11.028.

[61] A.J. Meinel, O. Germershaus, T. Luhmann, H.P. Merkle, L. Meinel, Electrospun matrices for localized drug delivery: Current technologies and selected biomedical applications, Eur. J. Pharm. Biopharm. 81 (2012) 1–13. doi:10.1016/j.ejpb.2012.01.016.

[62] X. Hu, S. Liu, G. Zhou, Y. Huang, Z. Xie, X. Jing, Electrospinning of polymeric nanofibers for drug delivery applications, J. Control. Release. 185 (2014) 12–21. doi:10.1016/j.jconrel.2014.04.018.

[63] C. Xie, X. Li, X. Luo, Y. Yang, W. Cui, J. Zou, et al., Release modulation and cytotoxicity of hydroxycamptothecin-loaded electrospun fibers with 2-hydroxypropyl-β-cyclodextrin inoculations, Int. J. Pharm. 391 (2010) 55–64. doi:10.1016/j.ijpharm.2010.02.016.

[64] S. Shao, L. Li, G. Yang, J. Li, C. Luo, T. Gong, et al., Controlled green tea polyphenols release from electrospun PCL/MWCNTs composite nanofibers, Int. J. Pharm. 421 (2011) 310–320. doi:10.1016/j.ijpharm.2011.09.033.

[65] J.B. Wolinsky, Y.L. Colson, M.W. Grinstaff, Local drug delivery strategies for cancer treatment: Gels, nanoparticles, polymeric films, rods, and wafers, J. Control. Release. 159 (2012) 14–26. doi:10.1016/j.jconrel.2011.11.031.

[66] S. Liu, G. Zhou, D. Liu, Z. Xie, Y. Huang, X. Wang, et al., Inhibition of Orthotopic Secondary Hepatic Carcinoma in Mice by Doxorubicin-Loaded Electrospun Polylactide Nanofibers, J. Mater. Chem. B. 1 (2013) 101–109. doi:10.1039/c2tb00121g.

[67] X. Xu, X. Chen, Z. Wang, X. Jing, Ultrafine PEG-PLA fibers loaded with both paclitaxel and doxorubicin hydrochloride and their in vitro cytotoxicity, Eur. J. Pharm. Biopharm. 72 (2009) 18–25. doi:10.1016/j.ejpb.2008.10.015.

[68] N. Mayet, Y.E. Choonara, P. Kumar, L.K. Tomar, C. Tyagi, L.C. Du Toit, et al., A comprehensive review of advanced biopolymeric wound healing systems, J. Pharm. Sci. 103 (2014) 2211–2230. doi:10.1002/jps.24068.

[69] M. Abrigo, S.L. McArthur, P. Kingshott, Electrospun nanofibers as dressings for chronic wound care: Advances, challenges, and future prospects, Macromol. Biosci. 14 (2014) 772–792. doi:10.1002/mabi.201300561.

[70] K. Kataria, A. Gupta, G. Rath, R.B. Mathur, S.R. Dhakate, In vivo wound healing performance of drug loaded electrospun composite nanofibers transdermal patch, Int. J. Pharm. 469 (2014) 102–110. doi:10.1016/j.ijpharm.2014.04.047.

[71] R.A. Thakur, C.A. Florek, J. Kohn, B.B. Michniak, Electrospun nanofibrous polymeric scaffold with targeted drug release profiles for potential application as wound dressing, Int. J. Pharm. 364 (2008) 87–93. doi:10.1016/j.ijpharm.2008.07.033.

[72] T.H.B. Eriksen, E. Skovsen, P. Fojan, Release of Antimicrobial Peptides from Electrospun Nanofibres as a Drug Delivery System, J. Biomed. Nanotechnol. 9 (2013) 492–498. doi:10.1166/jbn.2013.1553.

[73] M.P. Prabhakaran, L. Ghasemi-Mobarakeh, S. Ramakrishna, Electrospun composite nanofibers for tissue regeneration, J. Nanosci. Nanotechnol. 11 (2011) 3039–3057. doi:10.1166/jnn.2011.3753.

[74] J.E. Trachtenberg, P.M. Mountziaris, F.K. Kasper, A.G. Mikos, Fiber-based composite tissue engineering scaffolds for drug delivery, Isr. J. Chem. 53 (2013) 646–654. doi:10.1002/ijch.201300051.

[75] W. Cui, Y. Zhou, J. Chang, Electrospun nanofibrous materials for tissue engineering and drug delivery, Sci. Technol. Adv. Mater. 11 (2010) 014108. doi:10.1088/1468-6996/11/1/014108.

[76] Y.J. Son, W.J. Kim, H.S. Yoo, Therapeutic applications of electrospun nanofibers for drug delivery systems, Arch. Pharm. Res. 37 (2014) 69–78. doi:10.1007/s12272-013-0284-2.

[77] Y.-F. Goh, I. Shakir, R. Hussain, Electrospun fibers for tissue engineering, drug delivery, and wound dressing, J. Mater. Sci. 48 (2013) 3027–3054. doi:10.1007/s10853-013-7145-8.

[78] G. Jin, M.P. Prabhakaran, D. Kai, S. Ramakrishna, Controlled release of multiple epidermal induction factors through core-shell nanofibers for skin regeneration, Eur. J. Pharm. Biopharm. 85 (2013) 689–698. doi:10.1016/j.ejpb.2013.06.002.

[79] H. Seager, Drug-delivery products and the Zydis fast-dissolving dosage form, J. Pharm. Pharmacol. 50 (1998) 375–382.

[80] C.A. Squier, P.W. Wertz, Permeability and the pathophysiology of oral mucosa, Adv. Drug Deliv. Rev. 12 (1993) 13–24. doi:10.1016/0169-409X(93)90038-6.

[81] P. Vrbata, P. Berka, D. Stránská, P. Doležal, M. Musilová, L. Čižinská, Electrospun drug loaded membranes for sublingual administration of sumatriptan and naproxen, Int. J. Pharm. 457 (2013) 168–176. doi:10.1016/j.ijpharm.2013.08.085.

[82] J.K.W. Lam, Y. Xu, A. Worsley, I.C.K. Wong, Oral transmucosal drug delivery for pediatric use, Adv. Drug Deliv. Rev. 73 (2014) 50–62. doi:10.1016/j.addr.2013.08.011.

[83] U.E. Illangakoon, H. Gill, G.C. Shearman, M. Parhizkar, S. Mahalingam, N.P. Chatterton, et al., Fast dissolving paracetamol/caffeine nanofibers prepared by electrospinning, Int. J. Pharm. 477 (2014) 369–379. doi:10.1016/j.ijpharm.2014.10.036.

[84] X. Li, M.A. Kanjwal, L. Lin, I.S. Chronakis, Electrospun polyvinyl-alcohol nanofibers as oral fast-dissolving delivery system of caffeine and riboflavin, Colloids Surfaces B Biointerfaces. 103 (2013) 182–188. doi:10.1016/j.colsurfb.2012.10.016.

[85] S.R.D. A. Sharma, A. Gupta, G. Rath, A. Goyal, R. B. Mathur, Electrospun composite nanofiber-based transmucosal patch for anti-diabetic drug delivery, J. Mater. Chem. B. 1 (2013) 3410–3418. doi:10.1039/c3tb20487a.

[86] C. Dott, C. Tyagi, L.K. Tomar, Y.E. Choonara, P. Kumar, L.C. Du Toit, et al., A mucoadhesive electrospun nanofibrous matrix for rapid oramucosal drug delivery, J. Nanomater. 2013 (2013) 1–19. doi:10.1155/2013/924947.

[87] N. Salamat-Miller, M. Chittchang, T.P. Johnston, The use of mucoadhesive polymers in buccal drug delivery, Adv. Drug Deliv. Rev. 57 (2005) 1666–1691. doi:10.1016/j.addr.2005.07.003.

[88] W. Samprasit, R. Kaomongkolgit, M. Sukma, T. Rojanarata, T. Ngawhirunpat, P. Opanasopit, Mucoadhesive electrospun chitosan-based nanofibre mats for dental caries prevention, Carbohydr. Polym. 117 (2015) 933–940. doi:10.1016/j.carbpol.2014.10.026.

[89] S. Wongsasulak, S. Pathumban, T. Yoovidhya, Effect of entrapped α-tocopherol on mucoadhesivity and evaluation of the release, degradation, and swelling characteristics of zein-chitosan composite electrospun fibers, J. Food Eng. 120 (2014) 110–117. doi:10.1016/j.jfoodeng.2013.07.028.

[90] S. Wongsasulak, N. Puttipaiboon, T. Yoovidhya, Fabrication, Gastromucoadhesivity, Swelling, and Degradation of Zein-Chitosan Composite Ultrafine Fibers, J. Food Sci. 78 (2013) N926–35. doi:10.1111/1750-3841.12126.

[91] H. Kutchai, The Gastrointestinal System, in: P.S. Leung (Ed.), Physiology, Springer, 2004: pp. 539–565. doi:10.1007/978-94-017-8771-0.

[92] M. Narvekar, H.Y. Xue, J.Y. Eoh, H.L. Wong, Nanocarrier for Poorly Water-Soluble Anticancer Drugs-Barriers of Translation and Solutions, AAPS PharmSciTech. 15 (2014) 822–833. doi:10.1208/s12249-014-0107-x.

[93] B.P.K. Reddy, H.K.S. Yadav, D.K. Nagesha, A. Raizaday, A. Karim, Polymeric Micelles as Novel Carriers for Poorly Soluble Drugs— Review, J. Nanosci. Nanotechnol. 15 (2015) 4009–4018. doi:10.1166/jnn.2015.9713.

[94] K.R. Vandana, Y. Prasanna Raju, V. Harini Chowdary, M. Sushma, N. Vijay Kumar, An overview on in situ micronization technique - An emerging novel concept in advanced drug delivery, Saudi Pharm. J. 22 (2013) 283–289. doi:10.1016/j.jsps.2013.05.004.

[95] F. Ignatious, L. Sun, C.-P. Lee, J. Baldoni, Electrospun nanofibers in oral drug delivery, Pharm. Res. 27 (2010) 576–588. doi:10.1007/s11095-010-0061-6.

[96] G. Verreck, I. Chun, J. Peeters, J. Rosenblatt, M.E. Brewster, Preparation and characterization of nanofibers containing amorphous drug dispersions generated by electrostatic spinning, Pharm. Res. 20 (2003) 810–817. doi:10.1023/A:1023450006281.

[97] X.Y. Li, Y.C. Li, D.G. Yu, Y.Z. Liao, X. Wang, Fast disintegrating quercetin-loaded drug delivery systems fabricated using coaxial electrospinning, Int. J. Mol. Sci. 14 (2013) 21647–21659. doi:10.3390/ijms141121647.

[98] P. Vrbata, P. Berka, D. Stránská, P. Doležal, M. Lázníček, Electrospinning of diosmin from aqueous solutions for improved dissolution and oral absorption, Int. J. Pharm. 473 (2014) 407–413. doi:10.1016/j.ijpharm.2014.07.017.

[99] S. Alborzi, L.-T. Lim, Y. Kakuda, Release of folic acid from sodium alginate-pectin-poly(ethylene oxide) electrospun fibers under in vitro conditions, LWT - Food Sci. Technol. 59 (2014) 383–388. doi:10.1016/j.lwt.2014.06.008.

[100] R. Wulff, C.S. Leopold, Coatings from blends of Eudragit® RL and L55: A novel approach in pH-controlled drug release, Int. J. Pharm. 476 (2014) 78–87. doi:10.1016/j.ijpharm.2014.09.023.

[101] D.-G. Yu, Y. Xu, Z. Li, L.-P. Du, B.-G. Zhao, X. Wang, Coaxial Electrospinning with Mixed Solvents: From Flat to Round Eudragit L100 Nanofibers for Better Colon-Targeted Sustained Drug Release Profiles, J. Nanomater. 2014 (2014) 1–8. doi:10.1155/2014/967295.

[102] G. Weiss, A. Knoch, A. Laicher, F. Stanislaus, R. Daniels, Simple coacervation of hydroxypropyl methylcellulose phthalate (HPMCP). II. Microencapsulation of ibuprofen, Int. J. Pharm. 124 (1995) 97–105. doi:10.1016/0378-5173(95)00085-W.

[103] L. Wang, M. Wang, P.D. Topham, Y. Huang, Fabrication of magnetic drug-loaded polymeric composite nanofibres and their drug release characteristics, RSC Adv. 2 (2012) 2433. doi:10.1039/c2ra00484d.

[104] M. Wang, L. Wang, Y. Huang, Electrospun hydroxypropyl methyl cellulose phthalate (HPMCP)/erythromycin fibers for targeted release in intestine, J. Appl. Polym. Sci. 106 (2007) 2177–2184. doi:10.1002/app.25666.

[105] U.E. Illangakoon, T. Nazir, G.R. Williams, N.P. Chatterton, Mebeverine-loaded electrospun nanofibers: Physicochemical characterization and dissolution studies, J. Pharm. Sci. 103 (2014) 283–292. doi:10.1002/jps.23759.

[106] K. Karthikeyan, S. Guhathakarta, R. Rajaram, P.S. Korrapati, Electrospun zein/eudragit nanofibers based dual drug delivery system for the simultaneous delivery of aceclofenac and pantoprazole, Int. J. Pharm. 438 (2012) 117–122. doi:10.1016/j.ijpharm.2012.07.075.

[107] X. Shen, D. Yu, L. Zhu, C. Branford-White, K. White, N.P. Chatterton, Electrospun diclofenac sodium loaded Eudragit® L 100-55 nanofibers for colon-targeted drug delivery, Int. J. Pharm. 408 (2011) 200–207. doi:10.1016/j.ijpharm.2011.01.058.

[108] Q. Xu, N. Zhang, W. Qin, J. Liu, Z. Jia, H. Liu, Preparation, In Vitro and In Vivo Evaluation of Budesonide Loaded Core/Shell Nanofibers as Oral Colonic Drug Delivery System, J. Nanosci. Nanotechnol. 13 (2013) 149–156. doi:10.1166/jnn.2013.6920.

[109] R.A. Rader, (Re)defining biopharmaceutical, Nat. Biotechnol. 26 (2008) 743–51. doi:10.1038/nbt0708-743.

[110] Y. Aoki, M. Morishita, K. Takayama, Role of the mucous/glycocalyx layers in insulin permeation across the rat ileal membrane, Int. J. Pharm. 297 (2005) 98–109. doi:10.1016/j.ijpharm.2005.03.004.

[111] J.A. Fix, Oral controlled release technology for peptides: status and future prospects, Pharm. Res. 13 (1996) 1760–1764. doi:10.1023/A:1016008419367.

[112] B.F. Choonara, Y.E. Choonara, P. Kumar, D. Bijukumar, L.C. du Toit, V. Pillay, A review of advanced oral drug delivery technologies facilitating the protection and absorption of protein and peptide molecules, Biotechnol. Adv. 32 (2014) 1269–1282. doi:10.1016/j.biotechadv.2014.07.006.

[113] A.L. Smart, S. Gaisford, A.W. Basit, Oral peptide and protein delivery: intestinal obstacles and commercial prospects, Expert Opin. Drug Deliv. 11 (2014) 1323–35. doi:10.1517/17425247.2014.917077.

[114] Y. Zhang, W. Wei, P. Lv, L. Wang, G. Ma, Preparation and evaluation of alginate-chitosan microspheres for oral delivery of insulin, Eur. J. Pharm. Biopharm. 77 (2011) 11–9. doi:10.1016/j.ejpb.2010.09.016.

[115] N. Zhang, J. Li, W. Jiang, C. Ren, J. Li, J. Xin, et al., Effective protection and controlled release of insulin by cationic β-cyclodextrin polymers from alginate/chitosan nanoparticles, Int. J. Pharm. 393 (2010) 213–219. doi:10.1016/j.ijpharm.2010.04.006.

[116] A.H. Krauland, M.J. Alonso, Chitosan/cyclodextrin nanoparticles as macromolecular drug delivery system, Int. J. Pharm. 340 (2007) 134–142. doi:10.1016/j.ijpharm.2007.03.005.

[117] B. Sarmento, A. Ribeiro, F. Veiga, D. Ferreira, R. Neufeld, Oral bioavailability of insulin contained in polysaccharide nanoparticles, Biomacromolecules. 8 (2007) 3054–3060. doi:10.1021/bm0703923.

[118] Z. Ma, T.M. Lim, L.Y. Lim, Pharmacological activity of peroral chitosan-insulin nanoparticles in diabetic rats, Int. J. Pharm. 293 (2005) 271–280. doi:10.1016/j.ijpharm.2004.12.025.

[119] M.C. Chen, K. Sonaje, K.J. Chen, H.W. Sung, A review of the prospects for polymeric nanoparticle platforms in oral insulin delivery, Biomaterials. 32 (2011) 9826–9838. doi:10.1016/j.biomaterials.2011.08.087.

[120] A. Schoubben, P. Blasi, S. Giovagnoli, L. Perioli, C. Rossi, M. Ricci, Novel composite microparticles for protein stabilization and delivery, Eur. J. Pharm. Sci. 36 (2009) 226–234. doi:10.1016/j.ejps.2008.09.008.

[121] K. Park, I.C. Kwon, K. Park, Oral protein delivery: Current status and future prospect, React. Funct. Polym. 71 (2011) 280–287. doi:10.1016/j.reactfunctpolym.2010.10.002.

[122] J. Chin, K.A. Foyez Mahmud, S.E. Kim, K. Park, Y. Byun, Insight of current technologies for oral delivery of proteins and peptides, Drug Discov. Today Technol. 9 (2012) e105–e112. doi:10.1016/j.ddtec.2012.04.005.

[123] S.R. Hwang, Y. Byun, Advances in oral macromolecular drug delivery, Expert Opin. Drug Deliv. (2014) 1–13. doi:10.1517/17425247.2014.945420.

[124] L.A. Sharpe, A.M. Daily, S.D. Horava, N.A. Peppas, Therapeutic applications of hydrogels in oral drug delivery., Expert Opin. Drug Deliv. 11 (2014) 901–915. doi:10.1517/17425247.2014.902047.

[125] J.L. Zaro, Lipid-Based Drug Carriers for Prodrugs to Enhance Drug Delivery, AAPS J. 17 (2014) 83–92. doi:10.1208/s12248-014-9670-z.

[126] J.K. Vasir, K. Tambwekar, S. Garg, Bioadhesive microspheres as a controlled drug delivery system, Int. J. Pharm. 255 (2003) 13–32. doi:10.1016/S0378-5173(03)00087-5.

[127] D. Wheatherby, S. Ferguson, Blood Chemistry and CBC Analysis, Bear Mountain Publishing, 2004.

[128] S. Khansari, S. Duzyer, S. Sinha-Ray, A. Hockenberger, A.L. Yarin, B. Pourdeyhimi, Two-stage desorption-controlled release of fluorescent dye and vitamin from solution-blown and electrospun nanofiber mats containing porogens, Mol. Pharm. 10 (2013) 4509–4526. doi:10.1021/mp4003442.

[129] R. Srikar, A.L. Yarin, C.M. Megaridis, A. V Bazilevsky, E. Kelley, Desorption-limited mechanism of release from polymer nanofibers, Langmuir. 24 (2008) 965–974. doi:10.1021/la702449k.

[130] A.Y.A. Kaassis, N. Young, N. Sano, H.A. Merchant, D.-G. Yu, N.P. Chatterton, et al., Pulsatile drug release from electrospun poly(ethylene oxide)–sodium alginate blend nanofibres, J. Mater. Chem. B. 2 (2014) 1400. doi:10.1039/c3tb21605e.

[131] F. Han, H. Zhang, J. Zhao, Y. Zhao, X. Yuan, Diverse release behaviors of water-soluble bioactive substances from fibrous membranes prepared by emulsion and suspension electrospinning, J. Biomater. Sci. Polym. Ed. 24 (2013) 1244–59. doi:10.1080/09205063.2012.746510.

[132] C. Hu, S. Liu, Y. Zhang, B. Li, H. Yang, C. Fan, et al., Long-term drug release from electrospun fibers for in vivo inflammation prevention in the prevention of peritendinous adhesions, Acta Biomater. 9 (2013) 7381–7388. doi:10.1016/j.actbio.2013.03.040.

[133] Y. Wang, B. Wang, W. Qiao, T. Yin, A novel controlled release drug delivery system for multiple drugs based on electrospun nanofibers containing nanoparticles, J. Pharm. Sci. 99 (2010) 4805–4811. doi:10.1002/jps.22189.

[134] H. Jiang, Y. Hu, Y. Li, P. Zhao, K. Zhu, W. Chen, A facile technique to prepare biodegradable coaxial electrospun nanofibers for controlled release of bioactive agents, J. Control. Release. 108 (2005) 237–243. doi:10.1016/j.jconrel.2005.08.006.

[135] H. Jiang, D. Fang, B. Hsiao, B. Chu, W. Chen, Preparation and characterization of ibuprofen-loaded poly(lactide-co-glycolide)/poly(ethylene glycol)-g-chitosan electrospun membranes, J. Biomater. Sci. Polym. Ed. 15 (2004) 279–296. doi:10.1163/156856204322977184.

[136] M. Jannesari, J. Varshosaz, M. Morshed, M. Zamani, Composite poly(vinyl alcohol)/poly(vinyl acetate) electrospun nanofibrous mats as a novel wound dressing matrix for controlled release of drugs, Int. J. Nanomedicine. 6 (2011) 993–1003. doi:10.2147/IJN.S17595.

[137] L.K. MacRi, L. Sheihet, A.J. Singer, J. Kohn, R. a F. Clark, Ultrafast and fast bioerodible electrospun fiber mats for topical delivery of a hydrophilic peptide, J. Control. Release. 161 (2012) 813–820. doi:10.1016/j.jconrel.2012.04.035.

[138] J. Li, R. Fu, L. Li, G. Yang, S. Ding, Z. Zhong, et al., Co-delivery of Dexamethasone and Green Tea Polyphenols Using Electrospun Ultrafine Fibers for Effective Treatment of Keloid, Pharm. Res. 31 (2014) 1632–1643. doi:10.1007/s11095-013-1266-2.

[139] D. Steffens, M. Lersch, A. Rosa, C. Scher, T. Crestani, M.G. Morais, et al., A new biomaterial of nanofibers with the microalga spirulina as scaffolds to cultivate with stem cells for use in tissue engineering, J. Biomed. Nanotechnol. 9 (2013) 710–718. doi:10.1166/jbn.2013.1571.

[140] C. Kriegel, K.M. Kit, D.J. McClements, J. Weiss, Nanofibers as carrier systems for antimicrobial microemulsions. II. Release characteristics and antimicrobial activity, J. Appl. Polym. Sci. 118 (2010) 2859–2868. doi:10.1002/app.32563.

[141] P. Sofokleous, E. Stride, M. Edirisinghe, Preparation, characterization, and release of amoxicillin from electrospun fibrous wound dressing patches, Pharm. Res. 30 (2013) 1926–1938. doi:10.1007/s11095-013-1035-2.

[142] S. Maretschek, A. Greiner, T. Kissel, Electrospun biodegradable nanofiber nonwovens for controlled release of proteins, J. Control. Release. 127 (2008) 180–187. doi:10.1016/j.jconrel.2008.01.011.

[143] C. Alvarez-Lorenzo, B. Blanco-Fernandez, A.M. Puga, A. Concheiro, Crosslinked ionic polysaccharides for stimuli-sensitive drug delivery, Adv. Drug Deliv. Rev. 65 (2013) 1148–1171. doi:10.1016/j.addr.2013.04.016.

[144] R. Cheng, F. Meng, C. Deng, H.A. Klok, Z. Zhong, Dual and multi-stimuli responsive polymeric nanoparticles for programmed site-specific drug delivery, Biomaterials. 34 (2013) 3647–3657. doi:10.1016/j.biomaterials.2013.01.084.

[145] G.M. Whitesides, B. Grzybowski, Self-assembly at all scales, Science. 295 (2002) 2418–2421. doi:10.1126/science.1070821.

[146] S.L. Turgeon, C. Schmitt, C. Sanchez, Protein-polysaccharide complexes and coacervates, Curr. Opin. Colloid Interface Sci. 12 (2007) 166–178. doi:10.1016/j.cocis.2007.07.007.

[147] D. Hudson, A. Margaritis, Biopolymer nanoparticle production for controlled release of biopharmaceuticals, Crit. Rev. Biotechnol. 34 (2014) 161–79. doi:10.3109/07388551.2012.743503.

[148] I.J. Joye, D.J. McClements, Biopolymer-based nanoparticles and microparticles: Fabrication, characterization, and application, Curr. Opin. Colloid Interface Sci. 19 (2014) 417–427. doi:10.1016/j.cocis.2014.07.002.

[149] K. Kumar, N. Dhawan, H. Sharma, S. Vaidya, B. Vaidya, Bioadhesive polymers: Novel tool for drug delivery, Artif. Cells. Nanomed. Biotechnol. (2013) 1–10. doi:10.3109/21691401.2013.815194.

[150] B. Menchicchi, J.P. Fuenzalida, K.B. Bobbili, A. Hensel, M.J. Swamy, F.M. Goycoolea, Structure of Chitosan Determines Its Interactions with Mucin, Biomacromolecules. 15 (2014) 3550–3558. doi:10.1021/bm5007954.

[151] B. Menchicchi, J.P. Fuenzalida, A. Hensel, M.J. Swamy, L. David, C. Rochas, et al., Biophysical Analysis of the Molecular Interactions between Polysaccharides and Mucin, Biomacromolecules. (2015) 150218131922003. doi:10.1021/bm501832y.

[152] M. George, T.E. Abraham, Polyionic hydrocolloids for the intestinal delivery of protein drugs: Alginate and chitosan - a review, J. Control. Release. 114 (2006) 1–14. doi:10.1016/j.jconrel.2006.04.017.

[153] F.M. Goycoolea, G. Lollo, C. Remuñán-López, F. Quaglia, M.J. Alonso, Chitosan-alginate blended nanoparticles as carriers for the transmucosal delivery of macromolecules, Biomacromolecules. 10 (2009) 1736–1743. doi:10.1021/bm9001377.

[154] B. Sarmento, A. Ribeiro, F. Veiga, P. Sampaio, R. Neufeld, D. Ferreira, Alginate/chitosan nanoparticles are effective for oral insulin delivery, Pharm. Res. 24 (2007) 2198–2206. doi:10.1007/s11095-007-9367-4.

[155] D. Sağlam, P. Venema, E. van der Linden, R. de Vries, Design, properties, and applications of protein micro- and nanoparticles, Curr. Opin. Colloid Interface Sci. 19 (2014) 428–437. doi:10.1016/j.cocis.2014.09.004.

[156] C. Schmitt, S.L. Turgeon, Protein/polysaccharide complexes and coacervates in food systems, Adv. Colloid Interface Sci. 167 (2011) 63–70. doi:10.1016/j.cis.2010.10.001.

[157] J. Milanović, L. Petrović, V. Sovilj, J. Katona, Complex coacervation in gelatin/sodium caseinate mixtures, Food Hydrocoll. 37 (2014) 1–7. doi:10.1016/j.foodhyd.2013.10.016.

[158] Z. Zhang, R. Zhang, E.A. Decker, D.J. McClements, Development of food-grade filled hydrogels for oral delivery of lipophilic active ingredients: pH-triggered release, Food Hydrocoll. 44 (2015) 345–352. doi:10.1016/j.foodhyd.2014.10.002.

[159] Y.A. Antonov, P. Moldenaers, Structure formation and phase-separation behaviour of aqueous casein-alginate emulsions in the presence of strong polyelectrolyte, Food Hydrocoll. 25 (2011) 350–360. doi:10.1016/j.foodhyd.2010.06.013.

[160] Y. Zhao, F. Li, M.T. Carvajal, M.T. Harris, Interactions between bovine serum albumin and alginate: An evaluation of alginate as protein carrier, J. Colloid Interface Sci. 332 (2009) 345–353. doi:10.1016/j.jcis.2008.12.048.

[161] L. Chen, M. Subirade, Alginate-whey protein granular microspheres as oral delivery vehicles for bioactive compounds, Biomaterials. 27 (2006) 4646–4654. doi:10.1016/j.biomaterials.2006.04.037.

[162] T. Harnsilawat, R. Pongsawatmanit, D.J. McClements, Characterization of β-lactoglobulin-sodium alginate interactions in aqueous solutions: A calorimetry, light scattering, electrophoretic mobility and solubility study, Food Hydrocoll. 20 (2006) 577–585. doi:10.1016/j.foodhyd.2005.05.005.

[163] D.-Y. Kim, W.-S. Shin, Unique characteristics of self-assembly of bovine serum albumin and fucoidan, an anionic sulfated polysaccharide, under various aqueous environments, Food Hydrocoll. 44 (2015) 471–477. doi:10.1016/j.foodhyd.2014.10.011.

[164] I. Schmidt, F. Cousin, C. Huchon, F. Boué, M. a V Axelos, Spatial structure and composition of polysaccharide-protein complexes from small angle neutron scattering, Biomacromolecules. 10 (2009) 1346–1357. doi:10.1021/bm801147j.

[165] E. da S. Gulão, C.J.F. de Souza, F.A.S. da Silva, J.S.R. Coimbra, E.E. Garcia-Rojas, Complex coacervates obtained from lactoferrin and gum arabic: Formation and characterization, Food Res. Int. 65 (2014) 367–374. doi:10.1016/j.foodres.2014.08.024.

[166] G.Q. Huang, Y.T. Sun, J.X. Xiao, J. Yang, Complex coacervation of soybean protein isolate and chitosan, Food Chem. 135 (2012) 534–539. doi:10.1016/j.foodchem.2012.04.140.

[167] L. Chen, M. Subirade, Effect of preparation conditions on the nutrient release properties of alginate-whey protein granular microspheres, Eur. J. Pharm. Biopharm. 65 (2007) 354–362. doi:10.1016/j.ejpb.2006.10.012.

[168] S.A. Fioramonti, A.A. Perez, E.E. Aríngoli, A.C. Rubiolo, L.G. Santiago, Design and characterization of soluble biopolymer complexes produced by electrostatic self-assembly of a whey protein isolate andsodium alginate, Food Hydrocoll. 35 (2014) 129–136. doi:10.1016/j.foodhyd.2013.05.001.

[169] M. Bayarri, N. Oulahal, P. Degraeve, A. Gharsallaoui, Properties of lysozyme/low methoxyl (LM) pectin complexes for antimicrobial edible food packaging, J. Food Eng. 131 (2014) 18–25. doi:10.1016/j.jfoodeng.2014.01.013.

[170] I. Morfin, E. Buhler, F. Cousin, I. Grillo, F. Boué, Rodlike complexes of a polyelectrolyte (hyaluronan) and a protein (lysozyme) observed by SANS, Biomacromolecules. 12 (2011) 859–870. doi:10.1021/bm100861g.

[171] J.J. Water, M.M. Schack, A. Velazquez-Campoy, M.J. Maltesen, M. van de Weert, L. Jorgensen, Complex coacervates of hyaluronic acid and lysozyme: Effect on protein structure and physical stability, Eur. J. Pharm. Biopharm. 88 (2014) 325–331. doi:10.1016/j.ejpb.2014.09.001.

[172] S.M.H. Hosseini, Z. Emam-Djomeh, S.H. Razavi, A.A. Moosavi-Movahedi, A.A. Saboury, M.S. Atri, et al., β-Lactoglobulin-sodium alginate interaction as affected by polysaccharide depolymerization using high intensity ultrasound, Food Hydrocoll. 32 (2013) 235–244. doi:10.1016/j.foodhyd.2013.01.002.

[173] H. Yu, Q. Huang, Bioavailability and Delivery of Nutraceuticals and Functional Foods Using Nanotechnology, in: Bio-Nanotechnology A Revolut. Food, Biomed. Heal. Sci., 2013: pp. 593–604. doi:10.1002/9781118451915.ch35.

[174] L. Chen, G.E. Remondetto, M. Subirade, Food protein-based materials as nutraceutical delivery systems, Trends Food Sci. Technol. 17 (2006) 272–283. doi:10.1016/j.tifs.2005.12.011.

[175] X. Ding, P. Yao, Soy protein/soy polysaccharide complex nanogels: Folic acid loading, protection, and controlled delivery, Langmuir. 29 (2013) 8636–8644. doi:10.1021/la401664y.

[176] K.Y. Lee, D.J. Mooney, Alginate: Properties and biomedical applications, Prog. Polym. Sci. 37 (2012) 106–126. doi:10.1016/j.progpolymsci.2011.06.003.

[177] M. Rinaudo, Main properties and current applications of some polysaccharides as biomaterials, Polym. Int. 57 (2008) 397–430. doi:10.1002/pi.2378.

[178] D.A. Norris, N. Puri, P.J. Sinko, The effect of physical barriers and properties on the oral absorption of particulates, Adv. Drug Deliv. Rev. 34 (1998) 135–154. doi:10.1016/S0169-409X(98)00037-4.

[179] A. Sosnik, Alginate Particles as Platform for Drug Delivery by the Oral Route: State-of-the-Art, ISRN Pharm. 2014 (2014) 1–17. doi:10.1155/2014/926157.

[180] S.B. Patil, K.K. Sawant, Mucoadhesive microspheres: a promising tool in drug delivery, Curr. Drug Deliv. 5 (2008) 312–318. doi:10.2174/156720108785914970.

[181] H. Valizadeh, H. Fahimfar, S. Ghanbarzadeh, Z. Islambulchilar, P. Zakeri-Milani, Effect of anionic macromolecules on intestinal permeability of furosemide, Drug Dev. Ind. Pharm. 41 (2015) 190–193. doi:10.3109/03639045.2013.851210.

[182] E. Déat-Lainé, V. Hoffart, G. Garrait, E. Beyssac, Whey protein and alginate hydrogel microparticles for insulin intestinal absorption: Evaluation of permeability enhancement properties on Caco-2 cells, Int. J. Pharm. 453 (2013) 336–342. doi:10.1016/j.ijpharm.2013.06.016.

[183] A.T. Girgih, R. He, F.M. Hasan, C.C. Udenigwe, T.A. Gill, R.E. Aluko, Evaluation of the in vitro antioxidant properties of a cod (Gadus morhua) protein hydrolysate and peptide fractions, Food Chem. 173 (2015) 652–659. doi:10.1016/j.foodchem.2014.10.079.

[184] K.H. Sabeena Farvin, L.L. Andersen, H.H. Nielsen, C. Jacobsen, G. Jakobsen, I. Johansson, et al., Antioxidant activity of Cod (Gadus morhua) protein hydrolysates: In vitro assays and evaluation in 5% fish oil-in-water emulsion, Food Chem. 149 (2014) 326–334. doi:10.1016/j.foodchem.2013.03.075.

[185] S.W.A. Himaya, D.H. Ngo, B. Ryu, S.K. Kim, An active peptide purified from gastrointestinal enzyme hydrolysate of Pacific cod skin gelatin attenuates angiotensin-1 converting enzyme (ACE) activity and cellular oxidative stress, in: Food Chem., Elsevier Ltd, 2012: pp. 1872–1882. doi:10.1016/j.foodchem.2011.12.020.

[186] G. Pilon, J. Ruzzin, L.E. Rioux, C. Lavigne, P.J. White, L. Frøyland, et al., Differential effects of various fish proteins in altering body weight, adiposity, inflammatory status, and insulin sensitivity in high-fat-fed rats, Metabolism. 60 (2011) 1122–1130. doi:10.1016/j.metabol.2010.12.005.

[187] H.S. Ewart, D. Dennis, M. Potvin, C. Tiller, L. hua Fang, R. Zhang, et al., Development of a salmon protein hydrolysate that lowers blood pressure, Eur. Food Res. Technol. 229 (2009) 561–569. doi:10.1007/s00217-009-1083-3.

[188] E.C.Y. Li-Chan, S.L. Hunag, C.L. Jao, K.P. Ho, K.C. Hsu, Peptides derived from Atlantic salmon skin gelatin as dipeptidyl-peptidase IV inhibitors, J. Agric. Food Chem. 60 (2012) 973–978. doi:10.1021/jf204720q.

[189] K.B. Moore, C.D. Saudek, Therapeutic potential of dipeptidyl peptidase-IV inhibitors in patients with diabetes mellitus, Am. J. Ther. 15 (2008) 484–491. doi:10.1097/MJT.0b013e3180ed42dc.

[190] M. Lehrke, N. Marx, New antidiabetic therapies: innovative strategies for an old problem, Curr. Opin. Lipidol. 23 (2012) 569–575. doi:10.1097/MOL.0b013e328359b19f.

[191] V. Ouellet, S.J. Weisnagel, J. Marois, J. Bergeron, P. Julien, R. Gougeon, et al., Dietary cod protein reduces plasma C-reactive protein in insulin-resistant men and women, J. Nutr. 138 (2008) 2386–2391. doi:10.3945/jn.108.092346.

[192] V. Ouellet, J. Marois, S.J. Weisnagel, H. Jacques, Dietary cod protein improves insulin sensitivity in insulin-resistant men and women: A randomized controlled trial, Diabetes Care. 30 (2007) 2816–2821. doi:10.2337/dc07-0273.

[193] S. Kristoffersen, B. Vang, R. Larsen, R.L. Olsen, Pre-rigor filleting and drip loss from fillets of farmed Atlantic cod (Gadus morhua L.), Aquac. Res. 38 (2007) 1721–1731. doi:10.1111/j.1365-2109.2007.01843.x.

[194] V. Ferraro, I.B. Cruz, R. Ferreira Jorge, M.E. Pintado, P.M.L. Castro, Solvent extraction of sodium chloride from codfish (Gadus morhua) salting processing wastewater, Desalination. 281 (2011) 42–48. doi:10.1016/j.desal.2011.07.038.

[195] V. Ferraro, I.B. Cruz, R.F. Jorge, F. Xavier Malcata, P.M.L. Castro, M.E. Pintado, Characterisation of high added value compounds in wastewater throughout the salting process of codfish (Gadus morhua), Food Chem. 124 (2011) 1363–1368. doi:10.1016/j.foodchem.2010.07.090.

[196] V. Ferraro, I.B. Cruz, R.F. Jorge, F.X. Malcata, M.E. Pintado, P.M.L. Castro, Valorisation of natural extracts from marine source focused on marine by-products: A review, Food Res. Int. 43 (2010) 2221–2233. doi:10.1016/j.foodres.2010.07.034.

[197] V. Ferraro, R. Ferreira Jorge, I.B. Cruz, F. Antunes, B. Sarmento, P.M.L. Castro, et al., In vitro intestinal absorption of amino acid mixtures extracted from codfish (Gadus morhua L.) salting wastewater, Int. J. Food Sci. Technol. 49 (2014) 27–33. doi:10.1111/ijfs.12269.

[198] P.J. Goodhew, J. Humphreys, R. Beanland, Electron microscopy and analysis, Taylor & Francis Group, 2001.

[199] D. Chescoe, P.J. Goodhew, The Operation of Transmission and Scanning Electron Microscopes, Oxford University Press, 1990.

[200] R. Erni, M.D. Rossell, C. Kisielowski, U. Dahmen, Atomic-resolution imaging with a sub-50-pm electron probe, Phys. Rev. Lett. 102 (2009) 1–4. doi:10.1103/PhysRevLett.102.096101.

[201] R.L. Price, W.G. (Jay) Jerome, Basic confocal microscopy, Springer, 2011.

[202] C.J.R. Sheppard, D.M. Shotton, Confocal Laser Scanning Microscopy, Taylor & Francis Group, 1997.

[203] W.O. McClure, G.M. Edelman, Fluorescent probes for conformational states of proteins. I. Mechanism of fluorescence of 2-p-toluidinylnaphthalene-6-sulfonate, a hydrophobic probe., Biochemistry. 5 (1966) 1908–1919. doi:10.1021/bi00870a018.

[204] L. Stryer, The interaction of a naphthalene dye with apomyoglobin and apohemoglobin. A fluorescent probe of non-polar binding sites, J. Mol. Biol. 13 (1965) 482–495. doi:10.1016/S0022-2836(65)80111-5.

[205] A. Barth, The infrared absorption of amino acid side chains, Prog. Biophys. Mol. Biol. 74 (2000) 141–173. doi:10.1016/S0079-6107(00)00021-3.

[206] B.C. Smith, Fundamentals of Fourier Transform Infrared Sectroscopy, 2nd ed., Taylor & Francis Group, 2011.

[207] F.M. Mirabella, Internal Reflection Spectroscopy: Theory and Applications, Marcel Dekker, 1992.

[208] U.K. Laemmli, Cleavage of Structural Proteins during the Assembly of the Head of Bacteriophage T4, Nature. 227 (1970) 680–685. doi:10.1038/227680a0.

[209] W.B. Gratzer, D.A. Cowburn, Optical activity of biopolymers, Nature. 222 (1969) 426–431. doi:10.1038/222426a0.

[210] Malvern, Basic principles of particle size analysis. Technical report, 2013.

[211] M.M. Domingues, P.S. Santiago, M.A.R.B. Castanho, N.C. Santos, What can light scattering spectroscopy do for membrane-active peptide studies?, J. Pept. Sci. 14 (2008) 394–400. doi:10.1002/psc.1007.

[212] K. Qvortrup, F. Geneser, J. Tranum-Jensen, E.I. Brüel, Annemarie Christensen, Genesers Histologi, Munksgård Danmark, 2012.

[213] A.L. Daugherty, R.J. Mrsny, Transcellular uptake mechanisms of the intestinal epithelial barrier - Part one, Pharm. Sci. Technol. Today. 2 (1999) 144–151. doi:10.1016/S1461-5347(99)00142-X.

[214] P.S. Burton, R.A. Conradi, A.R. Hilgers, (B) Mechanisms of peptide and protein absorption. (2) Transcellular mechanism of peptide and protein absorption: Passive aspects, Adv. Drug Deliv. Rev. 7 (1991) 365–386. doi:10.1016/0169-409X(91)90014-4.

[215] P.W. Swaan, Recent advances in intestinal macromolecular drug delivery via receptor- mediated transport pathways, Pharm. Res. 15 (1998) 826–834. doi:10.1023/A:1011908128045.

[216] A.L. Daugherty, R.J. Mrsny, Regulation of the intestinal epithelial paracellular barrier, Pharm. Sci. Technol. Today. 2 (1999) 281–287. doi:10.1016/S1461-5347(99)00170-4.

[217] H.N. Nellans, (B) Mechanisms of peptide and protein absorption. (1) Paracellular intestinal transport: Modulation of absorption, Adv. Drug Deliv. Rev. 7 (1991) 339–364. doi:10.1016/0169-409X(91)90013-3.

[218] P. Artursson, K. Palm, K. Luthman, Caco-2 monolayers in experimental and theoretical predictions of drug transport, Adv. Drug Deliv. Rev. 46 (2001) 27–43. doi:10.1016/S0169-409X(00)00128-9.

[219] M. Pinto, S. Robine-Leon, M.-D. Appay, M. Kedinger, N. Triadou, E. Dussaulx, et al., Enterocyte-like differentiation and polarization of the human colon carcinoma cell line Caco-2 in culture, Biol. Cell. 47 (1983) 323–330.

[220] T.M. Buttke, J.A. McCubrey, T.C. Owen, Use of an aqueous soluble tetrazolium/formazan assay to measure viability and proliferation of lymphokine-dependent cell lines, J. Immunol. Methods. 157 (1993) 233–240. doi:10.1016/0022-1759(93)90092-L.

[221] R.A. Cone, Barrier properties of mucus, Adv. Drug Deliv. Rev. 61 (2009) 75–85. doi:10.1016/j.addr.2008.09.008.

[222] S.K. Lai, Y.Y. Wang, D. Wirtz, J. Hanes, Micro- and macrorheology of mucus, Adv. Drug Deliv. Rev. 61 (2009) 86–100. doi:10.1016/j.addr.2008.09.012.

[223] M. Boegh, S.G. Baldursdóttir, A. Müllertz, H.M. Nielsen, Property profiling of biosimilar mucus in a novel mucus-containing in vitro model for assessment of intestinal drug absorption, Eur. J. Pharm. Biopharm. 87 (2014) 227–235. doi:10.1016/j.ejpb.2014.01.001.

[224] D.J. Thornton, J.K. Sheehan, From mucins to mucus: toward a more coherent understanding of this essential barrier, Proc. Am. Thorac. Soc. 1 (2004) 54–61. doi:10.1513/pats.2306016.

[225] G.J. Mahler, M.L. Shuler, R.P. Glahn, Characterization of Caco-2 and HT29-MTX cocultures in an in vitro digestion/cell culture model used to predict iron bioavailability, J. Nutr. Biochem. 20 (2009) 494–502. doi:10.1016/j.jnutbio.2008.05.006.

[226] A. Wikman-Larhed, P. Artursson, Co-cultures of human intestinal goblet (HT29-H) and absorptive (Caco-2) cells for studies of drug and peptide absorption, Eur. J. Pharm. Sci. 3 (1995) 171–183. doi:10.1016/0928-0987(95)00007-Z.

[227] F. Antunes, F. Andrade, F. Araújo, D. Ferreira, B. Sarmento, Establishment of a triple co-culture in vitro cell models to study intestinal absorption of peptide drugs, Eur. J. Pharm. Biopharm. 83 (2013) 427–435. doi:10.1016/j.ejpb.2012.10.003.

[228] F. Araújo, B. Sarmento, Towards the characterization of an in vitro triple co-culture intestine cell model for permeability studies, Int. J. Pharm. 458 (2013) 128–134. doi:10.1016/j.ijpharm.2013.10.003.

[229] M. Boegh, M. García-Díaz, A. Müllertz, H.M. Nielsen, Steric and interactive barrier properties of intestinal mucus elucidated by particle diffusion and peptide permeation, Eur. J. Pharm. Biopharm. (2015). doi:10.1016/j.ejpb.2015.01.014.

[230] E.G. Shafrin, W.A. Zisman, Constitutive relations in the wetting of low energy surfaces and the theory of the retraction method of preparing monolayers, J. Phys. Chem. 64 (1960) 519–524. doi:10.1021/j100834a002.

[231] T. Chow, Wetting of rough surfaces, J. Phys. Condens. Matter. 10 (1998) 445–451. doi:10.1088/0953-8984/10/27/001.

[232] T. Young, An Essay on the Cohesion of Fluids, Philos. Trans. R. Soc. London. 95 (1805) 65–87. doi:10.1098/rstl.1805.0005.

[233] E. Iglesias, Enolization of Benzoylacetone in Aqueous Surfactant Solutions : A Novel Method for Determining Enolization Constants, 3654 (1996) 12592–12599.

[234] A.-M. Lambeir, C. Durinx, S. Scharpé, I. De Meester, Dipeptidyl-peptidase IV from bench to bedside: an update on structural properties, functions, and clinical aspects of the enzyme DPP IV, Crit. Rev. Clin. Lab. Sci. 40 (2003) 209–294. doi:10.1080/713609354.

[235] C.H.S. McIntosh, H.-U. Demuth, J.A. Pospisilik, R. Pederson, Dipeptidyl peptidase IV inhibitors: how do they work as new antidiabetic agents?, Regul. Pept. 128 (2005) 159–165. doi:10.1016/j.regpep.2004.06.001.

[236] W. Creutzfeldt, M. Nauck, Gut hormones and diabetes mellitus, Diabetes. Metab. Rev. 8 (1992) 149–177. doi:10.1016/S0168-8227(88)80281-X.

[237] K. Augustyns, P. Van der Veken, A. Haemers, Inhibitors of proline-specific dipeptidyl peptidases: DPP IV inhibitors as a novel approach for the treatment of Type 2 diabetes, Expert Opin. Ther. Pat. 15 (2005) 1387–1407. doi:10.1517/13543776.15.10.1387.

[238] K. Kojima, T. Hama, T. Kato, T. Nagatsu, Rapid chromatographic purification of dipeptidyl peptidase IV in human submaxillary gland, J. Chromatogr. 189 (1980) 233–240. doi:10.1016/S0021-9673(00)81523-X.

Appendices

Appendix I – Paper I

Paper I

Bioactive electrospun fish sarcoplasmic proteins as a drug delivery system

K. Stephansen, I.S. Chronakis, F Jessen

Colloids Surf. B. Biointerfaces. 122C (2014) 158–165

Colloids and Surfaces B: Biointerfaces 122 (2014) 158–165

Contents lists available at ScienceDirect

Colloids and Surfaces B: Biointerfaces

journal homepage: www.elsevier.com/locate/colsurfb

Bioactive electrospun fish sarcoplasmic proteins as a drug delivery system

Karen Stephansen*, Ioannis S. Chronakis, Flemming Jessen

National Food Institute, Technical University of Denmark, Søltofts Plads 227, 2800 Kongens Lyngby, Denmark

ARTICLE INFO

Article history:
Received 24 January 2014
Received in revised form 23 June 2014
Accepted 24 June 2014
Available online 1 July 2014

Keywords:
Electrospinning
Proteins
Drug delivery
Bioactive
Biodegradable
DPP-IV inhibitors

ABSTRACT

Nano-microfibers were made from cod (*Gadus morhua*) sarcoplasmic proteins (FSP) (M_w < 200 kDa) using the electrospinning technique. The FSP fibers were studied by scanning electron microscopy, and the fiber morphology was found to be strongly dependent on FSP concentration. Interestingly, the FSP fibers were insoluble in water. However, when exposed to proteolytic enzymes, the fibers were degraded. The degradation products of the FSP fibers proved to be inhibitors of the diabetes-related enzyme DPP-IV. The FSP fibers may have biomedical applications, among others as a delivery system. To demonstrate this, a dipeptide (Ala-Trp) was encapsulated into the FSP fibers, and the release properties were investigated in gastric buffer and in intestinal buffer. The release profile showed an initial burst release, where 30% of the compound was released within the first minute, after which an additional 40% was released (still exponential) within the next 30 min (gastric buffer) or 15 min (intestinal buffer). The remaining 30% was not released in the timespan of the experiment.

Introduction

Electrospinning processing is a straightforward technique suitable for the production of continuous and functional nano-microfibers from a wide range of (bio)polymers [1–3]. This electrostatic technique involves the use of a high-voltage electrostatic field to charge the surface of a polymer solution droplet, thereby inducing ejection of a liquid jet through a spinneret. On the way to the collector, the jet will be subjected to forces that allow it to stretch immensely. Simultaneously, the jet will solidify through solvent evaporation, and electrically charged nano-microfibers will remain, directed by electrical forces toward the collector.

Several proteins have been electrospun [4]. To name a few, the structural proteins collagen and gelatin were electrospun, among others, in an attempt to mimic the extra cellular matrix [5–7]. Dror et al. presented a study in which the globular protein bovine serum albumin was electrospun into nano-microfibers [8], and Barnes et al. have electrospun two other globular proteins, hemoglobin and myoglobin, aiming at the development of a biologic construct with the potential of being used as an oxygen delivery system [9]. In a study by Neal et al., laminin proteins were electrospun in order to mimic the basement membranes [10], and Woerderman et al. demonstrated that it was possible to electrospin a heterogeneous protein mixture, such as the commercial wheat gluten [11]. Moreover, electrospun silk proteins have been studied, especially for biomedical applications [12–15]. In many cases, however, proteins need a carrier system in order to be electrospun, and crosslinking to achieve, for instance, the desired mechanical properties, or to become insoluble. For example, crosslinking of hemoglobin and myoglobin fibers as well as collagen and gelatin have been studied [9,16,17]. Poly vinyl alcohol (PVA) has been used as a carrier system to achieve egg albumin spinnability [18], and poly(ethylene oxide) (PEO) facilitate electrospinning of whey proteins [19]. In a study by Jiang et al., poly (ε-caprolactone) (PCL) was co-axially electrospun together with zein proteins (PCL as the core material and zein as the shell), to increase the mechanical strength of the zein fibers [20].

Fish sarcoplasmic proteins account for 25–30% of the fish muscle proteins. They are easily accessible, and comprise peptides and proteins of up to ~200 kDa in molecular weight. Fish protein hydrolysates have been shown to comprise bioactive properties [21–23]. One example is inhibitory effects against dipeptidyl peptidase-4 (DPP-IV) [24], an enzyme with an essential role in glucose metabolism and linked to type 2 diabetes, and DPP-IV inhibitors may be used as a potential new treatment for type 2 diabetes [25,26]. Additionally, dietary cod proteins have been shown to improve insulin sensitivity in insulin-resistant subjects [27,28].

The usage of electrospun nano-microfibers for biomedical application has gained widespread interest [29–31], and more specific in the drug delivery fields of bio-functional scaffolds for

* Corresponding author. Tel.: +45 45 25 27 73.
E-mail addresses: kaste@food.dtu.dk, karenstephansen@gmail.com (K. Stephansen).

http://dx.doi.org/10.1016/j.colsurfb.2014.06.053
0927-7765/

regenerative medicine [32,33], wound dressing [34,35], as well as sublingual drug delivery systems [36]. Electrospun nano-microfibers can be used to enhance the solubility and release of poorly soluble drugs, due to the large aspect ratio of fibers. For instance the poorly water soluble drug nabumetone has been encapsulated into polyethylene oxide nano-microfibers [37], while itraconazole has been encapsulated into hydroxypropyl methyl cellulose [38]. Likewise, lipophilic drugs such as rifampicin and paclitaxel have also been encapsulated into polymeric nano-microfibers [39].

Few studies have been published on the application of drug-loaded nano-microfibers as oral drug delivery systems, which is the desired route of administration from a patient convenience point of view. These systems are mainly polymer-based matrices, such as the system described by Shen et al., where Eudragit® L 100-55 nano-microfibers were loaded with diclofenac sodium for colon-targeted delivery [40], or the loading of caffeine and riboflavin into polyvinyl-alcohol fibers, as described by Li et al. [41].

In this study, FSP were electrospun into nano-microfibers and characterized with respect to fiber morphology, protein composition, fiber solubility, fiber degradability and bioactivity. To illustrate how the FSP fibers may be used as a delivery system, a dipeptide (Ala-Trp) was encapsulated into the fibers and the release properties were investigated. Rhodamine B (RhdB) was also encapsulated to study the distribution of an encapsulated compound in the FSP fibers.

Experimental

Materials

Cod (*Gadus morhua*) from the North Sea was obtained from Hanstholm Fisk, Denmark. 1,1,1,3,3,3-Hexafluoro-2-propanol (HFIP), pepsin (activity of 3.260 units/mg protein), pancreatin (activity of 8× U.S.P. specifications), DPP-IV, diprotin, Gly-Pro-Nitroanilid and Ala-Trp were obtained from Sigma-Aldrich Company, St. Louis, USA. The remaining reagents were obtained from Sigma-Aldrich Company, St. Louis, USA, and used without further purification.

Methods

Preparation of FSP

FSP extract: fresh cod was filleted and frozen at −30 °C. The frozen fillet was defrosted, chopped, placed into centrifuge tubes and centrifuged for 15 min, 18,000 × *g*, 5 °C (4K15, Sigma Laboratory centrifuges, Germany).

FSP: FSP extract was transferred to a petri dish, frozen, freeze-dried (FD) and stored at −60 °C.

Electrospinning

FSP was dissolved in HFIP, added to a syringe and placed in a syringe pump (New Era Pump Systems, Inc., USA). A 22 G needle (Proto Advantage, Canada) was used. The syringe pump delivered the FSP solution with a flow rate of 0.02 ml/min. Using a high voltage power supply (Gamma High Voltage Research, USA), an electric field of 20 kV was applied between the spinneret of the syringe and a 5 × 5 cm collector plate made of stainless steel with alumina foil wrapped around it. The distance between the syringe tip and the collector plate was 15 cm. The electrospinning was conducted at room temperature, and samples were stored in an exicator until further analysis.

Protein composition of FSP

Sodium dodecyl sulfate polyacrylamide gel electrophoresis (SDS-PAGE) was performed according to the method of Laemmli [42] using pre-cast 4–20% acrylamide Tris–glycine Novex gels (Life Technologies, USA). FSP extract: 0.5 ml FSP extract was added to a 1.5 ml Eppendorf tube, centrifuged, and the supernatant was saved. FD FSP in water: 27.5 mg FD FSP was added to an Eppendorf tube together with 0.5 ml demineralized water, dissolved and centrifuged. This amount was chosen to obtain a FSP concentration of 55 mg/ml, which is the approximate protein concentration in the FSP extract. The supernatant was saved. FD FSP in HFIP: 27.5 mg FD FSP was added to an Eppendorf tube together with 0.5 ml HFIP, dissolved and centrifuged. The supernatant was saved.

10 μl of each sample was added to Eppendorf tubes together with 60 μl of SDS sample buffer (4.8% SDS, 1 mM EDTA, 0.1 M DTT, 20% (v/v) Glycerol, 125 mM Tris–HCl pH 6.8, 0.05% (w/v) Brom Phenol Blue) and heated for 2 min at 95 °C. 10 μl was loaded on the gel. In addition to the samples, 10 μl Mark12™ (Life Technologies, USA) was loaded. The gel was run at 125 V, 200 mA and 150 W.

Microscopy analysis

Fiber morphology was analyzed with scanning electron microscopy (SEM) (FEI Inspect, USA). A small area of the samples was cut out, placed on carbon tape and sputter coated with gold, 10 s, 40 mA. The diameters of 60 FSP fibers were analyzed with ImageJ [43]. For clarity reasons only images containing few fibers are reported. The polymer jet was stable and continuous, and the fibers shown here represent the collection of fibers obtained after further electrospinning.

The RhdB distribution in FSP fibers was analyzed with confocal microscopy (Zeiss LSM 780, Germany). FSP fibers with 0.05 wt% RhdB were prepared by mixing RhdB into the protein solution (125 mg/ml FSP) prior to electrospinning. The electrospinning was carried out as previously described. Rhodamine fluorescence was detected at 626 nm after excitation with 543 nm, and FSP fiber auto fluorescence was detected at 481 nm after excitation with 405 nm. The images were processed with the ZEN microscopy software (Zeiss, Germany).

Solubility and degradation of FSP fibers

1 ± 0.2 mg fiber was added to 4 × 7 Eppendorf tubes. 250 μl solvent (gastric buffer (2 mg/ml NaCl, 84 mM HCl), simulated gastric fluid (gastric buffer with 0.32% (w/v) pepsin), intestinal buffer (6.8 mg/ml KH_2PO_4, 15.4 mM NaOH, pH 6.8), or simulated intestinal fluid (intestinal buffer with 1% (w/v) pancreatin) was added to Eppendorf tubes and placed on an orbital shaker (90 RPM). At the times 1 min, 30 min, 1 h and 4 h after the addition of solvent, the tubes were centrifuged and supernatants were transferred to another Eppendorf tube containing SDS sample buffer. The samples were treated and SDS-PAGE was performed as described above.

The degradation of FSP fibers by enzymes was studied further in a similar set-up; with low activity simulated fluids (low activity simulated gastric fluid (gastric buffer with 0.0032% (w/v) pepsin) and low activity simulated intestinal fluid (intestinal buffer with 0.01% (w/v) pancreatin).

The degradation pattern of FD FSP was studied as in the case of the FSP fibers, except that the time point at 10 h was omitted and a control consisting of solvent without enzyme was added.

Bioactivity of the FSP fibers

Inhibitor dilution series: 60 mg of FSP fibers was added to an Eppendorf tube together with 1 ml simulated gastric fluid or simulated intestinal fluid. The Eppendorf tubes were placed on an orbital shaker (90 RPM). After 3 h, the Eppendorf tubes were centrifuged and the supernatants were transferred to another 1.5 ml tube and heated at 95 °C for 4 min. The Eppendorf tubes were subsequently centrifuged and the supernatants were saved. In parallel, samples containing only simulated fluids were prepared for control. From the samples, 3-fold dilution series were made using water. The

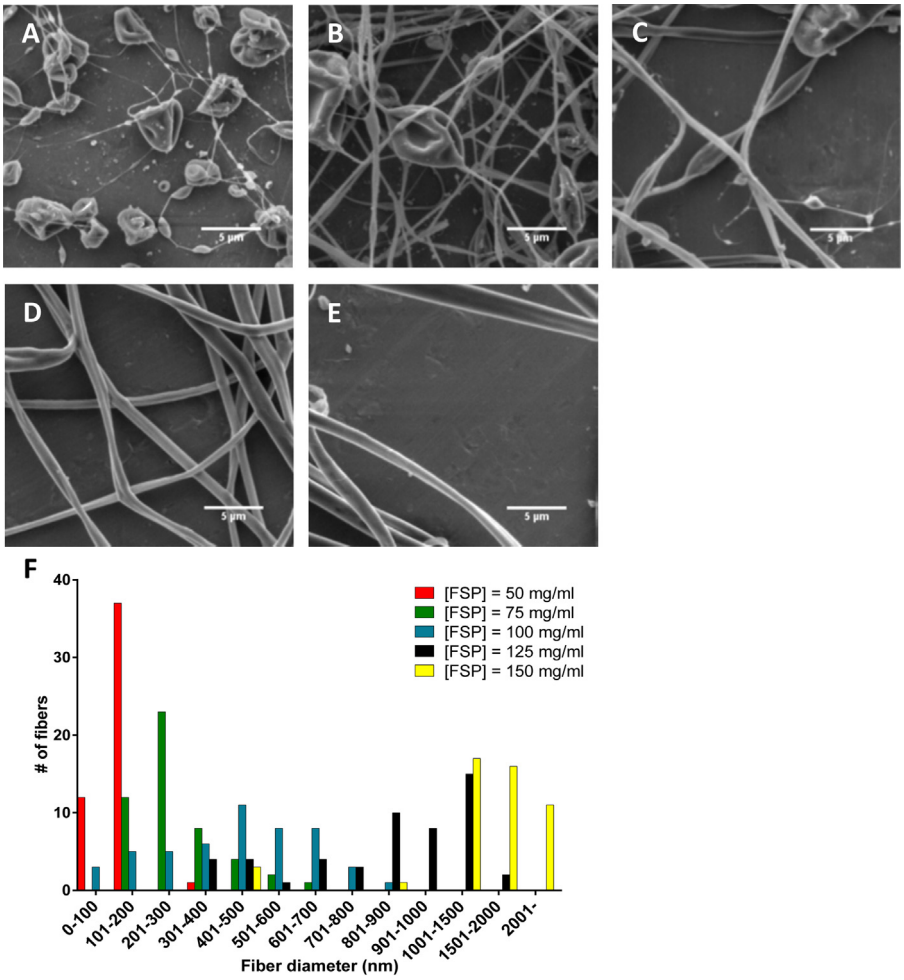

Fig. 1. SEM images of FSP fibers. (A)–(E) [FSP] = 50 mg/ml, 75 mg/ml, 100 mg/ml, 125 mg/ml, and 150 mg/ml, respectively. Magnification: ×5000, scale bar: 5 μm. (F) Size histogram of FSP fibers; 50 mg/ml (red), 75 mg/ml (green), 100 mg/ml (blue), 125 mg/ml (black) and 150 mg/ml (yellow). (For interpretation of the references to color in this figure legend, the reader is referred to the web version of this article.)

samples were pH adjusted to ~8. In parallel, a 3-fold dilution series of the well-known DPP-IV inhibitor diprotin was prepared.

DPP-IV assay: the assay was conducted as described by Li-Chan et al. [24]. In short, 25 μl of the inhibitor solution was added to the wells in a transparent flat bottom 96 well microtiter plate (Greiner bio-one, Switzerland) together with 50 μl DPP-IV (0.01 unit/ml in 100 mM TRIS). The plate was pre-incubated at 37 °C for 10 min. The substrate, 2.4 mM Gly-Pro-Nitroanilid in 100 mM TRIS, was pre-incubated (37 °C for 10 min) and 25 μl was transferred to the wells. Absorption at 405 nm was detected over time using a plate reader (Synergy 2 multi-mode microplate reader, Biotek, USA). In parallel, the known DPP-IV inhibitor, diprotin, was run.

All experiments (except the buffer control which were carried out in singlets) were carried out in triplicate; the mean values ± SDare reported.

FT-IR spectroscopy

Fourier-transform infrared (FT-IR) spectra were obtained on a Spectrum Two IR Spectrometers (PerkinElmer, USA). Washed fibers were obtained by adding the fibers to a 100 ml beaker with 50 ml demineralized water and stirring gently for 1 min. The samples were dried overnight in an exicator. The spectra were scanned from 4000 cm^{-1} to 550 cm^{-1} (only data from 1600 cm^{-1} to 1000 cm^{-1} were reported, as the spectra outside this region did not show anything of relevance), with 1 cm^{-1} resolution, and an average of 28 scans are reported.

Release of Ala-Trp from FSP fibers

FSP-(Ala-Trp) fiber: 1.7 mg Ala-Trp was dissolved in 1 ml HFIP together with 125 mg FSP. The solution was spun with similar conditions to the one described for FSP fiber formation.

FSP-(Ala-Trp) fiber and solvent were added to an Eppendorf tube to achieve 4 mg FSP fiber/ml and placed on an orbital shaker (90 RPM). At the times 1, 5, 10, 15, 30, 60, 120 and 180 min, the supernatant was transferred to another 1.5 ml tube, heated (95 °C for 4 min) and centrifuged. The supernatant was saved. 50 μl of sample was added to a black flat bottom 96 well microtiter plate (Corning Incorporated, USA) together with 50 μl of solvent, and fluorescence at 360 nm upon excitation with 280 nm was measured in a plate reader (Spectra Max Gemini, Molecular Devices, USA). Samples containing FSP-(Ala-Trp) fibers, FSP fibers and the solvent without any fibers were made for gastric buffer and intestinal buffer.

All experiments were carried out in triplicate, and the mean value ± SD are reported.

Results and discussion

Morphology of electrospun FSP fibers

The morphology of the electrospun fibers as a function of FSP concentration was investigated with SEM, Fig. 1A–E. At 50 mg/ml, the majority of the observed structures were particles. When

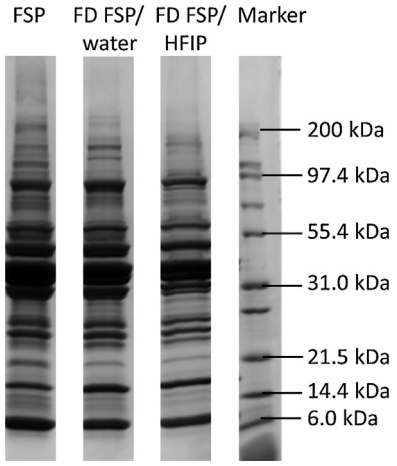

Fig. 2. SDS-PAGE showing the protein composition in FSP extract (lane 1), FD FSP dissolved in water (lane 2), FD FSP dissolved in HFIP (lane 3) and a marker (lane 4).

the FSP concentration was increased to 75 mg/ml and 100 mg/ml, respectively, a larger tendency toward fiber formation versus particle formation was observed, although beads and particle-like structures were still present. At a FSP concentration of 125 mg/ml, beads and particles were approximately eliminated, and there was an increased fiber diameter. Increasing the FSP concentration further had no large influence on the fiber morphology (data not shown). Fig. 1F shows the size distribution of the FSP fiber diameter (excluding particles). At low FSP concentrations, the fiber diameters were in the nano scale, e.g. for 75 mg/ml, fiber diameters were between 100 and 700 nm. At 125 mg/ml, the dominant fiber diameter was approximately 1000 nm (though still varying from hundreds of nm to several μm) and, at larger FSP concentrations, the fiber diameter increased further. Although most pronounced for low FSP concentration fibers, a large size distribution and irregularities were observed. This may originate as a result of low chain entanglement between the proteins. The solvent may also have an impact on the morphology (e.g. the double, spindle like fibers), which may arise as a result of solvent polarity and volatility. Since fibers made with an FSP concentration of 125 mg/ml were without beads or particles and the fiber diameters had the smallest variations, FSP fibers made from FSP at 125 mg/ml were chosen for further characterization. No attempts were made to modify the diameter of uniform FSP fibers by using surfactants and salts, for instance, as this was not the main focus of this study.

Analysis of FSP protein composition by SDS-PAGE

To investigate any potential loss of material during processing, FSP composition during the processing steps; FSP before FD (FSP), FSP after FD (FD FSP/water), and FD FSP dissolved in HFIP (FD FSP/HFIP), were analyzed with SDS-PAGE (Fig. 2). The band patterns for the three samples were alike, suggesting that the protein composition in the three solutions was similar. This indicates that the protein composition of FSP was preserved during freeze drying and dissolution in HFIP; hence, all water soluble proteins normally found in the cod muscle will also be present in the FSP fibers. This was supported by amino acid analysis, which showed very similar amino acid compositions for FSP, FD FSP and FSP fibers (data not shown).

Solubility and enzymatic degradation of FSP fiber

The solubility and enzymatic degradation of FSP fibers and FD FSP for a period of 4 h in gastric buffer, simulated gastric fluid, intestinal buffer and simulated intestinal fluid was investigated. Fig. 3A and E shows SDS-PAGE analyses of compounds released from the FSP fibers in gastric buffer and intestinal buffer. After a short amount of time, low molecular weight (MW) compounds were released in both systems. These compounds may have been attached to the fibers, however not as a part of the fiber network, and therefore they will be detached upon contact with water. Very weak bands corresponding to compounds with larger M_w (~25 kDa) were observed after 4 h in gastric buffer, Fig. 3A. Similar to the low M_w compounds released immediately, these compounds may be partially engaged in the fiber network; however, due to the larger size, they have more electrostatic interactions with the fiber and will consequently be released after a longer amount of time. Despite this minimal release of compounds from the fibers, the fibers were not solubilized over a period of 24 h in the enzyme free solutions (data not shown). Characteristic drawbacks of many electrospun nano-microfibers developed using natural biopolymers are their high dissolution and degradation rates in aqueous (thus also physiologically) environments. Hence they need thorough modifications (often with very toxic agents) to become insoluble. The FSP fibers stand out in this context, being insoluble in aqueous solutions, and can thus be used without further treatment. Another fiber system that has been reported to be insoluble in water without crosslinking is fibers made of the basement membrane protein laminin I [9]. The omission of crosslinkers resulted in maintained bioactivity of the laminin fibers, which enabled the use of laminin fibers to mimic the basement membranes.

When pepsin or pancreatin was present in the simulated fluids, it was observed by the naked eye that the fibers were degraded. Fig. 3B and F show SDS-PAGE analyses of the degradation fragments for fiber degradation in simulated gastric fluid or simulated intestinal fluid, respectively. In both situations all lanes contained the same band pattern, including the solvent control, and hence all bands in all lanes originated from the enzyme(s) in the solvent.

To further investigate the mechanism by which the fibers were enzymatically degraded, the amounts of enzymes were decreased 100 fold. SDS-PAGE analyses of the degradation fragments are seen in Fig. 3C and G. Again, by observing the fibers in the solvents by eye, it was evident that the fibers were degraded, though much more slowly; fibers in low activity simulated gastric fluid were not degraded completely until after 24 h (compared to after 30 min with the higher amount of pepsin), and fibers in low activity simulated intestinal fluid were only ~50% degraded after 24 h (compared to 100% with the higher amount of pancreatin). In Fig. 3C and G no bands corresponding to large degradation fragments were observed. However, the bands corresponding to compounds with M_w around 6 kDa in Fig. 3C and G, lanes 1–7, were not observed in the corresponding lanes in Fig. 3A and E; they may originate from degraded fiber.

Fig. 3D and H SDS-PAGE show analyses of degradation pattern of FD FSP in low activity simulated gastric fluid or low activity simulated intestinal fluid. In low activity simulated gastric fluid, proteins were partially degraded into larger fragments before being completely degraded. In low activity simulated intestinal fluid, compounds were partially degraded into rather stabile fragments, and after 4 h there was still a significant amount of compounds that were not degraded. The differences between degradation patterns for FD FSP and FSP fibers suggest that electrospun FSP does not follow the same degradation mechanism as FD FSP in solution. In the fibers, the proteins were most likely kept in an unfolded state (in contrast to FD FSP in solution, where the proteins may have been in a folded state), and therefore all cleavage sites were available for the enzymes. Consequently, the FSP proteins in the fibers were more prone to degradation, and complete degradation was thus possible. The fact that only small FSP fiber degradation products were observed indicates that the fibers were degraded

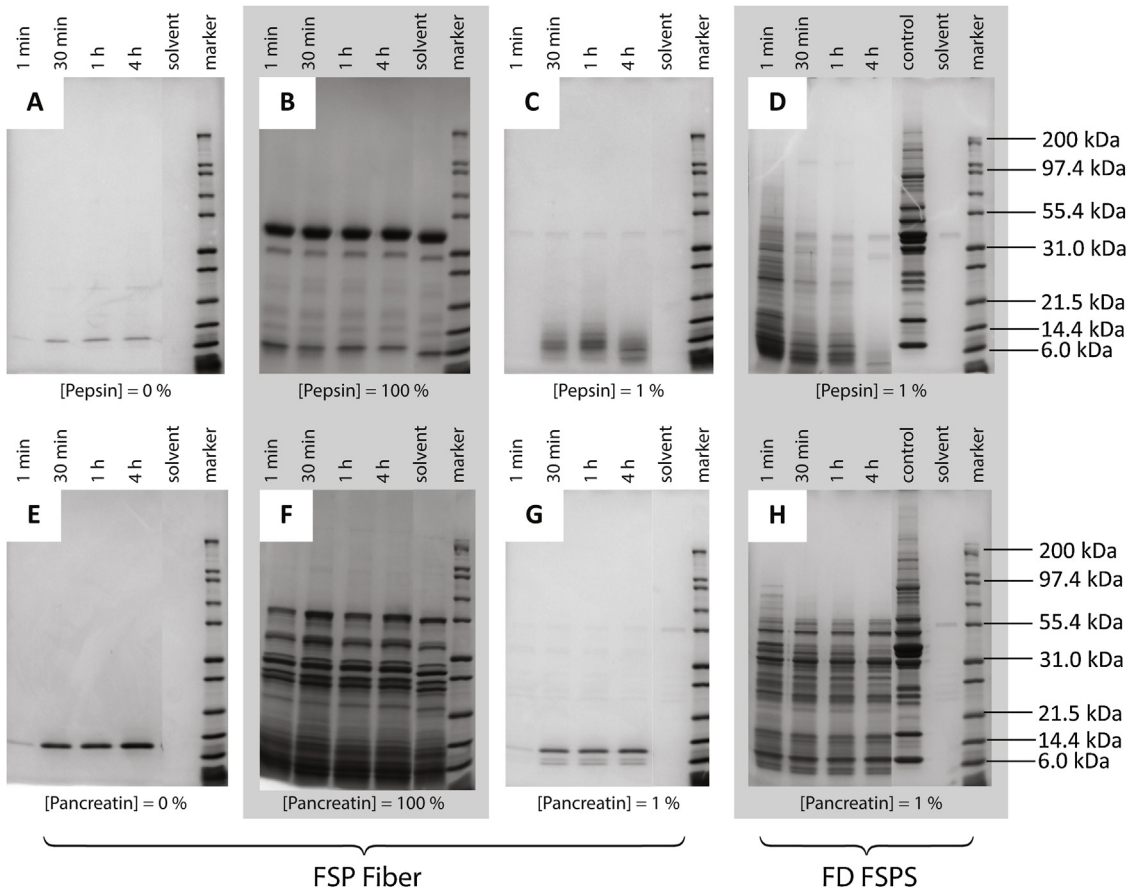

Fig. 3. Solubility and degradation of FSP fibers ((A)–(G)) and FD FSP ((D) and (H)) in gastric buffer (A), simulated gastric fluid (B), low activity simulated gastric fluid ((C) and (D)), intestinal buffer (E), simulated intestinal fluid (F) and low activity simulated intestinal fluid(G) and (H). (A)–(H) lanes 1–4 represent the protein composition in the supernatant after 1 min, 30 min, 1 h and 4 h, respectively. (A)–(C) and (E)–(F) lane 5: solvent and lane 6: marker. (D) and (H) lane 5: FD FSP in buffer without enzyme (control), lane 6: solvent and lane 7: marker.

directly into small fragments, rather than by initial degradation into large fragments, followed by sequential degradation to smaller fragments—as observed for the FD FSP.

To rule out that compounds (such as salts, small peptides, nucleotides etc.) other than the FSP proteins were causing the insoluble nature of the FSP fibers, the FSP extract was dialyzed (cut-off 6–8 kDa) prior to freeze drying. The dialyzed FD FSP was electrospun into fibers, and the fiber solubility in gastric buffer or intestinal buffer was investigated. These fibers were also found to be insoluble in the simulated fluids (data not shown). As the dialysis eliminated the majority of salts, small peptides, nucleotides etc., the majority of the remaining compounds in the FSP were proteins: hence the insoluble nature of the FSP fibers in aqueous solutions pertains to the proteins. The fact that the water soluble FSP became insoluble after electrospinning may be due to the proteins being in an unfolded state when turned into fibers. Unfolding may be caused either by the solvent or by the electrospinning process; however this was not further investigated in this study.

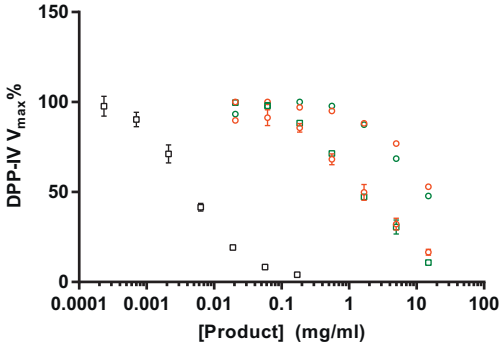

Fig. 4. Dose–response curves for FSP fibers degraded in simulated gastric fluid (□), FSP fibers degraded in simulated intestinal fluid (□), simulated gastric fluid (x), simulated intestinal fluid (x) and diprotin (○), against DPP-IV. Mean ± SD is reported, $n = 3$. The buffer controls were carried out in singlets.

Bioactivity of the FSP fibers

Degradation products from FSP fibers degraded by pepsin or pancreatin were investigated for inhibitory properties against DPP-IV. Dose-response curves for FSP fibers degraded in simulated gastric fluid, simulated gastric fluid, FSP fibers degraded in simulated intestinal fluid, simulated intestinal fluid, and diprotin, a known DPP-IV inhibitor, are shown in Fig. 4. The dose–response curves show that the DPP-IV activity decreases with increasing amount of inhibitor, indicating that the degraded FSP fibers contain inhibitory properties against DPP-IV. The origin of the bioactivity may be peptides containing proline (the proline content in the FSP fibers was ~4%), as peptides containing proline are known to have an inhibitory effect toward DPP-IV [44]. As the plots illustrate, the degradation products of FSP fibers, collectively, were not as potent inhibitors as diprotin. This was expected, as diprotin is a pure antagonist, whereas it is highly unlikely that all FSP fiber degradation products have inhibitory activity against DPP-IV, instead FSP

degradation products were a mixture of inhibitory peptides and peptides without any influence on DPP-IV activity.

FSP fibers as a carrier system

A large range of peptides contain bioactive properties. As the FSP fibers may be utilized as a carrier system for such bioactive peptides, a model system was set up to simulate the release profile of a peptide from the FSP fibers. Ala-Trp was chosen to simulate a bioactive peptide due to its inherent fluorescent properties, enabling the release of Ala-Trp from FSP fibers to be investigated by fluorescence. The following sections present the encapsulation of Ala-Trp into FSP fibers and the release of Ala-Trp from FSP-(Ala-Trp) fibers. In addition, RhdB was encapsulated into the FSP to visually demonstrate the distribution of an encapsulated compound in the FSP fiber.

Encapsulation of Ala-Trp into FSP fibers

The absorption of side chains in a protein may deviate from the absorption of side chains in a dipeptide as a result of, for instance, the surrounding environment [45]. This was utilized to verify that Ala-Trp was encapsulated into the FSP fibers, by recording FTIR spectra of Ala-Trp, FSP fibers and FSP-(Ala-Trp) fibers (Fig. 5).

The spectrum for Ala-Trp (Fig. 5C) contained a large degree of fine structure, and was simpler to analyze as it only represented one molecule. The spectra for FSP and FSP-Ala-Trp (Fig. 5A and B) were more complicated, as they were a combination of absorption spectra from many different compounds. The observed peaks may thus be a combination of several absorption bands from different compounds, leading to a decrease in fine structure. As all samples contained peptides, similar peak patterns were expected (especially for FSP and FSP-Ala-Trp). Comparing the spectra for FSP and FSP-Ala-Trp, large similarities were observed, however two peaks stand out (indicated with arrows), being present in the spectrum for FSP-Ala-Trp but not in the spectrum for FSP, most likely arising because of Ala-Trp. Comparing the peak patterns in the region where the spectrum for FSP-Ala-Trp deviates from FSP, with the peak pattern for Ala-Trp alone, the peak at 1098 cm^{-1} have shifted to 1090 cm^{-1} in Ala-Trp's spectrum. This peak is one of the characteristic peaks for the indole IR spectrum. The peak at 1192 cm^{-1} also stands out in the FSP-Ala-Trp spectrum. Compared to the Ala-Trp spectrum, several peaks are present in this region, and the peak in the FSP-Ala-Trp spectrum may arise as a result of a shift in the relative intensity of the overlapped bands, due to changes in the surrounding environment.

A washing procedure was carried out to reduce dipeptides located on the outside of the fiber; thus only Ala-Trp encapsulated into the fiber network was present. Fig. 5B shows spectra of the fibers after a washing procedure. The peak patterns did not change significantly, though the intensities were affected by washing. Nevertheless, the spectrum still contained peaks that could be ascribed to Ala-Trp, indicating that some amount of the dipeptide was still present inside the fiber network.

Release of Ala-Trp from the FSP fibers

Release profiles of Ala-Trp from FSP fibers in gastric buffer or intestinal buffer, without enzymes, are seen in Fig. 6. The inset figure is a zoom in on the release within the first 20 min. Within the first minute, the Ala-Trp concentration increased to ~30 μM in both solvents. In gastric buffer the maximum release (~60 μM) was obtained after ~30 min, whereas maximum release (~70 μM) in intestinal buffer was obtained after ~15 min. The reason for the extended release time in gastric buffer may have to do with the acidic environment, which leads to protonation of all protonation sites in the fibers. If Ala-Trp is released by diffusion, the rate of

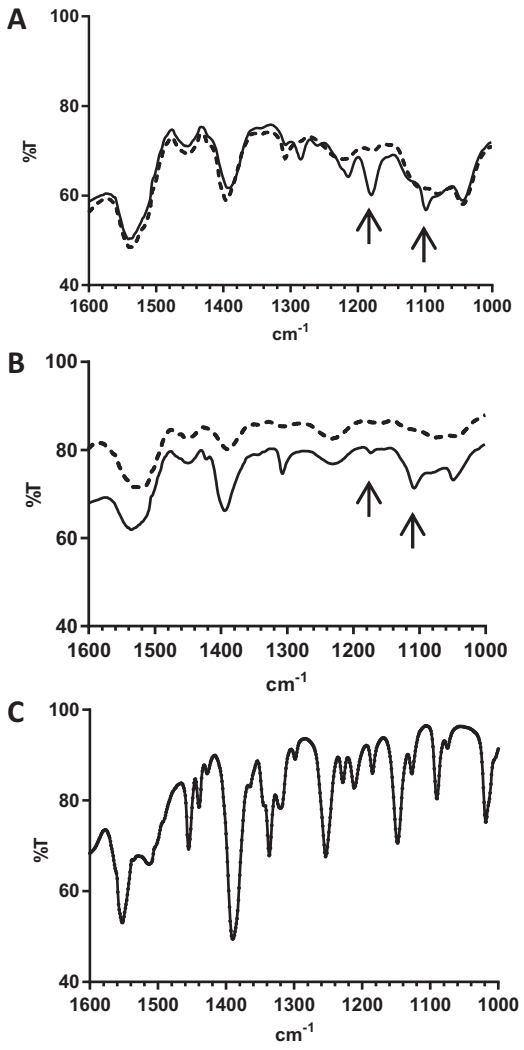

Fig. 5. FT-IR spectra of (A) FSP-(Ala-Trp) fibers (full line) and FSP fibers (dashed line), (B) FSP-(Ala-Trp) (full line) fibers and FSP fibers (dashed line) after a washing procedure and (C) Ala-Trp. The arrows highlight significant peaks for Ala-Trp and Ala-Trp in FSP-(Ala-Trp) fibers.

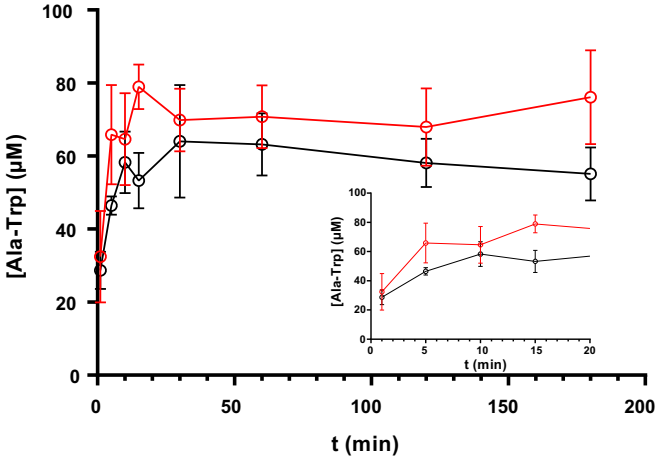

Fig. 6. Release profiles of Ala-Trp from FSP-(Ala-Trp) fibers in gastric buffer (●) or intestinal buffer (●). The inset figure is a zoom in on the release profile for the first 60 min. Mean ± SD, $n = 3$ is reported.

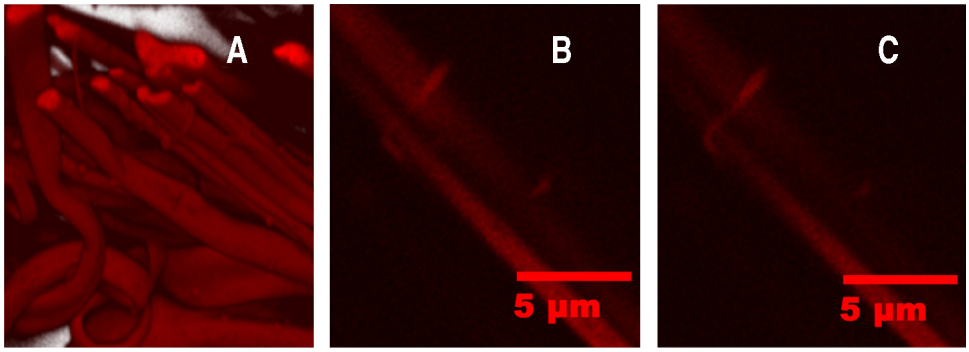

Fig. 7. Confocal images of FSP–RhdB fibers. (A) 3D representation of FSP–RhdB fibers constructed from multiple 2D images. (B) and (C) Scans at height $x + 300$ nm (A) and x (B).

release will depend on chemical interactions between Ala-Trp and the fiber network. Increased protonation of the FSP fibers will lead to increased chemical interactions and thus a prolonged release rate. The theoretical Ala-Trp concentration upon total release of Ala-Trp from the FSP fiber was 97.5 μM. Hence, ~30% of the encapsulated Ala-Trp dipeptide was potentially trapped inside the fibers and would not be released unless the fibers were degraded. In an attempt to release the remaining 30%, enzymes (pepsin or pancreatin) were added. Unfortunately, the background fluorescence from the enzymes made it impossible to distinguish the signal from Ala-Trp from the background signal. The release properties of the system may be tuned (e.g. prolonged release, continuous release, delayed release), for instance by post treatments of the fibers, or by changing the composition of the FSP solution, however this study focuses solely on the properties of the unmodified FSP fibers.

As a surrogate for Ala-Trp, RhdB, which is readily detectable in the presence of enzymes, was encapsulated into the FSP fibers (data not shown). Although RhdB is not a peptide, it is somewhat similar in size (M_w(RhdB) = 479 g/mol versus M_w(Ala-Trp) = 275 g/mol) and it contains some of the same functional groups. Moreover, RhdB is known to interact well with proteins (it is used as a staining agent for proteins). It was therefore hypothesized to mimic Ala-Trp with respect to encapsulation in the fiber network. When FSP fibers with RhdB were placed in gastric buffer or intestinal buffer, without enzymes being added, ~70% of the RhdB was released, compared to when enzymes were present. This corresponded very well to the behavior of Ala-Trp, and it can be assumed that the remaining 30% Ala-Trp may be released upon fiber degradation.

Distribution of compounds encapsulated in the FSP fibers

Encapsulation of Ala-Trp and RhdB was carried out by mixing the respective compound together with the FSP protein solution prior to electrospinning. FSP–RhdB fibers were studied with confocal microscopy to verify that the RhdB was uniformly distributed throughout the fiber. The steady RhdB fluorescence observed from the cross sections of the fibers indicates that RhdB was distributed throughout the fiber, Fig. 7A. This was further supported by looking at the RhdB fluorescence in two different planes of the FSP–RhdB fiber, Fig. 7B and C. Here similar fluorescence was observed in both planes, indicating that RhdB was distributed throughout the fiber. Studying the auto fluorescence from unloaded FSP fibers (data not shown), showed small areas around in the sample with an increased autofluorescence, which may be a result of increased protein density. In FSP–RhdB fibers comparable areas were observed as dark spots—areas with decreased RhdB fluorescence. These observations may be explained by a dense FSP network, with correspondingly limited RhdB. The dense FSP network causes increased autofluorescence, decreased amount of RhdB causes decreased RhdB fluorescene, and thus dark spots.

Conclusion

Nano-microfibers were made from FSP using the electrospinning process. The FSP concentration had a large influence on the morphology of the electrospun FSP fibers. The FSP fibers were insoluble in gastric buffer and intestinal buffer, but the fibers were degraded when enzymes were present. The enzymes degraded the fibers into small peptides rather than into large fragments that were subsequently degraded to small peptides. The residual FSP fiber degradation products were inhibitors of the diabetes related DPP-IV, providing an inherent bioactivity to the FSP fibers. When encapsulating a compound into the FSP fibers, the compound was distributed uniformly throughout the fiber, except for small areas where the protein network was densely packed. The release profile of a dipeptide from the FSP fibers was composed of a burst release within one minute followed by a slower, although still fast, release. In gastric buffer, the maximum release of the dipeptide was released within 30 min, and in intestinal buffer maximum release was obtained after 15 min. ~30% of the encapsulated compound was not released in the timespan of the experiment.

Acknowledgements

This study was funded by the Danish Strategic Research Council (DSF-10-93456, FENAMI Project). The authors would also like to thank Prof. Klaus Qvotrup (the Core Facility for Integrated Microscopy, University of Copenhagen), for assistance with confocal imaging.

References

[1] N. Bhardwaj, S.C. Kundu, Electrospinning: a fascinating fiber fabrication technique, Biotechnol. Adv. 28 (2010) 325–347.
[2] P. Supaphol, O. Suwantong, P. Sangsanoh, S. Srinivasan, R. Jayakumar, S.V. Nair, Electrospinning of biocompatible polymers and their potentials in biomedical applications, Biomed. Appl. 246 (2012) 213–240.
[3] A. Frenot, I.S. Chronakis, Polymer nanofibers assembled by electrospinning, Curr. Opin. Colloid Interface Sci. 8 (2003) 64–75.
[4] D.B. Khadka, D.T. Haynie, Protein- and peptide-based electrospun nanofibers in medical biomaterials, Nanomedicine 8 (2012) 1242–1262.
[5] Z.-M. Huang, Y. Zhang, S. Ramakrishna, C. Lim, Electrospinning and mechanical characterization of gelatin nanofibers, Polymer (Guildford) 45 (2004) 5361–5368.
[6] J.A. Matthews, G.E. Wnek, D.G. Simpson, G.L. Bowlin, Electrospinning of collagen nanofibers, Biomacromolecules 3 (2002) 232–238.
[7] P. Songchotikunpan, J. Tattiyakul, P. Supaphol, Extraction and electrospinning of gelatin from fish skin, Int. J. Biol. Macromol. 42 (2008) 247–255.
[8] Y. Dror, T. Ziv, V. Makarov, H. Wolf, A. Admon, E. Zussman, Nanofibers made of globular proteins, Biomacromolecules 9 (2008) 2749–2754.

[9] C.P. Barnes, M.J. Smith, G.L. Bowlin, S.A. Sell, J.A. Matthews, D.G. Simpson, et al., Feasibility of electrospinning the globular proteins hemoglobin and myoglobin, J. Eng. Fibers Fabr. 1 (2006) 16–29.
[10] R.A. Neal, S.G. McClugage, M.C. Link, L.S. Sefcik, R.C. Ogle, E.A. Botchwey, Laminin nanofiber meshes that mimic morphological properties and bioactivity of basement membranes, Tissue Eng., C: Methods 15 (2009) 11–21.
[11] D.L. Woerdeman, P. Ye, S. Shenoy, R.S. Parnas, G.E. Wnek, O. Trofimova, Electrospun fibers from wheat protein: investigation of the interplay between molecular structure and the fluid dynamics of the electrospinning process, Biomacromolecules 6 (2005) 707–712.
[12] R. Machado, A. da Costa, V. Sencadas, C. Garcia-Arévalo, C.M. Costa, J. Padrão, et al., Electrospun silk-elastin-like fibre mats for tissue engineering applications, Biomed. Mater. 8 (2013) 065009.
[13] F. Zhang, B. Zuo, Z. Fan, Z. Xie, Q. Lu, X. Zhang, et al., Mechanisms and control of silk-based electrospinning, Biomacromolecules 13 (2012) 798–804.
[14] T. Elakkiya, G. Malarvizhi, S. Rajiv, T.S. Natarajan, Curcumin loaded electrospun *Bombyx mori* silk nanofibers for drug delivery, Polym. Int. 63 (2014) 100–105.
[15] J. Chutipakdeevong, U.R. Ruktanonchai, P. Supaphol, Process optimization of electrospun silk fibroin fiber mat for accelerated wound healing, J. Appl. Polym. Sci. 130 (2013) 3634–3644.
[16] S. Baiguera, C. Del Gaudio, E. Lucatelli, E. Kuevda, M. Boieri, B. Mazzanti, et al., Electrospun gelatin scaffolds incorporating rat decellularized brain extracellular matrix for neural tissue engineering, Biomaterials 35 (2014) 1205–1214.
[17] Y.Z. Zhang, J. Venugopal, Z.-M. Huang, C.T. Lim, S. Ramakrishna, Crosslinking of the electrospun gelatin nanofibers, Polymer (Guildford) 47 (2006) 2911–2917.
[18] X. Liu, X. Wang, J. Zhang, X. Wang, Y. Lu, H. Tu, et al., Electrospun poly(vinyl alcohol)/albumin egg/rectorite composite nanofibrous mats and their cytotoxicity, RSC Adv. 4 (2014) 8867–8873, http://dx.doi.org/10.1039/c3ra45344h.
[19] A.-C. Vega-Lugo, L.-T. Lim, Effects of poly(ethylene oxide) and pH on the electrospinning of whey protein isolate, J. Polym. Sci., Part B: Polym. Phys. 50 (2012) 1188–1197.
[20] H. Jiang, P. Zhao, K. Zhu, Fabrication and characterization of zein-based nanofibrous scaffolds by an electrospinning method, Macromol. Biosci. 7 (2007) 517–525.
[21] S.W.a. Himaya, D.-H. Ngo, B. Ryu, S.-K. Kim, An active peptide purified from gastrointestinal enzyme hydrolysate of Pacific cod skin gelatin attenuates angiotensin-1 converting enzyme (ACE) activity and cellular oxidative stress, Food Chem. 132 (2012) 1872–1882.
[22] G. Pilon, J. Ruzzin, L.-E. Rioux, C. Lavigne, P.J. White, L. Frøyland, et al., Differential effects of various fish proteins in altering body weight, adiposity, inflammatory status, and insulin sensitivity in high-fat-fed rats, Metabolism 60 (2011) 1122–1130.
[23] H.S. Ewart, D. Dennis, M. Potvin, C. Tiller, L. Fang, R. Zhang, et al., Development of a salmon protein hydrolysate that lowers blood pressure, Eur. Food Res. Technol. 229 (2009) 561–569.
[24] E.C.Y. Li-Chan, S. Hunag, C. Jao, K. Ho, K. Hsu, Peptides derived from Atlantic salmon skin gelatin as dipeptidyl-peptidase IV inhibitors, J. Agric. Food Chem. 60 (2012) 973–978.
[25] K.B. Moore, C.D. Saudek, Therapeutic potential of dipeptidyl peptidase-IV inhibitors in patients with diabetes mellitus, Am. J. Ther. 15 (2008) 484–491.
[26] M. Lehrke, N. Marx, New antidiabetic therapies: innovative strategies for an old problem, Curr. Opin. Lipidol. 23 (2012) 569–575.
[27] V. Ouellet, J. Marois, S.J. Weisnagel, H. Jacques, Dietary cod protein improves insulin sensitivity in insulin-resistant men and women: a randomized controlled trial, Diabetes Care 30 (2007) 2816–2821.
[28] V. Ouellet, S.J. Weisnagel, J. Marois, J. Bergeron, P. Julien, R. Gougeon, et al., Dietary cod protein reduces plasma C-reactive protein in insulin-resistant men and women, J. Nutr. 138 (2008) 2386–2391.
[29] Q.P. Pham, U. Sharma, A.G. Mikos, Electrospinning of polymeric nanofibers for tissue engineering applications: a review, Tissue Eng. 12 (2006) 1197–1211.
[30] T.J. Sill, H. a von Recum, Electrospinning: applications in drug delivery and tissue engineering, Biomaterials 29 (2008) 1989–2006.
[31] M. Zamani, M.P. Prabhakaran, S. Ramakrishna, Advances in drug delivery via electrospun and electrosprayed nanomaterials, Int. J. Nanomed. 8 (2013) 2997–3017.
[32] Y.-F. Goh, I. Shakir, R. Hussain, Electrospun fibers for tissue engineering, drug delivery, and wound dressing, J. Mater. Sci. 48 (2013) 3027–3054.
[33] H. Liu, X. Ding, G. Zhou, P. Li, X. Wei, Y. Fan, Electrospinning of nanofibers for tissue engineering applications, J. Nanomater. 2013 (2013) 1–11.
[34] L.K. Macri, L. Sheihet, A.J. Singer, J. Kohn, R.a.F. Clark, Ultrafast and fast bioerodible electrospun fiber mats for topical delivery of a hydrophilic peptide, J. Controlled Release 161 (2012) 813–820.
[35] M. Jannesari, J. Varshosaz, M. Morshed, M. Zamani, Composite poly(vinyl alcohol)/poly(vinyl acetate) electrospun nanofibrous mats as a novel wound dressing matrix for controlled release of drugs, Int. J. Nanomed. 6 (2011) 993–1003.
[36] P. Vrbata, P. Berka, D. Stránská, P. Doležal, M. Musilová, L. Cižinská, Electrospun drug loaded membranes for sublingual administration of sumatriptan and naproxen, Int. J. Pharm. 457 (2013) 168–176.
[37] F. Ignatious, L. Sun, C.-P. Lee, J. Baldoni, Electrospun nanofibers in oral drug delivery, Pharm. Res. 27 (2010) 576–588.
[38] G. Verreck, I. Chun, J. Peeters, J. Rosenblatt, M.E. Brewster, Preparation and characterization of nanofibers containing amorphous drug dispersions generated by electrostatic spinning, Pharm. Res. 20 (2003) 810–817.
[39] J. Zeng, X. Xu, X. Chen, Q. Liang, X. Bian, L. Yang, et al., Biodegradable electrospun fibers for drug delivery, J. Controlled Release 92 (2003) 227–231.
[40] X. Shen, D. Yu, L. Zhu, C. Branford-White, K. White, N.P. Chatterton, Electrospun diclofenac sodium loaded Eudragit® L 100-55 nanofibers for colon-targeted drug delivery, Int. J. Pharm. 408 (2011) 200–207.
[41] X. Li, M. a Kanjwal, L. Lin, I.S. Chronakis, Electrospun polyvinyl-alcohol nanofibers as oral fast-dissolving delivery system of caffeine and riboflavin, Colloids Surf., B: Biointerfaces 103 (2013) 182–188.
[42] U.K. Laemmli, Cleavage of structural proteins during the assembly of the head of bacteriophage T4, Nature 227 (1970) 680–685.
[43] C. a Schneider, W.S. Rasband, K.W. Eliceiri, NIH Image to ImageJ: 25 years of image analysis, Nat. Methods 9 (2012) 671–675.
[44] K. Augustyns, P. Van der Veken, A. Haemers, Inhibitors of proline-specific dipeptidyl peptidases: DPP IV inhibitors as a novel approach for the treatment of Type 2 diabetes, Expert Opin. Ther. Pat. 15 (2005) 1387–1407.
[45] A. Barth, The infrared absorption of amino acid side chains, Prog. Biophys. Mol. Biol. 74 (2000) 141–173.

Appendix II – Paper II

Paper II

Bioactive protein-based nanofibers promotes transepithelial permeation of intact therapeutic protein by interactions with biological components

K. Stephansen, M. García-Díaz, F. Jessen, I.S. Chronakis, H.M. Nielsen

Macromolecular Bioscience (in revision)

Bioactive protein-based nanofibers promotes transepithelial permeation of intact therapeutic protein by interactions with biological components

Karen Stephansen[1,2], María García-Díaz[2], Flemming Jessen[1], Ioannis S. Chronakis[1*], Hanne Mørck Nielsen[2*]

[1] National Food Institute, Technical University of Denmark, Søltofts Plads 227, DK-2800 Kgs. Lyngby, Denmark.

[2] Department of Pharmacy, Faculty of Health and Medical Sciences, University of Copenhagen, Universitetsparken 2, DK-2100 Copenhagen, Denmark.

***Corresponding authors:**

Hanne Mørck Nielsen; mail: hanne.morck@sund.ku.dk, phone: +45 35 33 63 46, address: Department of Pharmacy, Faculty of Health and Medical Sciences, University of Copenhagen, Universitetsparken 2, DK-2100 Copenhagen, Denmark.

Ioannis S. Chronakis; mail: ioach@food.dtu.dk, phone: +45 45 25 27 16, address: National Food Institute, Technical University of Denmark, Søltofts Plads 227, DK-2800 Kgs. Lyngby, Denmark

Abstract

In the present study the potential of using bioactive electrospun fish proteins (FSP) as a carrier matrix for small therapeutic proteins was demonstrated especially focusing on the challenges with oral delivery. The inherent structural and chemical properties of FSP as a biomaterial facilitated interactions with cells and enzymes found in the gastrointestinal tract and displayed excellent biocompatibility. More specifically, insulin was efficiently encapsulated into FSP fibers maintaining its conformation, and subsequent controlled release was obtained in simulated intestinal fluid. The encapsulation of insulin into FSP fibers provided protection against chymotrypsin degradation, and resulted in an increase in insulin transport to around 12% without compromising the cellular viability. This increased transport was driven by interactions upon contact between the nanofibers and the Caco-2 cell monolayer leading to the opening of the tight junction proteins. Overall, electrospun FSP may constitute a novel material for oral delivery of biopharmaceuticals.

Introduction

The interest in exploring the potential of oral delivery for biopharmaceuticals, mainly peptides and small proteins, becomes increasingly clear both from a therapeutic and from a patient convenience point of view. These compounds deviates from small molecules especially with regards to their larger size and vulnerability towards enzymatic degradation[1], which make it extremely challenging to obtain a therapeutic effect after non-injectable administration. Delivery via the oral route implies a series of challenges; such as ensuring sufficient structural and chemical stability of the drug by protection against the harsh acidic environment in the stomach and the enzymes in the gastrointestinal (GI) tract. Further, permeation through the mucosa may

be hindered by the properties of these drugs[2,3]. Despite many promising attempts to develop new oral formulations for biopharmaceuticals, especially focused on particle-based drug delivery systems, none has so far succeeded and new biomaterials and approaches are needed[4–10].

During the last decade, electrospinning has gained increasing interest as a promising technique for biomedical applications. This straightforward and scalable technique is suitable for the production of continuous and functional nano- and microfibers from a wide range of (bio)polymers[11–13]. Due to their similarity to the extracellular matrix, electrospun fibers have been extensively studied for tissue engineering, wound healing, and nerve and bone regeneration[14–17]. The large surface to volume ratio of the fibers can also be exploited to enhance the solubility and release of poorly soluble drugs and thus increase the dissolution rate[18–20].

For therapeutically active macromolecules, a number of reports have arisen regarding the encapsulation of proteins into electrospun polymer fibers[15,17,21]. Administration of macromolecules through the oral cavity using nanofibers has been investigated recently[22–24] showing promising results for electrospun scaffolds as non-injectable and non-invasive drug delivery systems. But despite of the associated challenges, oral delivery is still the most preferred route of administration - a route already utilized by nature for delivery nutrients. However, intestinal delivery of macromolecules using nanofibers has not yet been explored.

The homogeneity and elongated structure make polymers an excellent material for electrospinning. However, only few are biodegradable and biocompatible; properties that are essential for use in biomedical systems. To address the need for such properties, attention has been drawn towards some of nature's own materials, proteins, as they are biocompatible, as well as degradable by proteolytic enzymes. They are easy accessible in large quantities either from

natural sources or from biological expression, and several proteins have been successfully electrospun[25]. In a previous study, we introduced electrospinning of water soluble cod sarcoplasmic proteins (FSP)[26]. FSP is a heterogeneous mixture of proteins, containing up to 200 kDa large proteins. As a result, the FSP fibers displayed an interesting morphology; containing fiber diameters from hundreds of nanometers to few microns. The fibers were insoluble in aqueous media, but degraded by proteolytic enzymes – even more degraded than FSP in solution. These properties make the FSP fibers a very interesting carrier material, as various post electrospinning treatments (e.g. crosslinking of the fibers) normally are required for obtaining insolubility of fibers made from water soluble materials[27,28]. The numerous health benefits of consuming fish[29–31] make FSP fibers appealing carriers for oral drug formulations. Further, the inhibitory effects of FSP on dipeptidyl peptidase-4 (DPP-IV)[32], an enzyme with an essential role in glucose metabolism and linked to type 2 diabetes, makes FSP fibers an attractive platform for the delivery of antidiabetic drugs like insulin[33,34]. From an economical and sustainable point of view, many of the proteins that comprise the FSP are also found in waste water from the fish industry[35], which can thus provide a large and cheap FSP source. Despite the heterogeneity of the FSP, the material has proven to be very stable, and no variation in eletrospinning or fiber properties have been observed between different batches. Proteins are ideal candidate components to develop new "soft" materials for biomedical, food and biotechnological applications, particularly, when they, like FSP, already are common constituents of food.

It is our hypothesis that the FSP will serve as an excellent material for, among others, oral delivery applications. The inherent chemical properties of the proteins, together with the structural properties of the nanofibers, will ensure good interactions with the biological components comprising the barrier for obtaining efficient delivery of labile drugs. Additionally,

the FSP fibers will serve to physically protect and thus minimizing the degradation of insulin. To the best of our knowledge, no attempt has been made to utilize the properties of protein nano-microfibers for insulin encapsulation, and evaluate such for oral administration.

Materials and Methods

Materials

Cod (*Gadus morhua*) from the North Sea was obtained from Hanstholm Fisk (Hanstholm, Denmark). Human insulin was kindly provided by Sanofi-Aventis Deutschland (Frankfurt, Germany). Soy-bean phosphatidylcholine (SPC, purity 98%) was purchased from Lipoid (Ludwigshafen, Germany). 4-(2-Hydroxyethyl)piperazine-1-ethanesulfonic acid (HEPES) was acquired from AppliChem (Darmstadt, Germany). 1,1,1,3,3,3-Hexafluoro-2-propanol (HFIP), 2-(N-morpholino)ethane sulfonic acid (MES), Hank´s balanced salt solution (HBSS), sodium taurocholate hydrate (purity > 97%), α-chymotrypsin (Type II, from bovine pancreas, ≥ 40 units/mg protein) and phenazine methosulfate (PMS), fluorescein isothiocyanate (FITC), dimethylsulfoxide (DMSO) and DPX Mountant for histology were obtained from Sigma-Aldrich (St. Louis, MO, USA). 3-(4,5-Dimethylthiazol-2-yl)-5-(3-carboxymethoxyphenyl)-2-(4-sulfophenyl)-2H-tetrazolium (MTS) was purchased from Promega (Madison, WI, USA). Anti-ZO-1 monoclonal antibody (mouse, AlexaFluor 594 conjugate) and anti-Claudin-4 monoclonal antibody (mouse, AlexaFluor 488 conjugate) were purchased from Invitrogen (Carlsbad, CA, USA).

All the other reagents were obtained commercially at analytical grade and used without further purification, and the chromatographic solvents were of HPLC grade. Ultrapure water from

Barnstead NanoPure Systems (Thermo Scientific, Waltham, MA, USA) was used throughout the studies.

Preparation of FSP-Ins Fibers

FSP were isolated from fresh cod and fibers were prepared as previously described[26] (see Supplementary data S1, S2). A concentration of 125 mg/mL FSP was used together with 20 mg/mL insulin. The electrospinning was conducted at room temperature, and samples were stored at -20°C until further analysis. Prior to experiments fiber mats were cut into 3×6 mm sheets. For some cell experiments fiber sheets of 3×3 mm, 3×6 mm or 6×6 mm were also used. To evaluate the distribution of insulin in the fibers, insulin was labeled with FITC similar to the method described by Clausen *et al*.[36] (Supplementary data S3) and encapsulated into the FSP fibers together with unlabeled insulin at a ratio of 1:4 (w/w) following the standard procedure.

Characterization of Electrospun Fibers

The morphology of the fibers was investigated using scanning electron microscopy (SEM) (FEI Inspect, Hillsboro, OR, USA). Approximately 0.5×0.5 cm of the fiber sheet was placed on carbon tape and sputter coated with gold, 10 s, 40 mA utilizing a Cressington 208HR Sputter Coater (Cressington Scientific Instruments, Watford, England). The diameters of 60 fibers were measured with the imaging processing software ImageJ[37]. The localization of FITC-insulin was analyzed with laser scanning confocal microscopy (LSCM) (Zeiss LSM 780, Jena, Germany) detected at 519 nm after excitation with 495 nm, and compared to the bright field image of the fibers. The images were processed using ZEN 2012 lite software (Zeiss, Jena, Germany).

Analysis of Insulin by RP-HPLC

Insulin concentrations were analyzed by reverse phase high-pressure liquid chromatography (RP-HPLC) using a Prominence system (Shimadzu, Kyoto, Japan) equipped with an Aeris WIDEPORE XB-C18 column (100×2.10 mm, 3.6 μm) (Phenomenex, Allerød, Denmark) and a PDA detector (SPD-M20A, Shimadzu). The mobile phase A consisted of 95% H_2O/5% acetonitrile (AcCN)/0.1% trifluoroacetic acid (TFA) (vol%) and mobile phase B consisted of 95% AcCN/5% H_2O/0.1% TFA (vol%). The autosampler temperature was 4°C. Insulin was eluted using a linear gradient of mobile phase B from 20-50% over 3.5 min at a constant flow of 0.8 mL/min and 40°C. Insulin was quantified using automatic integration of the peak at 218 nm (retention time 2.7 min). Limit of detection (LOD) and limit of quantification (LOQ) were 0.2 μg/mL and 0.8 μg/mL (n=3), respectively.

Release of Insulin From FSP-Ins Fibers

In vitro release of insulin from the fibers was performed in 10 mM HEPES-HBSS buffer (pH 7.4), 10 mM MES-HBSS buffer (pH 6.5) or simulated small intestine fluid SSIF-HBSS (10 mM MES, 3 mM sodium taurocholate and 0.2 mM SPC in HBSS, pH 6.5) during 8 h at 37°C with continuous orbital mixing. FSP-Ins fibers were placed in the pre-warmed buffers at a concentration of 3.5 mg/mL. Aliquots of 100 μl of the supernatant were taken at regular time points and replaced with fresh buffer. The samples were analyzed with RP-HPLC as previously described. The experiment was carried out in triplicates.

Quantification of Encapsulation Efficiency

A concentration of 3.5 mg/mL FSP-Ins fibers were added to 18 mM SDS in 10 mM MES-HBSS buffer and incubated at 37°C with continuous orbital mixing. After 2 h the fibers were fully degraded, and the insulin concentration was quantified by using RP-HPLC, as previously described. The experiment was carried out in triplicates.

Conformational Stability of Insulin

The tertiary structure of insulin after release from the fibers was analyzed using circular dichroism (CD). A concentration of 3.5 mg/mL FSP-Ins or FSP fibers were incubated for 4 h at 37°C in 10 mM HEPES buffer (pH 7.4). The supernatants were analyzed on a J-815 Jasco CD spectrometer (Jasco, Tokyo, Japan). A 0.5 mg/mL insulin solution was used as control. Near-UV spectra (250-350 nm) were recorded with a 0.5 nm step size, and an average of 5 repeats was reported. A quartz cell (l = 0.5 cm) was used. CD spectra of the appropriate reference were recorded and subtracted. All spectra were normalized according to the insulin concentration and 2^{nd} order smoothing was performed.

Enzymatic Degradation Studies

A concentration of 3.5 mg/mL FSP-Ins fibers or 0.5 mg/mL insulin solution was incubated with SSIF-HBSS buffer (pH 6.5) in the presence of α-chymotrypsin (0.05 U/mL) at 37°C with continuous orbital mixing. Aliquots of 30 µl were taken at regular time points and added to ice cold HPLC vials to stop the enzymatic degradation. The samples were analyzed immediately on RP-HPLC as previously described. The experiment was carried out in triplicates.

Cell Culture

Caco-2 cells (DSMZ, Braunschweig, Germany) were cultured in DMEM supplemented with 10% (vol%) FBS, penicillin/streptomycin (100 U/mL and 100 μg/mL), 1% (vol%) L-glutamine and 1% (vol%) non-essential amino acids at 37 °C in an atmosphere of 5% CO_2. Cells grown in T75 culture flasks were passaged weekly. The cells were seeded at a density of 1 x 10^5 cells/insert onto 12-well polycarbonate Transwell® filter inserts (1.12 cm^2 growth area, 0.4 μm pore size) (Corning Costar, Tewksbury, MA, USA). The apical and basolateral media were replaced every other day and the cells were used after 20 days of culturing. All experiments were performed within a range of 11 successive passages.

Permeability Studies

Insulin transport across Caco-2 cell monolayers was studied during 4 h at 37 °C on a Max Q 200 horizontal shaker (Thermo Scientific, Waltham, MA, USA), (75 rpm). Culture media was removed and Caco-2 cell monolayers were washed with 10 mM HEPES-HBSS buffer (pH 7.4). For insulin permeability studies, sheets of FSP-Ins fibers were added to the apical side together with 0.5 mL buffer (HEPES-HBSS, MES-HBSS or SSIF-HBSS). The concentrations obtained were normalized according to the weight of the fibers. As controls, 0.5 mg/mL insulin solutions in the different buffers were used. In all cases, 1 mL HEPES-HBSS was added to the basolateral side. Samples of 100 μl were withdrawn from the basolateral side at fixed time points and replaced with pre-heated buffer. The samples were stored at -20 ˚C until analysis with RP-HPLC. All experiments were carried out in triplicates or more and in at least 3 different cell passage numbers.

The apparent permeability coefficient (P_{app}) was calculated according to Equation (1):

$$P_{app} = (\partial Q/\partial t)\ x\ 1/(A\ x\ C_0) \qquad (1)$$

where $\partial Q/\partial t$ is the steady state rate of permeation, A is the diffusion area, and C_0 the initial donor concentration.

Epithelial Integrity

The transepithelial electrical resistance (TEER) of Caco-2 cell monolayers was monitored before and after the permeability experiments using an Endohm^{TM} chamber connected to an EVOM voltohmmeter (World Precision Instruments, Berlin, Germany). Additionally, TEER was monitored before and after 4 h incubation with fiber sheets of sizes 3×3 mm, 3×6 mm and 6×6 mm, 3×6 mm fiber sheets placed in baskets or low molecular weight (LMW) compounds released from FSP fibers. TEER measurements were performed before and after the experiment in HEPES-HBSS buffer upon equilibration to room temperature. The initial TEER value was 465 ± 63 Ω×cm^2 (n = 231).

TEER recovery experiments were performed after the permeability studies with FSP-Ins fibers. After the 4 h permeability study, the epithelium was washed, the test medium was changed to DMEM supplemented with 10% FBS and the cells were incubated at 37 °C in an atmosphere of 5% CO_2. Recovery of TEER values was followed over 24 h.

Cellular Compatibility

The cell viability was determined by the dehydrogenase activity in the Caco-2 cells in monolayers after treatment using the MTS/PMS assay. After 4 h incubation with the test solutions, the cells were gently washed twice with HEPES-HBSS buffer and incubated with 320

µl of freshly prepared MTS/PMS reagent. The cells were incubated at 37 °C for 2 h on a horizontal shaker (75 rpm). A volume of 100 µl of the supernatant was transferred to a 96-well plate and the absorbance was measured at 492 nm on a FLUOstar OPTIMA plate reader (BMG Labtech, Offenburg, Germany). Cells incubated with insulin in HEPES-HBSS were used as positive control, and MTS/PMS solution was used as negative control.

Tight Junction Protein Connectivity

Caco-2 cell monolayers were incubated with FSP-Ins fibers for 4 h in HEPES-HBSS buffer. After incubation, cells were washed with Dulbecco´s phosphate buffered saline and fixed with 4% (vol%) paraformaldehyde. Cells were permeabilized with 0.5% (vol%) Triton-X100 for 5 min and blocked with 2% (wt%) bovine serum albumin (BSA) for 30 min at room temperature. Anti-ZO-1 monoclonal antibody or anti-Claudin-4 monoclonal antibody was incubated with the cell monolayer for 45 min at the concentration 5 µg/mL in PBS. Cells were then washed with PBS and the filter material was carefully removed from the plastic support with a scalpel, transferred to a microscope slide and mounted in DPX Mountant for histology. The samples were analyzed on a confocal microscopy (Zeiss LSM 780, Jena, Germany) equipped with Intune excitation laser system. For analysis of Claudin-4, a 490 nm laser was used, and for analysis of ZO-1, a 595 nm laser was used.

Statistics

Statistical analysis was performed using GraphPad (GraphPad, La Jolla, CA, USA). Unpaired Student's *t* test was used for assessment of statistically significant differences.

Results and Discussion

Successful Encapsulation of Insulin Into FSP Fibers

Water soluble FSP was successfully electrospun together with insulin into solid nanofibers. In general, encapsulation by mixing prior to electrospinning is very effective. Sharma *et al.*[24] reported 99% encapsulation efficiency when encapsulating insulin into polymeric composite nanofibers, and in this study the encapsulation efficiency was found to be 98.6 ± 2.9 %. The loading capacity of insulin into FSP fibers was 14% under the tested conditions. No difference in the morphology was observed between fibers obtained from electrospinning of FSP without insulin (Figure 1A) and FSP together with insulin (Figure 1B) indicating that the presence of insulin did not have an effect on the macroscopic structure of the fibers or on the fiber average diameter (349 ± 23 nm for FSP fibers and 360 ± 37 nm for FSP-Ins fibers). The effect of different insulin loadings up to 33% on the fiber morphology was also investigated. Interestingly, the macroscopic morphology revealed no significant dependency on the loaded amount of insulin within the investigated range (see Supplementary data S4). This revealed a possibility of a very high loading of therapeutic protein into the fibers, and even higher loadings may be explored.

In order to visualize the distribution of insulin throughout the fibers, FITC-labeled insulin was electrospun with FSP, and the fibers were evaluated by confocal microscopy (Figure 1C-E). The fluorescence from the FITC-insulin co-localized with the fiber structure obtained from the brightfield image, and the z-stack fluorescence images of FITC-insulin in the fibers demonstrated a uniform distribution throughout the whole fiber (data not shown).

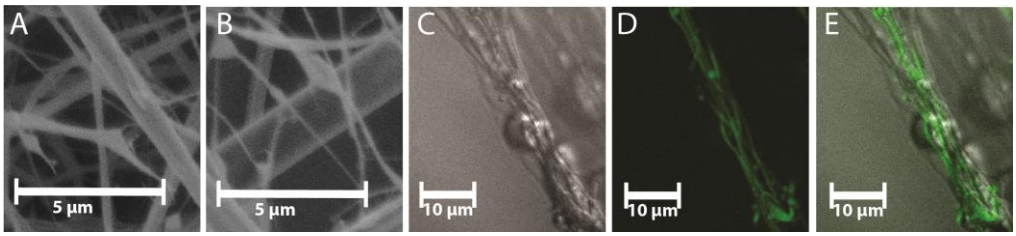

Figure 1. Representative scanning electron microscopy images of electrospun FSP fibers (A) and FSP-Ins fibers (B). LSCM representative images of FITC-insulin loaded FSP fibers, with bright-field image (C), confocal image (D), and overlay of confocal and bright field images (E).

The Tertiary Structure of Insulin is Preserved after Encapsulation and Release from FSP Fibers

Insulin release from FSP-Ins fibers was studied at 37 °C in three different buffers: HEPES-HBSS (pH 7.4), MES-HBSS (pH 6.5) and SSIF-HBSS (pH 6.5) (Figure 2A). Insulin was released gradually reaching a plateau after 2 h in SSIF-HBSS and after 3 h in MES-HBSS and HEPES-HBSS. The release profiles in HEPES-HBSS and MES-HBSS showed very similar kinetics with rate constants of $2.7 \pm 0.5 \times 10^{-4}$ s^{-1} and $2.4 \pm 0.1 \times 10^{-4}$ s^{-1}, respectively. In total, 45 ± 6% insulin was released from FSP-Ins in HEPES-HBSS buffer and 50 ± 13% was released in MES-HBSS buffer. Surprisingly, the release kinetic rate constant was increased to $3.7 \pm 0.4 \times 10^{-4}$ s^{-1} in SSIF-HBSS as well as the maximum amount of released insulin that was increased up to 75 ± 6%. Uncompleted release of an encapsulated compound from the nanofibers has previously been observed for other insoluble fibers, and the maximum possible release was explained to depend on the porosity of the fibers[38,39]. They also showed that the release was facilitated by a two-step mechanism; a rate limiting step being desorption of the compound from the nanoporous surface of the fibers, followed by diffusion into the buffer. As a result, only

compounds situated at the surface of the fibers will be released, as long as the fibers are intact. Addition of for instance porogens such as poly(ethylene glycol) or varying the polymer nature, concentration or molecular weight, will modulate the porosity, and thus the surface area, of the fibers, modifying the maximum release and also the release profile of the compound[39–41]. The increased insulin release in SSIF-HBSS was most likely due to interactions between the fibers with the mixed-micelles formed with sodium taurocholate and phosphatidylcholine. A similar interaction between micelles and polymeric films was shown in a study by Sett *et al.*[42]. For all buffers, maximum release was achieved after 3 h of incubation, which is convenient for achieving absorption from the small intestine as the transit time is 3-4 h.

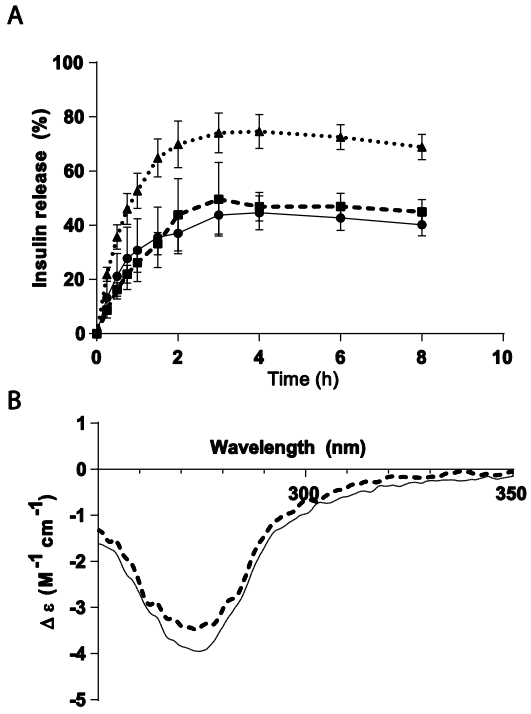

Figure 2. In vitro insulin release profiles of insulin from FSP-Ins fibers in HEPES-HBSS (solid line), MES-HBSS (dashed line) and SSIF-HBSS (dotted line). Data represent mean ± SD, n = 3 (A). Near-UV CD spectra of unprocessed insulin (solid line) and insulin released from FSP-Ins

fibers (dashed line). An average of 5 scans is reported. The spectra were normalized according to the insulin concentration, and the curves submitted to 2nd order smoothing (B).

Proteins are generally sensitive towards stressful processing conditions. In fact, one of the main concerns about incorporating proteins into electrospun fibers is the loss of bioactivity of the biomolecules after blend electrospinning[43]. Since maintaining the native structure of the protein is crucial for preservation of the activity, the effect of electrospinning on the insulin structure was investigated by collection of near-UV CD spectra of unprocessed insulin and insulin released from FSP-Ins fibers (Figure 2B). The spectrum for released insulin was similar to the spectrum for unprocessed insulin, indicating that the tertiary structure of insulin was similar to the native form of insulin after release from FSP-Ins fibers. Since the tertiary structure does not necessarily correlate with the bioactivity of a protein, the presence of intact insulin was further supported using ELISA and RP-HPLC analysis (data not shown). Previous studies of insulin in electrospun fibers[23,44], and insulin that have been exposed to HFIP[45], also found that insulin activity was not compromised during processing, which further emphasized that the combination of electrospinning and HFIP would not affect the activity of insulin.

Ins-FSP Fibers Demonstrate Enhanced Stability of Insulin Against Enzymatic Degradation

A significant challenge for delivering biopharmaceuticals by the oral route of administration is sufficient protection against degradation by intestinal proteases; mainly chymotrypsin and trypsin. To investigate whether the encapsulation of insulin into FSP fibers implied also protective effects against enzymatic degradation, the concentration of monomeric insulin during

the study of release from FSP-Ins fibers was monitored in SSIF-HBSS in the presence of 0.05 U/mL α-chymotrypsin (Figure 3) to which the insulin is most labile[46]. The insulin concentration as a function of time followed the expected rise-and-decay shape kinetics of an intermediate product of irreversible consecutive reactions (equations in Supplementary data S5). The kinetic analysis of the data yielded rate constants of $k_1 = 4 \pm 1 \times 10^{-4}$ s^{-1} for the insulin release and $k_2 = 2 \pm 1 \times 10^{-4}$ s^{-1} for the degradation. In order to assess the protective effect of the fibers, enzymatic degradation studies were also performed with insulin in solution (Firgure 3). As previous studies showed that LMW compounds were released from the fibers upon contact with a buffer[26], the degradation of insulin in solution was studied with the LMW compounds. In this case, the degradation happened fast with a degradation rate constant of $k = 11 \pm 1 \times 10^{-4}$ s^{-1}, and after 1 h, all the insulin was degraded. When encapsulated in the fibers, insulin could be detected in solution for up to 8 h. The degradation of insulin by chymotrypsin was also studied without the LMW compounds, however no effect of the LMW compounds was observed. These results clearly show a protecting effect from enzymatic degradation when insulin is encapsulated in the FSP fibers, and that the protection comes from the encapsulation of insulin into the fibers and not from a competition of the LMW compounds previously reported to be released from the fibers. In addition to protection against intestinal enzymes, protection against acidic pH and pepsin in the stomach are essential for the effectiveness of an oral delivery system. Current methods to overcome these barriers rely on e.g. enteric coating; however this has not been implemented in the current study.

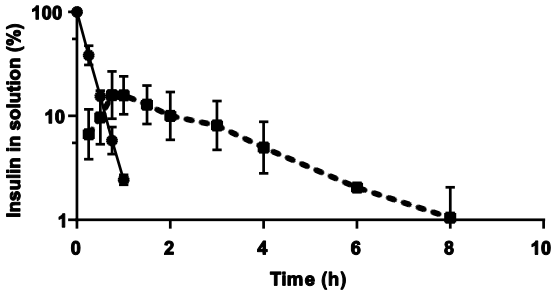

Figure 3. Enzymatic degradation profiles of insulin in solution (solid line) and insulin released from FSP-Ins fibers (dashed line). Data represent mean ± SD, n = 6.

Enhanced Transport of Insulin across Caco-2 Cell Monolayers upon Interaction with FSP-Ins Fibers

The influence of 3×6 mm sheets of FSP-Ins fibers on the transport of insulin across a Caco-2 cell monolayer was studied in HEPES-HBSS (Figure 4A), MES-HBSS and SSIF-HBSS. When encapsulated in fibers, insulin permeated through the Caco-2 monolayer after dosing in all three buffers HEPES-HBSS, MES-HBSS and SSIF-HBSS (Figure 4B), whereas the amount of transported insulin was below the LOD of the analytical method when a comparable amount (0.5 mg/mL) of insulin was applied as a solution. In HEPES-HBSS the amount of transported insulin reached 12 ± 4% within 4 h. There was no significant difference between the insulin transport in MES-HBSS and SSIF-HBSS (both pH 6.5), however in HEPES-HBSS (pH 7.4) the P_{app} value was increased, indicating that pH had a significant influence on the permeation across the membrane. Interestingly, the increased insulin release from FSP-Ins fibers observed in SSIF-HBSS did not result in an overall increased insulin transport. No degradation of insulin was observed during the transport experiments (data not shown), and the structural retention and

binding affinity after permeation across the Caco-2 cell monolayer of insulin was confirmed by RP-HPLC and ELISA (data not shown).

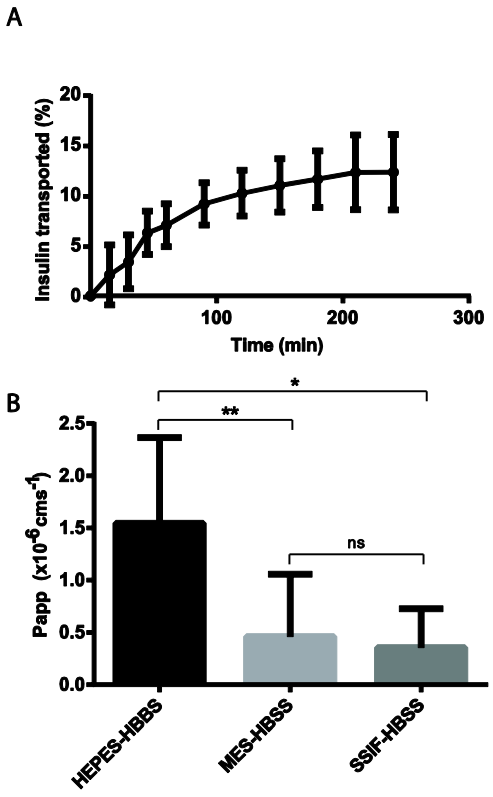

Figure 4. Permeation of insulin across a Caco-2 cell monolayer after release from FSP-Ins fibers in HEPES-HBSS (A). Data represent mean ± SD, n > 6. Apparent permeability (P_{app}) values for transport of insulin released from FSP-Ins fibers in HEPES-HBSS, MES-HBSS and SSIF-HBSS (B). Data represent mean ± SD, n > 3 (* $p < 0.05$, ** $p < 0.01$).

FSP-Ins fibers were placed close to the monolayer, hence when released from the fibers a relatively high concentration of insulin is exposed to the monolayer, resulting in an increased insulin transport across the epithelium due to a concentration gradient-driven flux. Alterations in

the tight junction structure, as reflected by changes in the TEER of the monolayer, may also be the reason for increased permeation of insulin. The FSP-Ins fibers (3×6 mm) caused an approximate two-fold decrease in the TEER values after incubation for 4 h in the different buffers (Figure 5A), however the effect seemed to be the least pronounced in SSIF-HBSS buffer. In order to evaluate whether the contact area between the fibers and the cells was crucial for the effect on TEER, three different sizes of fiber sheets (3×3 mm, 3×6 mm, 6×6 mm) were applied to the cell monolayer (Figure 5B). An area-dependent decrease in the TEER was observed (Figure 5B) suggesting that contact between the fibers and the cell monolayer is necessary to obtain an effect.

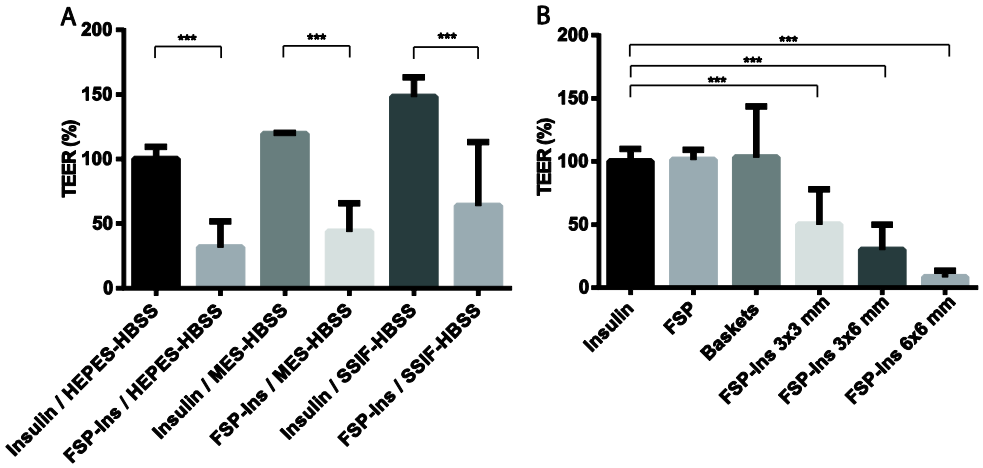

Figure 5. The relative change in TEER after incubation with insulin or 3×6 mm FSP-Ins sheets in HEPES-HBSS, MES-HBSS and SSIF-HBSS (A). The relative change in the TEER after incubation for 4 h in HEPES-HBSS with insulin in solution, supernatant after incubation with FSP fibers for 4 h, FSP-Ins fibers placed in baskets ensuring no direct contact to the cell monolayer, FSP-Ins size 3×3 mm, FSP-Ins size 3×6 mm and FSP-Ins size 6×6 mm (B). Mean ± SD, n > 6 (*** $p<0.001$).

To evaluate if the LMW compounds released from the fibers in solution had any influence on the integrity of the monolayer and thus the permeation of insulin, the effect of compounds released from FSP fibers in buffer during 4 h, and subsequently applied to the cell monolayer was investigated. It is shown that the compounds released from FSP fibers to a solution did not decrease the TEER of the monolayer (denoted "FSP" in Firgure 5B), emphasizing that it was the interaction between the fibers and the monolayer that induced a decrease in TEER. This conclusion was further supported by the fact that no decrease in TEER was observed when the fibers were placed in a basket above the monolayer, in a similar set-up as the one described by Sander *et al.*[47] (denoted "baskets" in Figure 5B). As the increased permeation was induced by close proximity of the fibers to the monolayer, the transient drop in TEER and thus increase in P_{app} values for insulin permeation was sensitive to variations in the FSP-Ins positioning on the monolayer, which to some extent may account for the observed SD. Future studies will focus on developing a material with more distinct contact to the cell monolayer. To investigate if the change in integrity was reversible, the TEER was monitored after the permeability experiment (see Supplementary data SI 6). After 24 h recovery, 50 ± 35% (n = 9) of the integrity that was lost during direct contact with the fibers, was regained, which indicated that the change in monolayer integrity was reversible. To rule out that the decrease in TEER was associated with detrimental effects on the cells, the viability of the cells in the presence of the FSP-Ins fiber sheets of different sizes was investigated. The MTS/PMS assay was applied to assess the effect after 4 h incubation with 3×3 mm, 3×6 mm and 6×6 mm FSP-Ins sheets in HEPES-HBSS, 3×6 mm sheets placed in baskets or in MES-HBSS or SSIF-HBSS (Figure 6). For all treatments the cell viability was > 90% and not significantly different from the control, except for exposure to

the 6×6 mm sheet where the cell viability decreased to 74 ± 4% after 4 h of exposure. Additionally, the cell viability 24 h after the 4 h incubation, corresponding to the TEER recovery, was higher than 90% (data not shown). The generally high cellular compatibility observed after incubation with FSP-Ins fibers substantiates that the decrease in TEER was not due to cell death.

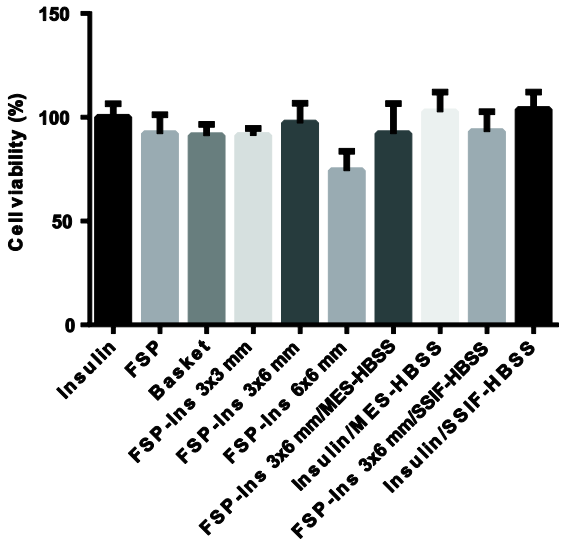

Figure 6. The relative biocompatibility after incubation for 4 h in HEPES-HBSS with insulin in solution, supernatant after incubation with FSP fibers for 4 h, FSP-Ins fibers placed in baskets ensuring no direct contact to the cell monolayer, FSP-Ins size 3×3 mm, FSP-Ins size 3×6 mm and FSP-Ins size 6×6 mm, 3×6 mm FSP-Ins sheets in MES-HBSS, MES-HBSS with insulin in solution, 3×6 mm FSP-Ins sheets in SSIF-HBSS or SSIF-HBSS with insulin in solution. Data show mean ± SD, n > 6.

Some of the main proteins responsible for the junction tightness are the transmembrane proteins (e.g. claudins) and cytoplasmic plaque proteins (e.g. zonula occludens proteins). To further investigate if the observed increase in insulin permeation was related to modifications of the tight junctions, the Caco-2 cell monolayer was incubated with FSP-Ins fiber sheets, stained with anti zonula occludens-1 (ZO-1) and claudin-4 (CL-4) antibodies labeled with a fluorophore and studied with confocal microscopy. Untreated Caco-2 monolayers contained continuous and circumferential ZO-1 and CL-4 distribution indicating intact tight junctions (Figure 7). After incubation for 4 h with FSP-Ins fibers different scenarios were observed when scanning the monolayer; one displaying a similar ZO-1 and CL-4 distribution as compared to the control (FSP-Ins A, Figure 7), and one that displayed less distinct cellular boarders, indicating that the tight junctions were affected by FSP-Ins (FSP-Ins B, Figure 7). These differences show that only a certain part of the monolayer was affected by the presence of FSP-Ins fibers, and support the hypothesis that direct contact between the fibers and the cell monolayer is important to mediate an effect. It is thus in line with the correlation between the area of the fiber sheets and the decrease in TEER, and substantiate the conclusion that the direct interaction between the fibers and the monolayer induces changes in the tight junctions and thus an increase in permeation at local hot spots on the epithelial barrier.

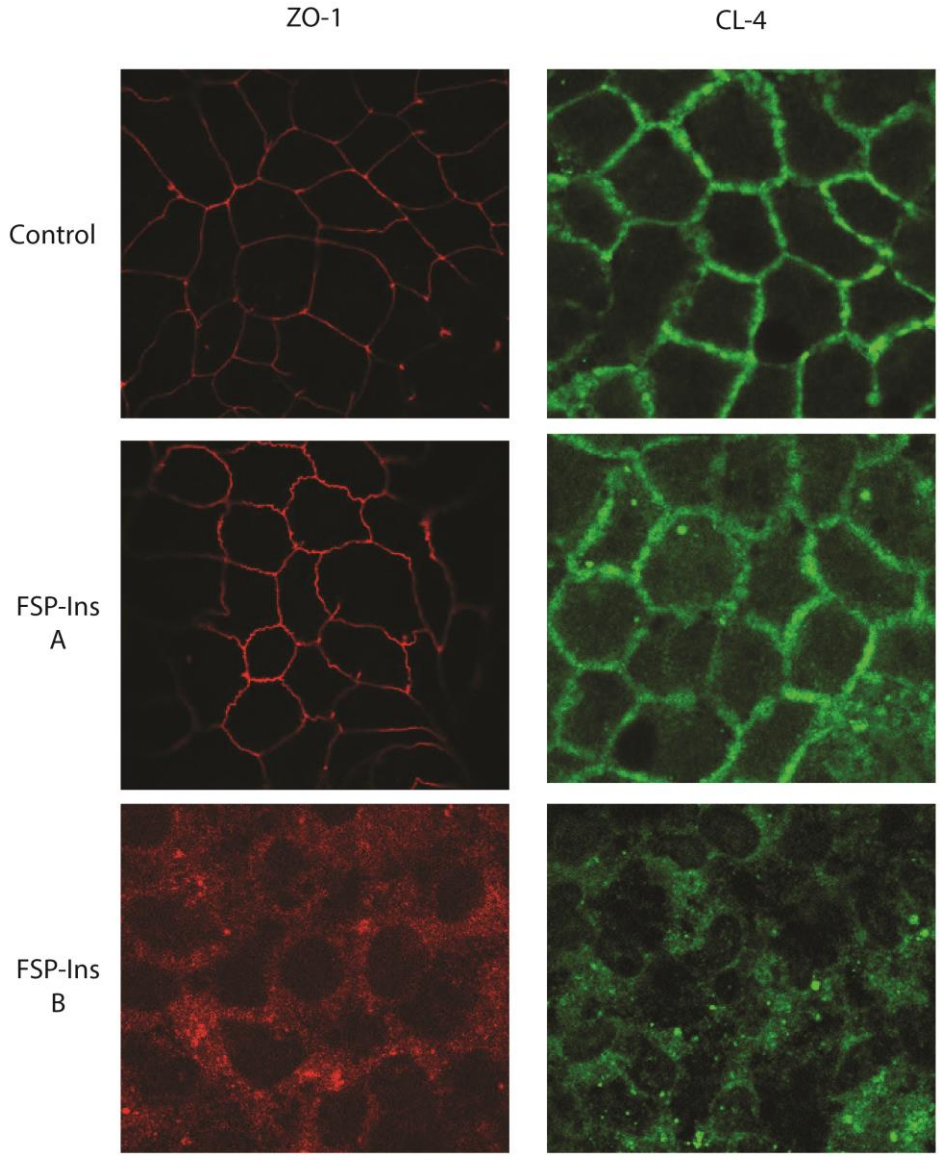

Figure 7. Confocal images of Caco-2 cell monolayers stained with Alexa-598 labeled anti ZO-1 and Alexa-488 labelled anti CL-4. FSP-Ins A and B represent two different scenarios on the same filter insert with a Caco-2 cell monolayer after incubation with FSP-Ins fibers in HEPES-HBSS.

Conclusion

Insulin was successfully encapsulated into water soluble FSP nanofibers without affecting the structure of the insulin. Interactions between the fibers and mixed micelles of bile salts present in the simulated intestinal release medium resulted in an increase in insulin release, as 75 ± 6% was released in SSIF-HBSS, compared to only 45 ± 6% in HEPES-HBSS and 50 ± 13% in MES-HBSS buffer. By encapsulation into the FSP fibers, insulin was detected in α-chymotrypsin-containing buffer for up to 8 h as compared to 1 h when insulin was not embedded in the fibers. Overall, the permeation of insulin across Caco-2 cell monolayers was increased to 12 ± 4% by applying FSP-Ins in HEPES-HBSS to the apical surface of the cells, evidently by exerting a specific effect on the tight junctions as shown by a decrease in integrity. Further, it was found that FSP-Ins fibers induced tight junction modulations dependent on the direct contact to the cell monolayer, as the tight junction proteins ZO-1 and CL-4 was disturbed only in specific regions.

Acknowledgments

Sanofi-Aventis is acknowledged for kindly supplying the human insulin. Authors are thankful to Senior Technician Maria L. Pedersen and Technician Thara Hussein for cell culturing. Authors acknowledge the Core Facility for Integrated Microscopy at Faculty of Health and Medical Sciences, University of Copenhagen and Peter Waaben Thulstrup, University of Copenhagen for access to CD apparatus. The research leading to these results has received support from the Danish Strategic Research Council (DSF -10-93456, FENAMI Project) and Innovative Medicines Initiative Joint Undertaking under grant agreement n°115363 resources, which are composed of financial contribution from the European Union's Seventh Framework Programme (FP7/2007-2013) and EFPIA companies in kind contribution.

Keywords: electrospinning, oral drug delivery, insulin, protein, intestinal delivery,

References

1. R. A. Rader, *Nat. Biotechnol.* **2008**, *26*, 743.

2. Y. Aoki, M. Morishita, K. Takayama, *Int. J. Pharm.* **2005**, *297*, 98.

3. J. A. Fix, *Pharm. Res.* **1996**, *13*, 1760.

4. Y. Zhang, W. Wei, P. Lv, L. Wang, G. Ma, *Eur. J. Pharm. Biopharm.* **2011**, *77*, 11.

5. N. Zhang *et al.*, *Int. J. Pharm.* **2010**, *393*, 212.

6. A. H. Krauland, M. J. Alonso, *Int. J. Pharm.* **2007**, *340*, 134.

7. B. Sarmento, A. Ribeiro, F. Veiga, D. Ferreira, R. Neufeld, *Biomacromolecules* **2007**, *8*, 3054.

8. Z. Ma, T. M. Lim, L. Y. Lim, *Int. J. Pharm.* **2005**, *293*, 271.

9. M.-C. Chen, K. Sonaje, K.-J. Chen, H.-W. Sung, *Biomaterials* **2011**, *32*, 9826.

10. A. Schoubben *et al.*, *Eur. J. Pharm. Sci.* **2009**, *36*, 226.

11. N. Bhardwaj, S. C. Kundu, *Biotechnol. Adv.* **2010**, *28*, 325.

12. P. Supaphol *et al.*, *Adv Polym Sci* **2012**, *246*, 213.

13. A. Frenot, I. S. Chronakis, *Curr. Opin. Colloid Interface Sci.* **2003**, *8*, 64.

14. Q. P. Pham, U. Sharma, A. G. Mikos, *Tissue Eng.* **2006**, *12*, 1197.

15. T. J. Sill, H. a von Recum, *Biomaterials* **2008**, *29*, 1989.

16. V. Leung, F. Ko, *Polym. Adv. Technol.* **2011**, *22*, 350.

17. Y.-F. Goh, I. Shakir, R. Hussain, *J. Mater. Sci.* **2013**, *48*, 3027.

18. F. Ignatious, L. Sun, C.-P. Lee, J. Baldoni, *Pharm. Res.* **2010**, *27*, 576.

19. G. Verreck, I. Chun, J. Peeters, J. Rosenblatt, M. E. Brewster, *Pharm. Res.* **2003**, *20*, 810.

20. J. Zeng *et al.*, *J. Control. Release* **2003**, *92*, 227.

21. X. Hu *et al.*, *J. Control. Release* **2014**, *185*, 12.

22. D. C. Aduba *et al.*, *Acta Biomater.* **2013**, *9*, 6576.

23. L. Xu *et al.*, *Pharm. Res.* **2015**, *32*, 275.

24. A. Sharma *et al.*, *J. Mater. Chem. B* **2013**, *1*, 3410.

25. D. B. Khadka, D. T. Haynie, *Nanomedicine Nanotechnology, Biol. Med.* **2012**, *8*, 1242.

26. K. Stephansen, I. S. Chronakis, F. Jessen, *Colloids Surf. B. Biointerfaces* **2014**, *122C*, 158.

27. B. D. Walters, J. P. Stegemann, *Acta Biomater.* **2014**, *10*, 1488.

28. R. Krishnan, S. Sundarrajan, S. Ramakrishna, *Macromol. Mater. Eng.* **2013**, *298*, 1034.

29. S. W. A. Himaya, D. H. Ngo, B. Ryu, S. K. Kim, *Food Chem.* **2012**, *132*, 1872.

30. G. Pilon *et al.*, *Metabolism.* **2011**, *60*, 1122.

31. H. S. Ewart *et al.*, *Eur. Food Res. Technol.* **2009**, *229*, 561.

32. E. C. Y. Li-Chan, S. L. Hunag, C. L. Jao, K. P. Ho, K. C. Hsu, *J. Agric. Food Chem.* **2012**, *60*, 973.

33. K. B. Moore, C. D. Saudek, *Am. J. Ther.* **2008**, *15*, 484.

34. M. Lehrke, N. Marx, *Curr. Opin. Lipidol.* **2012**, *23*, 1.

35. S. Kristoffersen, B. Vang, R. Larsen, R. L. Olsen, *Aquac. Res.* **2007**, *38*, 1721.

36. A. E. Clausen, A. Bernkop-Schnürch, *J. Pharm. Sci.* **2000**, *89*, 1253.

37. C. A. Schneider, W. S. Rasband, K. W. Eliceiri, *Nat. Methods* **2012**, *9*, 671.

38. R. Srikar, A. L. Yarin, C. M. Megaridis, A. V Bazilevsky, E. Kelley, *Langmuir* **2008**, *24*, 965.

39. M. Gandhi, R. Srikar, a L. Yarin, C. M. Megaridis, R. a Gemeinhart, *Mol. Pharm.* **2009**, *6*, 641.

40. S. Khansari *et al.*, *Mol. Pharm.* **2013**, *10*, 4509.

41. I. C. Liao, S. Y. Chew, K. W. Leong, *Nanomedicine (Lond).* **2006**, *1*, 465.

42. S. Sett, R. P. Sahu, S. Sinha-Ray, A. L. Yarin, *Langmuir* **2014**, *30*, 2619.

43. W. Ji *et al.*, *Pharm. Res.* **2011**, *28*, 1259.

44. C. Yong *et al.*, *Int. J. Nanomedicine* **2014**, *9*, 985.

45. W. K. Snavely, B. Subramaniam, R. a Rajewski, M. R. Defelippis, *J. Pharm. Sci.* **2002**, *91*, 2026.

46. R. Schilling, A. Mitra, *Pharm. Res.* **1991**, *8*, 721.

47. C. Sander, H. M. Nielsen, J. Jacobsen, *Int. J. Pharm.* **2013**, *458*, 254.

Text for the table of contents

This study presents new and promising properties of electrospun fibers, here applied to an intestinal delivery system for biomacromolecules. Inherent fiber properties facilitated protection of the model protein, insulin, from enzymatic degradation, and increased transepithelial permeation of intact therapeutic protein – two critical barriers within intestinal delivery. This study promotes electrospun fibers for delivery of biopharmaceuticals through the small intestine.

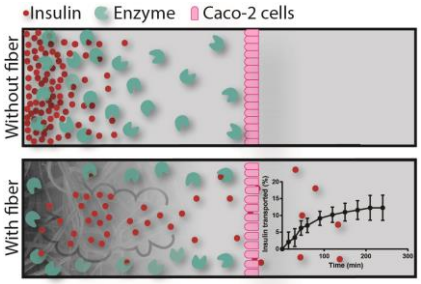

Supplementary data

Bioactive protein-based nanofibers promotes transepithelial permeation of intact therapeutic protein by interactions with biological components

Karen Stephansen[1,2], *María García-Díaz*[2], *Flemming Jessen*[1], *Ioannis S. Chronakis*[1*], *Hanne Mørck Nielsen*[2*]

[1] National Food Institute, Technical University of Denmark, Søltofts Plads 227, DK-2800 Kgs. Lyngby, Denmark.

[2] Department of Pharmacy, Faculty of Health and Medical Sciences, University of Copenhagen, Universitetsparken 2, DK-2100 Copenhagen, Denmark.

***Corresponding authors:**

Hanne Mørck Nielsen; mail: hanne.morck@sund.ku.dk, phone: +45 35 33 63 46, fax: +45 35 33 60 01, address: Department of Pharmacy, Faculty of Health and Medical Sciences, University of Copenhagen, Universitetsparken 2, DK-2100 Copenhagen, Denmark.

Ioannis S. Chronakis; mail:ioach@food.dtu.dk, phone: +45 45 25 27 16, address: National Food Institute, Technical University of Denmark, Søltofts Plads 227, DK-2800 Kgs. Lyngby, Denmark

S1: Preparation of FSP

Fresh cod (*Gadus morhua*) was filleted and frozen at -30˚C. The frozen fillet was defrosted, chopped into approximately 1x1x2 mm sized pieces, placed into centrifuge tubes and centrifuged for 15 min, 18,000 g, 5˚C (4K15, Sigma Laboratory centrifuges, Osterode am Harz, Germany). The supernatant was transferred to a petri dish, frozen, freeze dried and stored at -60˚C.

S2: Preparation of FSP-Ins fibers

FSP (125 mg/mL) and insulin (20 mg/mL) were dissolved in HFIP, added to a syringe and placed in a syringe pump (New Era Pump Systems, Farmingdale, NY, USA). A 30 G needle (Proto Advantage, Ancaster, ON, Canada) was used. The syringe pump delivered the FSP-Ins solution with a flow rate of 0.04 mL/min. Using a high voltage power supply (Gamma High Voltage Research, Ormond Beach, FL, USA), an electric field of 25 kV was applied between the spinneret of the syringe and a the 5×5 cm collector plate made of stainless steel covered by alumina foil. The distance between the syringe tip and the collector plate was 15 cm. For control experiments, FSP (125 mg/mL) was dissolved in HFIP, and electrospun under the same conditions.

S3: Labeling of insulin with FITC

FITC (2 mg/mL) was dissolved in DMSO and gradually added in aliquot volumes of 5 µl to 5 mg/mL insulin dissolved in 0.1 M $NaHCO_3$. After 8 h of incubation at 4 °C, NH_4Cl was added to a final concentration of 50 mM to stop the coupling reaction. The resulting conjugates were incubated for 2 h at 4 °C, dialyzed for 24 h at 4 °C against ultrapure water (Slide-A-Lyzer® Dialysis Cassette (3,500 MWCO), Thermo Scientific, Waltham, MA, USA), and lyophilized (-20°C, 0,1 mbar) using a Christ Epsilon 2-4 LSC freezedryer (Martin Christ, Osterode am Harz, Germany).

S4: SEM images of FSP-Ins

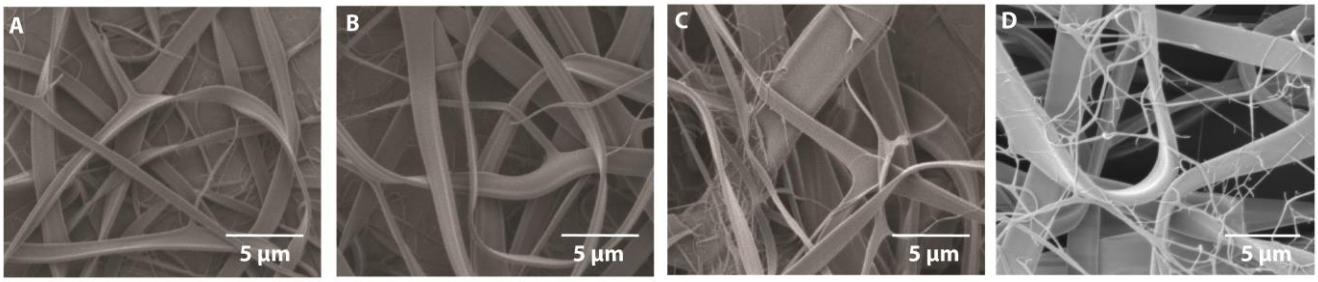

Fig. SI 4

Fig. SI 4. Representative SEM images of insulin encapsulated into fibers of dialyzed FSP, containing 0% (A), 9% (B), 20% (C) and 33% (D) insulin.

S5: *Equations describing the kinetics of insulin degradation*

$$FSP - Ins \overset{k_1}{\rightarrow} Ins \overset{k_2}{\rightarrow} Ins_{degraded}$$

where

$$[Ins] = \frac{k_1 \cdot FSP - Ins_0}{k_2 - k_1} \cdot (e^{-k_1 t} - e^{-k_2 t})$$

S6: *TEER recovery*

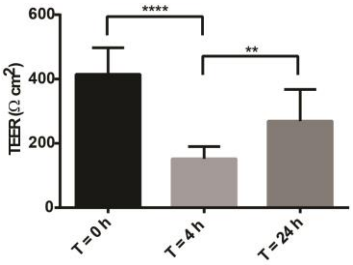

Fig. SI 6

Fig. SI 6. TEER values before incubation with FSP-Ins fibers (T = 0 h), after incubation with FSP-Ins fibers (T = 4 h) and after 24 h recovery (T = 24 h).

Appendix III – Paper III

Paper III

Interactions between surfactants in solution and electrospun protein fibers - Effects on release behavior and fiber properties.

K. Stephansen, M. García-Díaz, F. Jessen, I.S. Chronakis, H.M. Nielsen

RSC Biomaterials Science (prepared for submission)

Interactions between surfactants in solution and electrospun protein fibers - effects on release behavior and fiber properties.

Karen Stephansen[1,2], María García-Díaz[2], Flemming Jessen[1], Ioannis S. Chronakis[1*], Hanne M. Nielsen[2*]

[1]National Food Institute, Technical University of Denmark, Søltofts Plads 227, DK-2800 Kgs. Lyngby, Denmark.

[2]Department of Pharmacy, Faculty of Health and Medical Sciences, University of Copenhagen, Universitetsparken 2, DK-2100 Copenhagen, Denmark.

*Corresponding author:

Hanne Mørck Nielsen; mail: hanne.morck@sund.ku.dk, phone: +45 35 33 63 46, fax: +45 35 33 60 01, address: Department of Pharmacy, Faculty of Health and Medical Sciences, University of Copenhagen, Universitetsparken 2, DK-2100 Copenhagen, Denmark.

Ioannis S. Chronakis; mail:ioach@food.dtu.dk, phone: +45 45 25 27 16, address: National Food Institute, Technical University of Denmark, Søltofts Plads 227, DK-2800 Kgs. Lyngby, Denmark

Abstract

Interactions between compounds found in the human body such as proteins, bile salts, etc. and electrospun compounds has hitherto been an unstudied phenomena, dispite the exposure of fibers to such biorelevant compounds in many biomedical applications such as tissue engineering, wound healing and drug delivery. In this study we present a systematic investigation of how surfactants and proteins, as physiological relevant components, interact with insulin loaded fish sarcoplasmic protein (FSP) electrospun fibers (FSP-Ins fibers) and thereby affect fiber properties such as hydrophilicity, stability and release characteristics of an encapsulated drug. Interactions between insulin-loaded protein fibers and five anionic surfactants (the bile salts sodium taurocholate, sodium taurodeoxycholate, sodium glycocholate and sodium glycodeoxycholate, and sodium dodecyl sulfate), a cationic surfactant (benzalkonium chloride) and a neutral surfactant (Triton X-100) were studied. The anionic surfactants increased the insulin release in a concentration-dependent manner, whereas the neutral surfactant did not have a significant effect on the release. Interestingly, almost no insulin was released from the fibers when benzalkonium chloride was present. The FSP-Ins fibers were dense after incubation with this cationic surfactant, whereas high fiber porosity was observed after incubation with anionic or neutral surfactants. Contact angle measurements and staining with the hydrophobic dye 8-anilino-1-naphthalenesulfonic acid indiated that the FSP-Ins fibers where hydrophobic, and showed that the fiber surface properties were affected differently by the surfactants. Bovine serum albumin also affected insulin release *in vitro*, indicating that also proteins can affect the fiber performance.

Keywords: Electrospinning, proteins, surfactants, drug delivery, tissue engineering

Introduction

Electrospun nanofibers have a large range of biomedical applications within e.g tissue engineering, regenerative medicine and drug delivery[1–5]. The nanofibers can be functionalized in order to improve the performance *in vivo*, for example by addition of proteins to increase biocompatibility[6,7], addition of a polymer to strengthen the mechanical properties[7], addition of drugs such as antibiotics in wound dressing[8–10] or growth factors or DNA in tissue engineering[11–15]. Even cells can be electrospun to promote regeneration of new tissue[16–18]. During optimization of the fiber properties, special attention is given to the hydrophilicity of the fibers, fiber stability and drug release profiles (in case of encapsulated compounds)[12]. Drug release and stability properties are often studied *in vitro* in water[19,20], phosphate buffer[21], phosphate buffered saline[8,22–33] or other similar buffers not containing specific physiological compounds[34,35]. Depending on the application of the electrospun fibers, they will be exposed to different physiological environments, which contain compounds such as bile salts, proteins, salts, etc. However, the effects of physiological components on fiber stability and drug release characteristics are rarely taken into account, eventhough any deviation in fiber performance *in vivo*, from what was expected based on *in vitro* evaluation, may be critical. In our previous study we found that release of insulin from protein fibers was increased in simulated small intestinal fluid containing lipids and sodium taurocholate[36]. The study also showed that transport of insulin across a Caco-2 cells monolayer was increased, due to interactions between the cells and fibers. In a study by Alborzi *et al.*, release of folic acid from alginate-pectin/polyethylene oxide electrospun fibers was studied in a simulated intestinal fluid with a bile extract added, and the authors found that the release was decreased in the presence of bile extract[37]. Sofokleous *et al.* studied release of amoxicillin from poly(D,L-lactide-co-glycolide) (PLGA) for wound healing purposes, and found the drug release from the PLGA dressings

to be different in the tested media (water, simulated body fluid and phosphate buffered saline)[10]. Moreover, Maretschek *et al.* found release of cytochrome C from poly(L-lactide) fibers to be increased when Tween 20 was present in the release medium[38]. Despite of those observations, no study has been dedicated to further investigate the potential effects on the performance of electrospun fiber scaffolds caused by interactions with biorelevant compounds. In the current study we investigated how biorelevant compounds can have an effect on electrospun fibers, by systematically studying the interactions between insulin-loaded electrospun protein fibers and four different bile salts present in the human intestinal fluid (sodium taurocholate (TC), sodium taurodeoxycholate (TDC), sodium glycocholate (GC) and sodium glycodeoxycholate (GDC)). In order to further elucidate the mechanism accounting for the drug release induced by biological surfactants, different synthetic surfactants were also included in the study: the anionic sodium dodecyl sulfate (SDS), the cationic benzalkonium chloride (BC) and the neutral Triton X-100. The effect of the different surfactants on the insulin release profile, fiber porosity and fiber surface properties were studied

Materials and methods

Materials

Cod (*Gadus morhua*) from the North Sea was obtained from Hanstholm Fisk (Hanstholm, Denmark). Human insulin was kindly provided by Sanofi-Aventis Deutschland (Frankfurt, Germany). 4-(2-Hydroxyethyl)piperazine-1-ethanesulfonic acid (HEPES) was acquired from AppliChem (Darmstadt, Germany). 1,1,1,3,3,3-Hexafluoro-2-propanol (HFIP), 2-(N-morpholino)ethane sulfonic acid (MES), Hank´s balanced salt solution (HBSS), TC, TDO, GC, GDO, Triton X-100, SDS, and 8-anilinonaphtalene-1-sulfonic acid (ANS) and benzoylacetone (BZA) were obtained from Sigma-

Aldrich (St. Louis, MO, USA), and BC was obtained from Nomeco (Copenhagen, Denmark). All the other reagents were obtained commercially at analytical grade and used without further purification, and the chromatographic solvents were of HPLC grade. Ultrapure water from Barnstead NanoPure Systems (Thermo Scientific, Waltham, MA, USA) was used throughout the studies.

Preparation of FSP-Ins fibers

Fish sarcoplasmic proteins (FSP) were isolated from fresh cod and fibers were prepared as previously described[39] (Supplementary data S1, S2). A concentration of 125 mg/mL FSP was used together with 20 mg/mL insulin (Ins) for production of the FSP-Ins fibers. Electrospinning was conducted at room temperature, and samples were stored at -20°C until further analysis.

In vitro release studies

The *in vitro* release of insulin from FSP-Ins fibers was performed in 10 mM MES-HBSS buffer (pH 6.5) containing varying amounts (1.5 mM, 3 mM or 6 mM) of surfactant (TC, TDC, GC, GDC, Triton X-100, SDS or BC) during 5 h at 37°C with continuous orbital mixing. FSP-Ins fibers were placed in the pre-warmed buffers at a concentration of 3.5 mg/mL. Aliquots of 30 μl were taken from the supernatant at regular time points and replaced with fresh buffer. The samples were analyzed for contenct of insulin by using reverse phase high-pressure liquid chromatography (RP-HPLC) as described below. The experiment was carried out at least in triplicates.

Insulin quantification

Insulin concentrations were analyzed by RP-HPLC using a Prominence system (Shimadzu, Kyoto, Japan) equipped with an Aeris WIDEPORE XB-C18 column (100×2.10 mm, 3.6 μm) (Phenomenex, Allerød, Denmark) and a PDA detector (SPD-M20A, Shimadzu). The mobile phase A consisted of

95% H_2O/5% acetonitrile (AcCN)/0.1% trifluoroacetic acid (TFA) (v/v/v) and mobile phase B consisted of 95% AcCN/5% H_2O/0.1% TFA (v/v/v). The autosampler temperature was 4°C. Insulin was eluted using a linear gradient of mobile phase B from 20-50% over 3.5 min at a constant flow of 0.8 mL/min and with a column temperature of 40°C. Insulin was quantified as the peak area obtained at 218 nm (retention time 2.7 min). Limit of detection and limit of quantification were 0.2 μg/mL and 0.8 μg/mL (n=3), respectively.

Internal fiber porosity

The internal porosity of FSP-Ins fibers was studied by using cryo-scanning electron microscopy (cryo-SEM) using a Quanta FEG 3D (FEI, Hillsboro, OR, USA) system equipped with a Leica cryo stage and the EM VCT100 Cryo transport system, in combination with the MED020 freeze fracture and Platinum/Carbon or Carbon coating unit (Leica, Wetzlar, Germany). The samples were incubated in 10 mM MES-HBSS pH 6.5 with 6 mM surfactant (TC, SDS, Triton X-100, BC), and subsequently put on a aluminum stub, that was mounted on a transport shuttle, and fixed to the stub with Carbon/contact medium. The sample was frozen in liquid nitrogen, in order to fracture the fibers with a cooled knife inside the MED020. Subsequently, the sample sublimated for 3 min. and sputter was coated with platinum (coating thickness of 5 nm).

Critical micelle concentrations

The critical micelle concentration (CMC) of the different surfactants in MES-HBSS was determined according to the method described by Dominguez *et al.*[40]. Briefly, BZA was added to a final concentration of 0.14 mM, together with varying concentrations of each of the surfactant (TC, GC, TDC, GDO, Triton X-100, SDS and BC) in 10 mM MES-HBSS pH 6.5. A total volume of 200 µl was added to a clear flat-bottomed 96-well UV-transparent plate (Corning Incorporated, Corning, NY,

USA), and absorption was measured at 313 nm at 37°C using a Safire^2 plate reader (Tecan Group Ltd., Männedorf, Switzerland).

Contact angle

The contact angle between FSP-Ins fibers and aqueous solutions of surfactants (6 mM TC, Triton X-100, SDS or BC in 10 mM MES-HBSS, pH 6.5) was measured using an optical tensiometer (Theta, Attension, Finland) with a highspeed camera (3000 fps, MotionXtra N3, IDT, USA). A volume of 7.5 µl of buffer was deposited on the fiber surface, and images were immediately recorded with 59 frame per sec the first 3.4 sec, and thereafter 1 frame per second until 34 sec. The contact angle was derived from the images as the angle between the tangent to the drop at the surface-liquid interface and the fiber. The contact angle, calculated as the mean of the left and right contact angle, was plotted as a function of time, and the initial contact angle was found by extrapolation these measurements.

Confocal microscopy

FSP-Ins fibers were placed in 10 mM MES-HBSS pH 6.5 with and without surfactants (6 mM TC, Triton X-100 or BC) and incubated for 3 h. After 2 h, ANS was added to a final concentration of 25 µM and incubated for 1 h. The fibers were transferred to a coverslip and images were obtained using a laser scanning confocal microscope (Zeiss LSM 780, Jena, Germany), using excitation at 405 nm and emission measured at 489 nm.

Statistics

Statistical analysis was performed using GraphPad (GraphPad, La Jolla, CA, USA). Unpaired Student's *t* test was used for assessment of statistically significant differences.

Results and discussion

Release of insulin from FSP-Ins fibers was affected by surfactants in solution

Insulin release from FSP-Ins fibers was studied at in MES-HBSS in the absence or presence of surfactants (Figure 1). The chosen surfactants are divided into four groups, i) biologic anionic surfactants (TC, TDC, GC, GDC), ii) synthetic anionic surfactant (SDS), iii) cationic surfactant (BC) and iv) neutral surfactant (Triton X-100) (for the chemical structures see Supplementary information S3). The release was studied at increasing surfactant concentrations, up to 6 mM, and the presence of bile salts increased the release of insulin in a concentration-dependent manner (Figure 1 A – D). No additional effect on release rate and amount was observed with bile salt concentrations higher than 6 mM (data not shown). The fibers were physically stable in the buffer during long periods of time, as no change in internal structure was observed even after 2 months of incubation (Supplementary data S4), and the fibers remained non-dissolved even longer. To investigate if the effect on the insulin release could be caused by surfactants in general, insulin release upon exposure to synthetic surfactants (SDS, BC and Triton X-100) was analyzed in a similar manner, Figure 1 E-H. SDS induced a similar behavior as the bile salts, with increasing SDS concentrations leading to increased insulin release. However, fibers that were exposed to high concentrations of SDS were degraded, as observed visually, and accordingly the release of insulin continued to increase, contrary to what was observed for the bile salts. The synthetic SDS is a well-known denaturing agent, and as a rule of thumb it takes 1.4 g SDS/g protein to denature a protein to an unfolded structure (saturation). Although the FSP-fibers were not saturated with SDS at 6 mM SDS, degradation of the fibers occured. A further increase in SDS concentration up to 18 mM led to complete release of entrapped insulin, due to extensive fiber degradation (data not shown). Complete drug release allowed for quantification of the insulin

encapsulation efficiency, which was found to be 98.6 ± 2.9 % (n = 3)[36]. Insulin release in 3 mM SDS was similar to the release in MES-HBSS, but noticeable, when lowering the SDS concentration to 1.5 mM SDS, insulin released decreased. The presence of the neutral surfactant, Triton X-100, did not alter the insulin release profile as compared to that observed in the MES-HBSS (Figure 1F), and no concentration-dependency was observed. Interestingly, almost no insulin was released from the FSP-Ins fibers upon incubation with the cationic surfactant BC (Figure 1 G). Approximately 1 % of the encapsulated insulin was released in the 3 mM and 6 mM BC solution as burst release, but after 2 h no insulin was detectable. The strength of the interactions between BC and FSP-Ins fibers was investigated by transferring the FSP-Ins fibers to 12 mM SDS, after five h of incubation in 3 mM BC, and surprisingly no insulin was released after addition to the SDS solution (data not shown). This indicated that the interaction between BC and the FSP-Ins fibers resulted in a significant stabilization of the fiber structure, preventing insulin release. The differences in the way the surfactants affected insulin release, suggested that i) the surfactants interacted with the FSP-Ins fibers, and ii) the interaction, and the results of the interaction, strongly depend on the properties of the surfactants. The CMC of the surfactants in MES-HBSS was determined to investigate if there was any relation between the CMC and the effect on release (Figure 1 H), however no correlation to the CMC was found in relation to the effect of the surfactants on the drug release, which indicated that the CMC did not affect the behavior of the surfactants with respect to fiber interactions. In our previous study the simulated intestinal fluid also contained lipids, however the lipids were found not to affect insulin release (data not shown). Bovine serum albumin (BSA) is a common protein in the human body, and for that reason the effect of BSA on insulin release was briefly touched upon. Boegh *et al.* have developed a biosimilar mucus, which contained 3.1 % BSA, and with that amount of BSA in the MES-HBSS buffer, release of

insulin was increased (Supplementary information S5), indicating that interaction with fibers and thereby alterating fiber properties is not limited to surfactants.

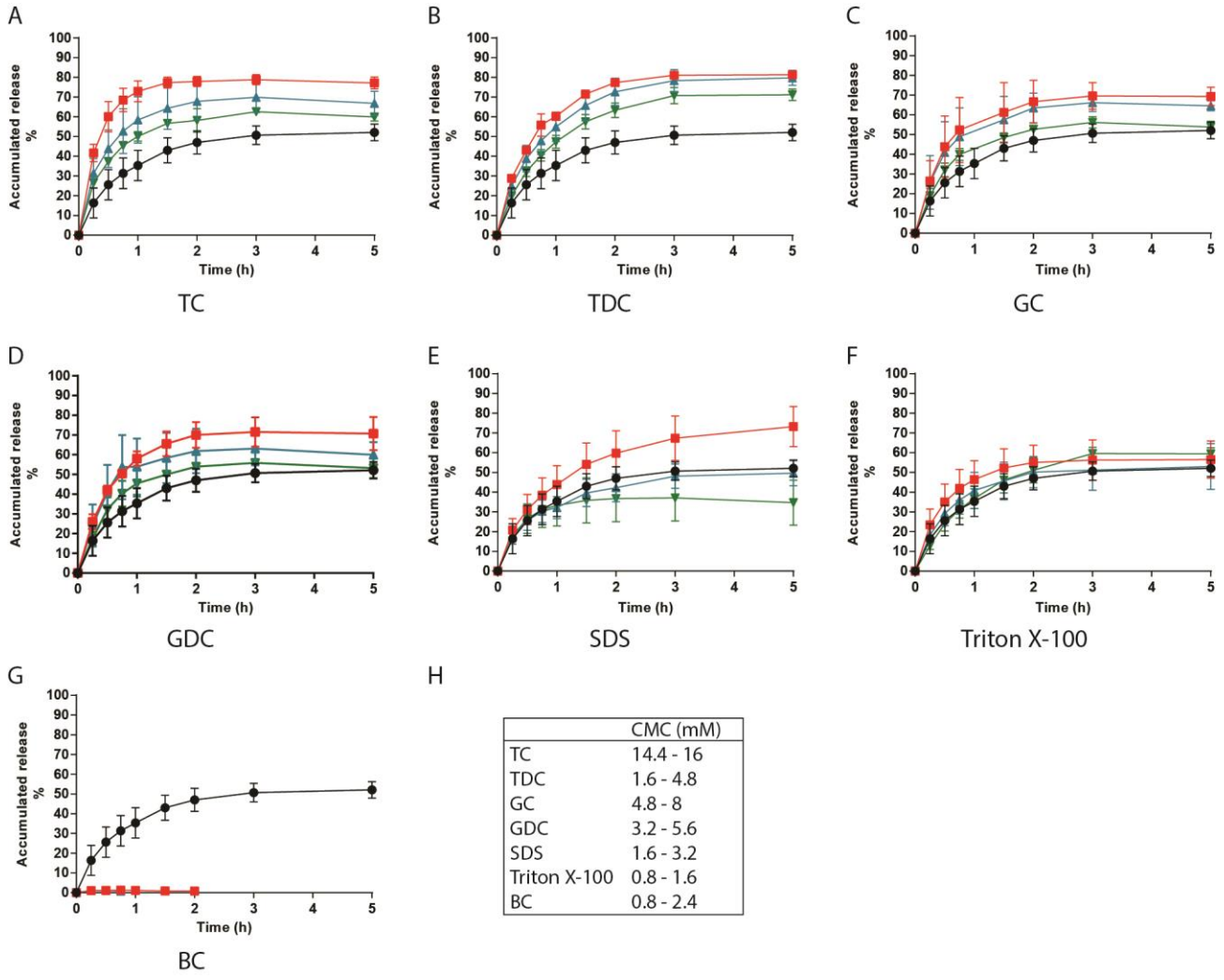

	CMC (mM)
TC	14.4 - 16
TDC	1.6 - 4.8
GC	4.8 - 8
GDC	3.2 - 5.6
SDS	1.6 - 3.2
Triton X-100	0.8 - 1.6
BC	0.8 - 2.4

Figure 1. Insulin release from FSP-Ins fibers *in vitro* in MES-HBSS with varying concentrations of TC (A), TDC (B), GC (C), GDC (D), SDS (E), Triton X-100 (F) and BC (G,H); 0 mM (black), 1.5 mM (green), 3 mM (blue) and 6 mM (red). Data represent mean ± SD, n ≥ 3.

Fiber porosity was affected by interactions with surfactant

In vitro release of a compound encapsulated in insoluble fibers has previously been correlated to the porosity of the fibers[19,20,41]. From those studies it was found that the release was facilitated by a two-step mechanism; desorption of the compound from the nanoporous surface of the fibers, as the rate limiting step, followed by diffusion from the fiber matrix into the buffer. As a result, only compounds situated at the surface of the fibers were released, as long as the fibers were intact. Modulating the porosity, and thus the surface area, for instance by addition of porogens, such as poly(ethylene glycol), or varying the polymer nature, concentration or molecular weight, modified the maximum released amount, and also the compound release profile [19,41,42]. In Figure 1the maximum release changed according to the type and the amount of surfactant present in the MES-HBSS buffer. To investigate if the observed tendencies were associated to changes in fiber porosity, the inner structure (cross-sections) of the FSP-Ins fibers after incubation in MES-HBSS, MES-HBSS with 6 mM TC or MES-HBSS with 6 mM BC, was analyzed with cryo-SEM, and compared to the inner structure of the fibers before incubation (Figure 2). Before incubation in a buffer, a small degree of porosity was observed throughout the fibers, and in some fibers the porosity in the core was increased, which most likely is caused by fast evaporation of the solvent (Figure 2D). After incubation in MES-HBSS and MES-HBSS with TC (Figure 2 A and B) the inner structure of the FSP-Ins fibers became more porous, whereas the fibers that had been exposed to BC became dense (Figure 2C). The trend in porosity correlated with insulin being released in MES-HBSS and MES-HBSS with TC, whereas release in MES-HBSS containing BC was negligible. The fact that the burst release in BC was almost nonexistent (Figure 1 G), suggested that BC instantaneously interacted with the surface of the fibers, and induced a

stabilizing effect thus precluding insulin release and causing the inner fiber structure to become dense. The inner structure of fibers exposed to Triton X-100 or SDS were also investigated (data not shown), and porosity was observed in both cases. As with MES-HBSS in the presence and absence of TC, porosity after exposure to Triton X-100 and SDS correlated with insulin being released from FSP-Ins fibers in both Triton X-100 and SDS solutions. It was not possible to study a potential connection between extend of insulin release and degree of porosity, since the porosity made the fibers fragile and sensitive to beam damage, which resulted in partly closing of the pores, which thereby prohibited quantitative analysis of the porosity.

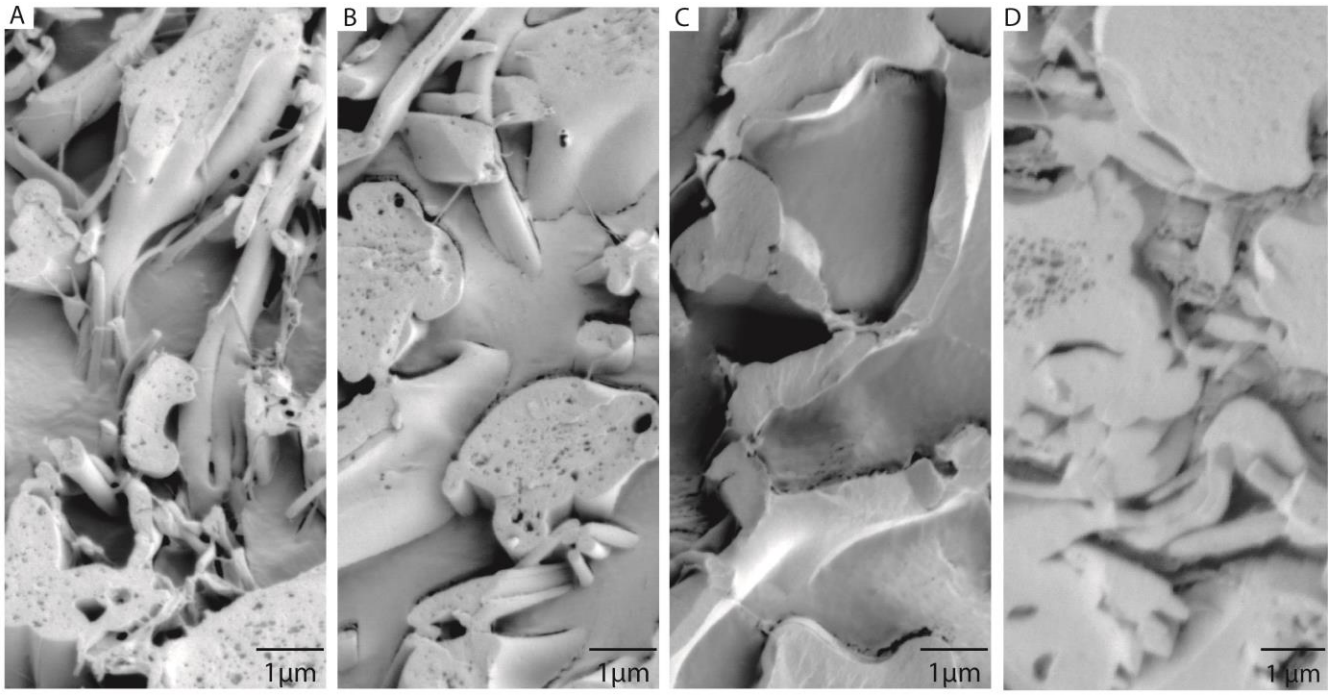

Figure 2. Cryo-SEM images of FSP-Ins fibers after incubation in MES-HBSS (A), MES-HBSS with 6 mM TC (B), MES-HBSS with 6 mM BC (C) and before incubation (D). Scale bars are 1 µm.

Interactions between surfactants and FSP-Ins fiber led to changes in the contact angles

The interactions between surfactants (TC, SDS, Triton X-100 and BC) in MES-HBSS and FSP-Ins fibers were further evaluated by contact angle measurements (Figure 3). MES-HBSS without surfactants displayed a large contact angle of 110 ± 8 degr., which indicated that the FSP-Ins fibers were hydrophobic. Addition of SDS caused no significant change in the contact angle (117 ± 7 degr.), whereas addition of TC increased the contact angle to 130 ± 6 degr. The presence of BC decreased the contact angle to 84 ± 21 deg. And Triton X-100 decreased the value even further to 37 ± 13 degr. The decreased contact angle caused by Triton X-100 and BC suggested that interactions between Triton X-100, or BC, and the fibers, facilitated increased surface hydrophilicity. The rate by which the liquid drop was absorbed into the fibers, varied in the order Triton X-100 > BC > SDS > TC > MES-HBSS. The differences in contact angle and time for complete liquid drop absorption emphasized that the surfactants interacted with the fibers in different ways, dependent on the properties of the surfactants. The effect of the surfactant concentration was investigated by comparing the contact angle for 3 mM ans 6 mM TC or SDS, but no dose-dependency was observed in this concentration range (Figure 3 B)

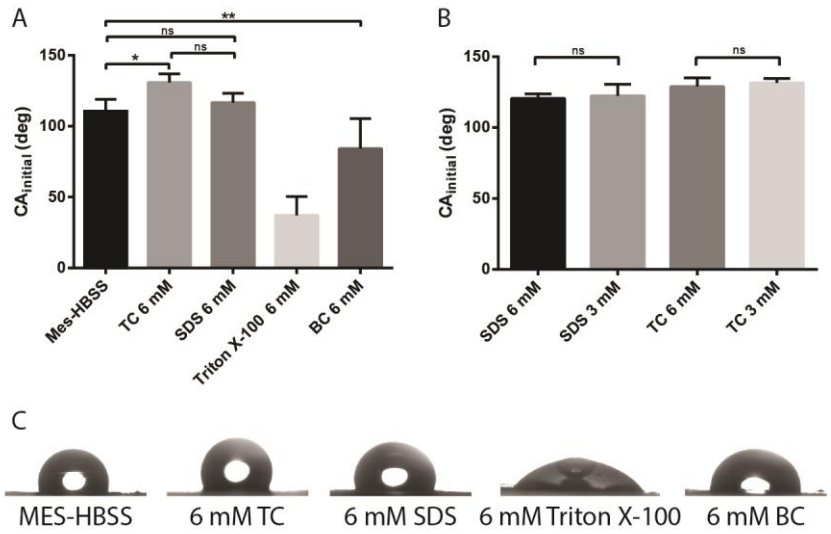

Figure 3. Contact angles between FSP-Ins and MES-HBSS with or without surfactants (A) and comparison of contact angles between FSP-Ins fibers and MES-HBSS containing either 3 mM or 6 mM surfactant (B). Data represent mean value ± SD, n > 3. Representative images of a drop of buffer (MES-HBSS with or without surfactants) on FSP-Ins fibers (C).

Surface properties of the FSP-Ins fibers were affected by interactions with surfactants

The hydrophobic nature of the FSP-Ins fibers was studied by ANS fluorescence (Figure 4). ANS is widely used to visualize hydrophobic regions in e.g. fibrillar aggregates and fibers, as its fluorescence is enhanced when ANS interacts with hydrophobic environments[43,44]. Increase in fluorescence intensity can thus be ascribed to increased amounts of hydrophobic pockets. Figure 4 A shows the ANS fluorescence in fibers after incubation with MES-HBSS. The visualization of the FSP-Ins fibers by the application of ANS fluorescence verified that the surface of the FSP-Ins fibers were hydrophobic. The homogeneity of the fluorescence throughout the fiber matrix furthermore suggested that the properties of the surface were consistent, despite of the complexity of the FSP matrix. The presence of 6 mM TC in the MES-HBSS buffer did not alter the ANS fluorescence (Figure 4 B), indicating that a similar

amount of hydrophobic pockets were still available for interactions with ANS. Interesingly, esposure of the FSP-Ins fibers to 6 mM Triton X-100 or 6 mM BC caused a decrease in ANS fluorescence, as shown in Figure 4C and D, respectively. In both cases the ANS fluorescence decreased significantly, compared to fibers exposed to MES-HBSS without surfactants, indicating that the amount of accessible hydrophobic regions was decreased. This was in agreement with the contact angle measurements, where an increased hydrophilicity was caused by BC and Triton X-100, and hydrophobicity was observed for MES-HBSS in the presence and absence of TC. The loss in the amount of hydrophobic regions available for ANS binding can be explained by changes in the FSP-Ins fiber surface properties, and here we propose two possible explanations. In the electrospun fibers, the protein entanglements may cause the proteins to be in an energetically unfavorable state. Addition of surfactants to the buffer may cause a relaxation of the proteins, which results in small rearrangements in the protein structure, and thus shielding of hydrophobic regions. Another hypothesis rely on the strong interactions between surfactants and fibers, which will compete with and prevent the ANS molecules from interacting with the fibers. Irrespective of the exact mechanism, changes in the surface properties of the fibers upon incubation with neutral or cationic surfactants were evident.

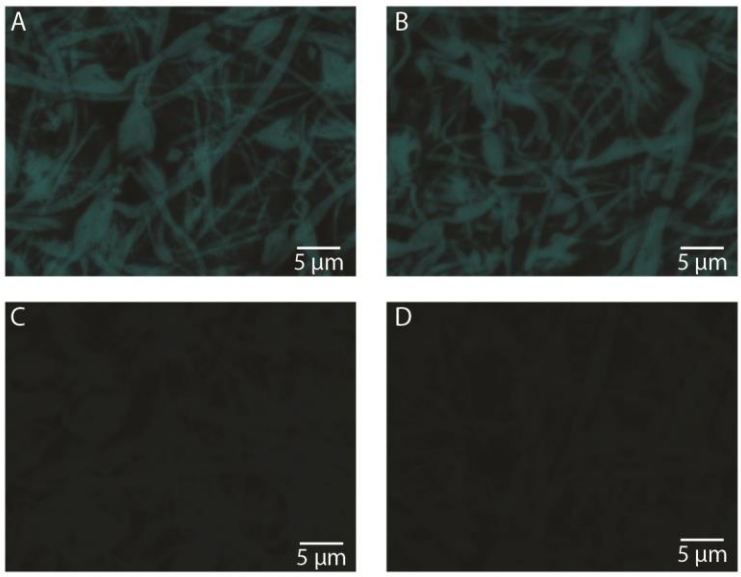

Figure 4. Cross-sectional confocal images of fibers displaying ANS fluorescence after incubation with FSP-Ins fibers in MES-HBSS (A), MES-HBSS with 6 mM TC (B), MES-HBSS with 6 mM Triton X-100 (C) and MES-HBSS with 6 mM BC (D). All images were recorded with the same settings.

Conclusion

The results presented in this study clearly indicate that biorelevant compounds interact with electrospun fibers. The interactions between surfactants in solution and electrospun protein fibers were found to significantly influence the release of entrapped cargo, the fiber stability, porosity and the fiber surface properties. Anionic surfactants were shown to have a concentration-dependent effect on insulin release, whereas addition of Triton X-100 did not cause a significant change in the amount released, and in MES-HBSS with BC, only negligible amounts of insulin were released. Cryo-SEM images of the fibers after incubation with the surfactants showed a correlation between release of cargo and increased porosity of the fibers, in the sense that when insulin was released, fiber porosity was observed. Contact angle measurements revealed that the surfactants had a significant influence on wetting of the fibers; for anionic surfactants a small increase in the contact angle was observed, whereas the presence of the

cationic surfactant, and especially the neutral surfactant, decreased the contact angle considerably. Interactions between fibers and surfactants were further elucidated, by decreased levels of interactions with the hydrophobic pocket fluorophore, ANS, after fiber incubation with neutral or cationic surfactants, as compared to anionic or no surfactants. Overall, this study emphasizes the importance of taking into account biologically relevant components, such as bile salts and proteins, with which electrospun fibers may be exposed to when used for tissue engineering, wound healing, drug delivery and other biomedical applications.

Acknowledgements

The authors would like to acknowledge Nis Korsgaard Andersen and Raphael Taboryski for access to the optical tensiometer, and the Core Facility of Integrated Microscopy for assistance with cryo-SEM. Laboratory technician Karina Vissing is acknowledged for assistance with CMC determinations. Sanofi-Aventis is acknowledged for kindly supplying the human insulin. The research leading to these results has received support from the Danish Strategic Research Council (DSF -10-93456, FENAMI Project) and Innovative Medicines Initiative Joint Undertaking under grant agreement n°115363 resources, which are composed of financial contribution from the European Union's Seventh Framework Programme (FP7/2007-2013) and EFPIA companies in kind contribution.

References

1 T. J. Sill and H. a von Recum, *Biomaterials*, 2008, 29, 1989–2006.

2 Q. P. Pham, U. Sharma and A. G. Mikos, *Tissue Eng.*, 2006, **12**, 1197–1211.

3 D. B. Khadka and D. T. Haynie, *Nanomedicine Nanotechnology, Biol. Med.*, 2012, 8, 1242–1262.

4 D. B. Patel, R. Deshmukh, P. K. Pawde, S. Tadavi and R. V Kshirsagar, *J. Pharm. Res.*, 2009, **2**, 1184–1187.

5 F. Ignatious, L. Sun, C.-P. Lee and J. Baldoni, *Pharm. Res.*, 2010, **27**, 576–588.

6 P. Kuppan, S. Sethuraman and U. M. Krishnan, *J. Biomed. Nanotechnol.*, 2013, **9**, 1540–1555.

7 H. R. Pant and C. S. Kim, *Polym. Int.*, 2013, **62**, 1008–1013.

8 K. Kataria, A. Gupta, G. Rath, R. B. Mathur and S. R. Dhakate, *Int. J. Pharm.*, 2014, **469**, 102–110.

9 R. A. Thakur, C. A. Florek, J. Kohn and B. B. Michniak, *Int. J. Pharm.*, 2008, **364**, 87–93.

10 P. Sofokleous, E. Stride and M. Edirisinghe, *Pharm. Res.*, 2013, **30**, 1926–1938.

11 J. E. Trachtenberg, P. M. Mountziaris, F. K. Kasper and A. G. Mikos, *Isr. J. Chem.*, 2013, 53, 646–654.

12 W. Cui, Y. Zhou and J. Chang, *Sci. Technol. Adv. Mater.*, 2010, 11, 014108.

13 Y. J. Son, W. J. Kim and H. S. Yoo, *Arch. Pharm. Res.*, 2014, 37, 69–78.

14 Y.-F. Goh, I. Shakir and R. Hussain, *J. Mater. Sci.*, 2013, **48**, 3027–3054.

15 G. Jin, M. P. Prabhakaran, D. Kai and S. Ramakrishna, *Eur. J. Pharm. Biopharm.*, 2013, **85**, 689–698.

16 D. Poncelet, P. de Vos, N. Suter and S. N. Jayasinghe, *Adv. Healthc. Mater.*, 2012, **1**, 27–34.

17 E. Ehler and S. N. Jayasinghe, *Analyst*, 2014, **139**, 4449–52.

18 A. Townsend-Nicholson and S. N. Jayasinghe, *Biomacromolecules*, 2006, **7**, 3364–3369.

19 S. Khansari, S. Duzyer, S. Sinha-Ray, A. Hockenberger, A. L. Yarin and B. Pourdeyhimi, *Mol. Pharm.*, 2013, **10**, 4509–4526.

20 R. Srikar, A. L. Yarin, C. M. Megaridis, A. V Bazilevsky and E. Kelley, *Langmuir*, 2008, **24**, 965–974.

21 A. Y. A. Kaassis, N. Young, N. Sano, H. A. Merchant, D.-G. Yu, N. P. Chatterton and G. R. Williams, *J. Mater. Chem. B*, 2014, **2**, 1400.

22 D. Brahatheeswaran, A. Mathew, R. G. Aswathy, Y. Nagaoka, K. Venugopal, Y. Yoshida, T. Maekawa and D. Sakthikumar, *Biomed. Mater.*, 2012, 7, 045001.

23 F. Han, H. Zhang, J. Zhao, Y. Zhao and X. Yuan, *J. Biomater. Sci. Polym. Ed.*, 2013, **24**, 1244–59.

24 C. Hu, S. Liu, Y. Zhang, B. Li, H. Yang, C. Fan and W. Cui, *Acta Biomater.*, 2013, **9**, 7381–7388.

25 Y. Wang, B. Wang, W. Qiao and T. Yin, *J. Pharm. Sci.*, 2010, **99**, 4805–4811.

26 H. Jiang, Y. Hu, Y. Li, P. Zhao, K. Zhu and W. Chen, *J. Control. Release*, 2005, **108**, 237–243.

27 H. Jiang, D. Fang, B. Hsiao, B. Chu and W. Chen, *J. Biomater. Sci. Polym. Ed.*, 2004, **15**, 279–296.

28 M. Jannesari, J. Varshosaz, M. Morshed and M. Zamani, *Int. J. Nanomedicine*, 2011, **6**, 993–1003.

29 U. E. Illangakoon, T. Nazir, G. R. Williams and N. P. Chatterton, *J. Pharm. Sci.*, 2014, **103**, 283–292.

30 L. K. MacRi, L. Sheihet, A. J. Singer, J. Kohn and R. a F. Clark, *J. Control. Release*, 2012, **161**, 813–820.

31 J. Li, R. Fu, L. Li, G. Yang, S. Ding, Z. Zhong and S. Zhou, *Pharm. Res.*, 2014, **31**, 1632–1643.

32 J. Hu, J. Wei, W. Liu and Y. Chen, *J. Biomater. Sci. Polym. Ed.*, 2012, 24, 1–14.

33 D. Steffens, M. Lersch, A. Rosa, C. Scher, T. Crestani, M. G. Morais, J. a. V. Costa and P. Pranke, *J. Biomed. Nanotechnol.*, 2013, **9**, 710–718.

34 T. Elakkiya, G. Malarvizhi, S. Rajiv and T. S. Natarajan, *Polym. Int.*, 2014, **63**, 100–105.

35 C. Kriegel, K. M. Kit, D. J. McClements and J. Weiss, *J. Appl. Polym. Sci.*, 2010, **118**, 2859–2868.

36 K. Stephansen, M. García-Díaz, F. Jessen, I. S. Chronakis and H. M. Nielsen, *Macromol. Biosci. (in Revis.*, 2015.

37 S. Alborzi, L.-T. Lim and Y. Kakuda, *LWT - Food Sci. Technol.*, 2014, **59**, 383–388.

38 S. Maretschek, A. Greiner and T. Kissel, *J. Control. Release*, 2008, **127**, 180–187.

39 K. Stephansen, I. S. Chronakis and F. Jessen, *Colloids Surfaces B Biointerfaces*, 2014, **122**, 158–165.

40 A. Domínguez, A. Fernández, N. González, E. Iglesias and L. Montenegro, *J. Chem. Educ.*, 1997, **74**, 1227–1231.

41 M. Gandhi, R. Srikar, a. L. Yarin, C. M. Megaridis and R. a. Gemeinhart, *Mol. Pharm.*, 2009, **6**, 641–647.

42 I. C. Liao, S. Y. Chew and K. W. Leong, *Nanomedicine (Lond).*, 2006, **1**, 465–471.

43 W. O. McClure and G. M. Edelman, *Biochemistry*, 1966, **5**, 1908–1919.

44 L. Stryer, *J. Mol. Biol.*, 1965, **13**, 482–495.

Supporting information

Interactions between surfactants in solution and electrospun protein fibers - effects on release behavior and fiber properties.

Karen Stephansen[1,2], *María García-Díaz*[2], *Flemming Jessen*[1], *Ioannis S. Chronakis*[1*], *Hanne M. Nielsen*[2*]

[1]National Food Institute, Technical University of Denmark, Søltofts Plads 227, DK-2800 Kgs. Lyngby, Denmark.

[2]Department of Pharmacy, Faculty of Health and Medical Sciences, University of Copenhagen, Universitetsparken 2, DK-2100 Copenhagen, Denmark.

*Corresponding author:

Hanne Mørck Nielsen; mail: hanne.morck@sund.ku.dk, phone: +45 35 33 63 46, fax: +45 35 33 60 01, address: Department of Pharmacy, Faculty of Health and Medical Sciences, University of Copenhagen, Universitetsparken 2, DK-2100 Copenhagen, Denmark.

Ioannis S. Chronakis; mail:ioach@food.dtu.dk, phone: +45 45 25 27 16, address: National Food Institute, Technical University of Denmark, Søltofts Plads 227, DK-2800 Kgs. Lyngby, Denmark

S1: Preparation of FSP

Fresh cod (*Gadus morhua*) was filleted and frozen at -30˚C. The frozen fillet was defrosted, chopped into approximately 1x1x2 mm sized pieces, placed into centrifuge tubes and centrifuged for 15 min, 18,000 g, 5˚C (4K15, Sigma Laboratory centrifuges, Osterode am Harz, Germany). The supernatant was transferred to a petri dish, frozen, freeze dried and stored at -60˚C.

S2: Preparation of FSP-Ins fibers

FSP (125 mg/mL) and insulin (20 mg/mL) were dissolved in HFIP, added to a syringe and placed in a syringe pump (New Era Pump Systems, Farmingdale, NY, USA). A 30 G needle (Proto Advantage, Ancaster, ON, Canada) was used. The syringe pump delivered the FSP-Ins solution with a flow rate of 0.04 mL/min. Using a high voltage power supply (Gamma High Voltage Research, Ormond Beach, FL, USA), an electric field of 25 kV was applied between the spinneret of the syringe and a the 5×5 cm collector plate made of stainless steel covered by alumina foil. The distance between the syringe tip and the collector plate was 15 cm. For control experiments, FSP (125 mg/mL) was dissolved in HFIP, and electrospun under the same conditions.

S3: Chemical structures of the surfactants.

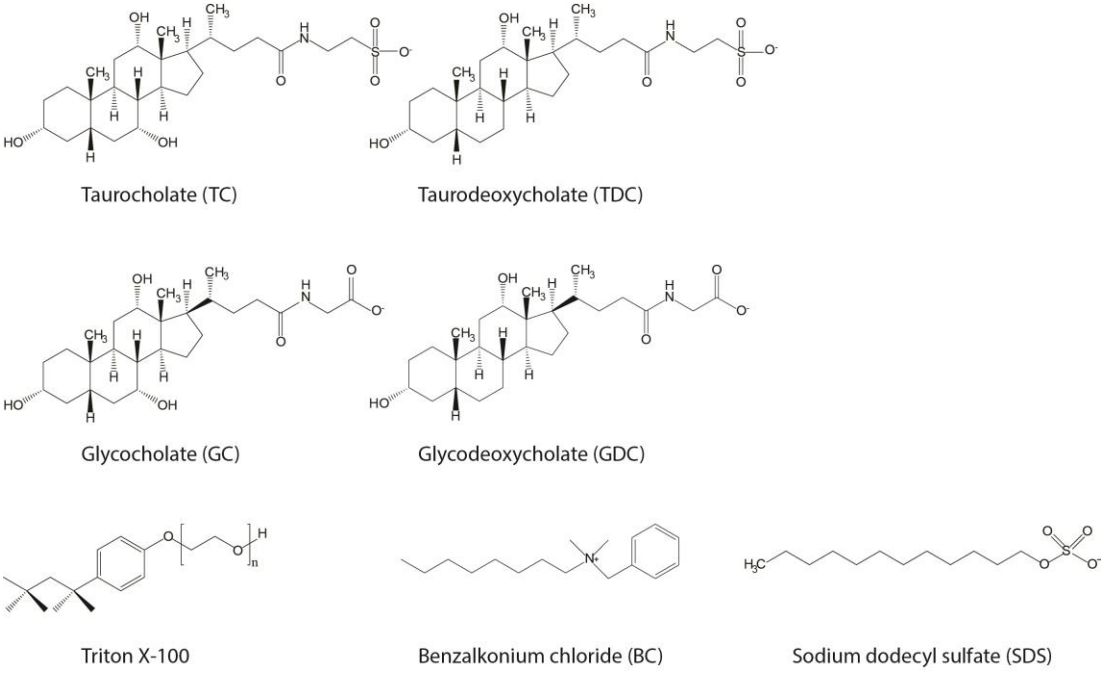

Figure 1. Chemical structures of the surfactants.

S4 Stability of FSP-Ins fibers

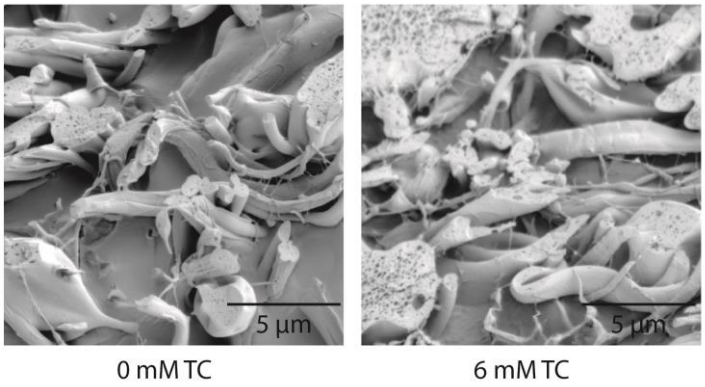

Figure 2. Structure of FSP-Ins after 2 months incubation in MES-HBSS with and without TC.

S4: Release of insulin from FSP-Ins fibers in the presence of 3.1% BSA

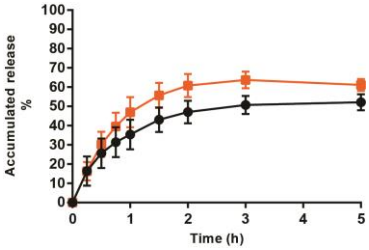

Figure 3. *In vitro* insulin release from FSP-Ins fibers in MES-HBSS with (orange) and without (black) BSA. Data represent mean ± SD, n ≥ 3.

Appendix IV – Paper IV

Paper IV

Design and characterization of self-assembled fish sarcoplasmic protein-alginate nanocomplexes

K. Stephansen, M. Mattebjerg, J. Wattjes, A. Milisavljevic, F. Jessen, K. Qvortrup, F. M. Goycoolea, I.S. Chronakis

International Journal of Biological Macromolecules 76 (2015) 146–152

International Journal of Biological Macromolecules 76 (2015) 146–152

Contents lists available at ScienceDirect

International Journal of Biological Macromolecules

journal homepage: www.elsevier.com/locate/ijbiomac

Design and characterization of self-assembled fish sarcoplasmic protein–alginate nanocomplexes

Karen Stephansen[a,***], Maria Mattebjerg[a], Jasper Wattjes[a,b], Ana Milisavljevic[a], Flemming Jessen[a], Klaus Qvortrup[c], Francisco M. Goycoolea[b,**], Ioannis S. Chronakis[a,*]

[a] Technical University of Denmark, DTU-Food, Søltofts Plads 227, DK-2800 Kgs Lyngby, Denmark
[b] IBBP, Westfälische Wilhelms-Universität Münster Schlossgarten 3, 48149 - Münster, Germany
[c] University of Copenhagen, Department of Biomedical Sciences, The Panum Institute, Blegdamsvej 3, DK-2200 Copenhagen N, Denmark

ARTICLE INFO

Article history:
Received 5 December 2014
Received in revised form 3 February 2015
Accepted 10 February 2015
Available online 20 February 2015

Keywords:
Alginate
Proteins
Particle
Nanocomplex
Drug delivery

ABSTRACT

Macrostructures based on natural polymers are subject to large attention, as the application range is wide within the food and pharmaceutical industries. In this study we present nanocomplexes (NCXs) made from electrostatic self-assembly between negatively charged alginate and positively charged fish sarcoplasmic proteins (FSP), prepared by bulk mixing. A concentration screening revealed that there was a range of alginate and FSP concentrations where stable NCXs with similar properties were formed, rather than two exact concentrations. The size of the NCXs was 293 ± 3 nm, and the zeta potential was −42 ± 0.3 mV. The NCXs were stable in water, gastric buffer, intestinal buffer and HEPES buffered glycose, and at all pH values from 2 to 9 except pH 3, where they aggregated. When proteolytic enzymes were present in the buffer, the NCXs were degraded. Only at high concentrations the NCXs caused a decreased viability in HeLa and U2OS cell lines. The simple processing procedure and the high stability of the NCXs, makes them excellent candidates for use in the food and pharmaceutical industry.

1. Introduction

The search for novel "supramolecular" nanostructured materials for use in biomedicine, pharmacy, food, biotechnology and other fields entails to identify constituting biopolymers that are not only biocompatible and biodegradable, but also are capable to confer the needed physical properties and functionality. Polysaccharide and proteins are natural "building blocks" of living systems, where they perform key functions, such as providing physical structure, conferring protection against pathogens, performing enzymatic reactions and signaling, among many more specialized functions. Complexes of polysaccharide and proteins can be classified as cognate or non-cognate. In the former, proteins and polysaccharides can be found in the same physiological environment and interact specifically as for example, lysozyme and glycosaminoglycans in mammalians' cartilages [1]. By contrast, non-cognate mixtures comprise pairs that are not necessarily interacting specifically. Hence, polysaccharides and proteins are ideal candidate components to develop new "soft" materials for biomedical, food, agriculture and biotechnological applications, particularly, when both macromolecules are already approved ingredients or common constituents of food.

Self-assembling (SA) refers to the process whereby components of a desired material associate themselves into supramolecular organized systems, obtained by non-covalent synthesis. Colloidal polyelectrolyte complexes comprising polysaccharides and proteins formed by spontaneous electrostatic interaction in aqueous medium, have been the focus of several studies [2–8]. The physicochemical properties of the constituent molecules determine not only the interactions among them, but also the supramolecular architecture of the resulting nanoassembly [9]. In the case of proteins, the proportion of polar, charged, aromatic or hydrophobic amino acids in the primary structure, along with the type of protein folding, are at play. Whereas in polysaccharides, the monosaccharide composition (e.g. charged versus non charged residues, degree, and position of the substituent groups) as well as their sequence in the chain (i.e. block, alternating, random) along with their linkage geometry, chain flexibility, and conformation in solution have a direct influence on the physicochemical properties such as the stability, particle size, phase equilibrium and structure at varying levels [9].

* Corresponding author at: Technical University of Denmark, Søltofts Plads 227, DK-2800 Kgs Lyngby, Denmark. Tel.: +45 45252716; fax: +45 45939600.
** Corresponding author at: Westfälische Wilhelms-Universität Münster, Schlossgarten 3, D-48149 Münster, Germany. Tel.: +49 2518324864; fax: +49 2518323823.
*** Corresponding author at: Technical University of Denmark, Søltofts Plads 227, DK-2800 Kgs Lyngby, Denmark. Tel.: +45 45252773; fax: +45 45939600.
E-mail addresses: kaste@food.dtu.dk (K. Stephansen), goycoole@uni-muenster.de (F.M. Goycoolea), ioach@food.dtu.dk (I.S. Chronakis).

http://dx.doi.org/10.1016/j.ijbiomac.2015.02.018
0141-8130/

Protein-polysaccharide systems have been applied in the development of drug delivery biocompatible carriers [10], or as self-assembled gelling complexes [11,12]. Polysaccharide/protein colloidal complexes that remain stable in liquid phase, and attain particle size dimensions in the sub-micron range, are here regarded as nanocomplexes (NCXs). The key to the formation of stable NCXs based on electrostatic SA of polysaccharide and proteins is to control the medium pH, as depending on the intrinsic pK (pK_o) of the polysaccharide and the p*I* of the protein, it is possible to assess a condition in which the components are oppositely charged. Other important parameters are the salinity, the molar ratio of charged groups and their total concentration. Often, the optimal conditions lie within a narrow range of composition or external conditions that avoid the aggregation and precipitation of the complex [13].

The focus of the present paper is the NCXs formed between sarcoplasmic proteins isolated from cod (FSP) and alginate, here referred to as FSP-Alg. FSP accounts for 25–30% of the fish muscle proteins. They are easily accessible, and comprise peptides and proteins of up to ~200 kDa in molecular weight. Fish protein hydrolysates have been shown to comprise bioactive properties [14–16]. One example is inhibitory effects against dipeptidyl peptidase-4 (DPP-IV) [17,18], an enzyme with an essential role in glucose metabolism and linked to type 2 diabetes, and DPP-IV inhibitors may be used as a potential new treatment for type 2 diabetes [19,20]. Additionally, dietary cod proteins have been shown to improve insulin sensitivity in insulin-resistant subjects [21,22]. Based on the multiple documented bioactive properties of FSPs, their inclusion in nanostructured materials is an interesting strategy to explore. Alginate is a linear block co-polymer constituted by homopolymeric (1→4)-linked poly-L-α guluronate (poly-G) and poly-D-β mannuronate (poly-M) and by alternate block of both residues. Its composition, summarized by the molar ratio of D-mannuroate to L-guluronate residues (M/G ratio), along with the molecular weight, are the main properties that dictate the physicochemical, functional and bioactive properties of alginate. Protein-polysaccharide complexes comprising alginate have been reported, for example with bovin serum albumin [4,8,10] or β-lactoglobulin, whey protein isolate, or lysozyme [4,5,9,13]. However, so far, to the best of our knowledge, nanometric complexes of alginate and a complex mixture of fish proteins have not been documented. Hence, in this study, we have aimed to address the formation of stable NCXs between these components, obtained by electrostatic SA complexation. We have established optimal conditions for their preparation, characterized their major physical properties and degradability, as well as their cytotoxicity in HeLa and U2OS cell cultures.

2. Material and methods

2.1. Materials

Alginate (Manucol LKX 50DR) was purchased from FMC Biopolymers (Philadelphia, PA, USA). The M/G ratio was 1.56 according with manufacturer specifications and the Mw 451 kDa (as determined by SEC-HPLC with intrinsic viscosity and DRI detectors and by use of a Universal Calibration curve of pullulan standards). Cod (*Gadus morhua*) from the North Sea was obtained from Hanstholm Fisk (Hanstholm, Denmark). All other reagents, unless otherwise stated, were obtained commercially at analytical grade from Sigma–Aldrich (St. Louis, MO, USA), and used without further purification.

2.2. Preparation of FSP-Alg NCXs

2.2.1. FSP extraction and dialysis

Muscle tissue from a cod was stored vacuum packed at −30 °C until use. The tissue samples were partly defrosted (30 min at room temperature) before extraction of the sarcoplasmic proteins. The fish muscles were cut into small 25 g pieces. A total volume of 250 mL of fish buffer (50 mM Tris–HCl, pH 7.4, 1 mM EDTA) was added. The mixture was kept on ice and homogenized at 8000 × *g* for 3 × 30 s with 2 min between each homogenization, followed by centrifugation (11,200 × *g*, 20 min, 3 °C) and subsequently the supernatant was dialyzed against water (Spectra/Por1 dialysis tubing, 6–8 kDa MWCO). Dialysis was performed for 48 h with change of water four times. The dialyses solution was centrifuged (11,200 × *g*, 20 min, 3 °C) and the supernatant freeze dried. The freeze dried protein was stored at −20 °C until use.

2.2.2. Zeta potential determination of FSP and alginate at different pH

The zeta potential (ζ) at varying pH was measured for FSP and alginate solutions in 0.1 M NaCl and titrated with dilute HCl solutions. This was conducted by mixed laser doppler electrophoresis and phase analysis light scattering (M3-PALS) in a Malvern Zetasizer NANO-ZS (Malvern Instruments, Worcestershire, UK) equipped with a 4 mW He/Ne laser beam operating at λ = 633 nm. The titration was conducted using an MPT-2 autotitration unit that enabled automatic addition of acid during the neutralization process. The measurements were made on a ZEN1060 folded capillary cell. Mean ± SD, *n* = 3 are reported.

2.2.3. NCX preparation and purification

Alginate stock solution (1.93 mg/mL) was stirred gently overnight to allow complete dissolution of the polymer. FSP stock solution (12.89 mg/mL) was prepared on the day of particle preparation and was filtered (0.4 μm filter) before use. The stock solutions of alginate and FSP were diluted with demineralized water to the desired concentrations, and pH was adjusted to 3.8. NCXs were formed in 24-well plates by rapidly mixing the FSP solution into the alginate solution in the volume ratio corresponding to 1.5 (e.g. 720 μL alginate solution and 1080 μL FSP solution), with a pipette. The particles were incubated for 30 min at room temperature in the 24-well plate, before transfer to Eppendorf tubes containing a glycerol bed (approximately 10% of the total volume of NCXs) to enable subsequent re-suspension. NCXs were purified by centrifugation (12,000 × *g*, 60 min, 25 °C), followed by removal of the supernatant, and then resuspension of the pellet in demineralized water. Particles were stored at 4 °C until further analysis.

2.3. NCX characterization

2.3.1. Measurement of particle size and zeta potential

The particle size and size distribution (PDI) was analyzed by dynamic light scattering with non-invasive back scattering (DLS-NIBS) at an angle of 173° with automatic attenuator setting and the zeta potential by mixed laser Doppler electrophoresis and phase analysis light scattering (M3-PALS). Both measurements were conducted in a Malvern Zetasizer NANO-ZS (Malvern Instruments, Worcestershire, UK) equipped with a 4 mW He/Ne laser beam operating at λ = 633 nm. The NCXs were diluted before transferring to the measurement cuvette (particle size: 20 μL NCX and 980 μL water; zeta potential: 10 μL NCX and 990 μL water). All measurements were performed at 25 ± 0.2 °C. Mean ± SD, *n* = 3 are reported.

2.3.2. Colloidal stability of the NCXs

The colloidal stability of the NCXs against aggregation in the different solvents (demineralized water, gastric buffer (GF) (34 mM NaCl pH 1.2)), intestinal buffer (IF) (50 mM KH_2PO_4 pH 6.8) or HEPES buffered glycose (HBG) (5% glucose, 20 mM HEPES, pH 7.0), and pH 2–9 was tested by adding an aliquot of NCXs to the solvent and incubate it for a given period of time at 37 ± 0.2 °C. The NCXs

were subsequently analyzed according to the method described in the section above. Mean ± SD, $n = 3$ are reported.

2.3.3. NCX morphology investigations by transmission electron microscopy

The NCXs were negatively stained with 1% phosphotungstic acid on copper 200 mesh grids. The NCXs were imaged with a transmission electron microscope (TEM) CM100 (Philips, Eindhoven).

2.3.4. Determination of FSP and NCXs protein composition

Sodium dodecyl sulfate polyacrylamide gel electrophoresis (SDS–PAGE) was performed according to Laemmli [23], to determine the protein composition in FSP, FSP-Alg NCXs and the supernatant after NCX formation. Samples were boiled for 2 min at 98 °C in loading buffer (0.25 M Tris/HCl pH 6.8, 1% (w/v) SDS, 20% v/v glycerol, 0.04% v/v bromphenol blue) before addition to tris–glycine gels (4–20%, Novex®, Life technologies Ltd., Paisley, UK). Mark 12™ unstained standard (Novex®, Life technologies Ltd., Paisley, UK) was used as molecular marker. Gels were run at a constant voltage of 125 V in an XCell II™ chamber (Novex®, Life technologies Ltd., Paisley, UK) and stained.

2.3.5. Determination of protein concentration

Protein concentration was determined according to the protocol of the BCA protein assay kit (Pierce, IL, USA). Absorbance was measured using a microplate reader (Synergy 2 Multi-Mode Microplate reader, BioTek®, VT, US). Mean ± SD, $n = 3$ are reported.

2.3.6. Determination of alginate concentration

Quantification of alginate was performed using the 3-Phenylphenol assay according to Blumenkrantz and Asboe-Hansen [24]. Briefly, 20 μL alginate containing sample was mixed with 1.2 mL H_2SO_4/sodium tetraborate solution (12.5 mM sodium tetraborate in concentrated H_2SO_4). Samples were heated to 98 °C for 5 min and 20 μL 3-phenyl-phenol solution (0.5% NaOH, 0.15% 3-phenylphenol) was added to the cooled sample. Absorbance at 520 nm was measured within 5 min. Mean ± SD, $n = 3$ are reported.

2.4. Enzymatic degradation of NCXs

For enzymatic degradation studies, NCXs (approximately 400 μg FSP/mL) or pure FSP were incubated for 0 or 2 h on a shaking table in either simulated gastric fluid (SGF) (34 mM NaCl, 4.5 μg/mL pepsin (activity of 3.260 units/mg protein), pH 1.2) or simulated intestinal fluid (SIF) (50 mM KH_2PO_4, 14.3 μg/mL pancreatin (activity of 8× U.S.P. specifications), pH 6.8). t_0 samples were drawn immediately after the NCXs/FSP was transferred to the enzyme-containing solutions. Protein compositions of enzyme treated samples were analyzed by SDS–PAGE.

2.5. Cytotoxicity of NCXs

The cytotoxicity of NCXs was evaluated using MTS assay (CellTiter 96® AQ_{ueous} Non-Radioactive Cell Proliferation assay, Promega, Madison, WI, USA). Cells (HeLa or U2OS) were seeded in 96-well plates at an initial density of 5000 cells per well. After 24 h the cells were washed with PBS buffer before addition of 100 μL samples containing different concentrations of FSP, alginate, or FSP-Alg NCXs. The samples were made by mixing different volumes of FSP, alginate, or FSP-Alg NCX stock solutions with DMEM without fetal bovine serum. Cells were incubated for 24 h with the samples before addition of 20 μL MTS reagent to each well. The metabolic activity was evaluated after incubation at 37 °C and 5% CO_2 for 1 h for HeLa cells, and 2 h for U2OS cells, by measuring absorbance at 490 nm using a Wallac Victor^3 plate reader (Perkin-Elmer, Waltham, MA, USA). Cytotoxicity was reported as percent cell viability using untreated cells as 100% viability. Mean ± SD, $n = 3$ are reported.

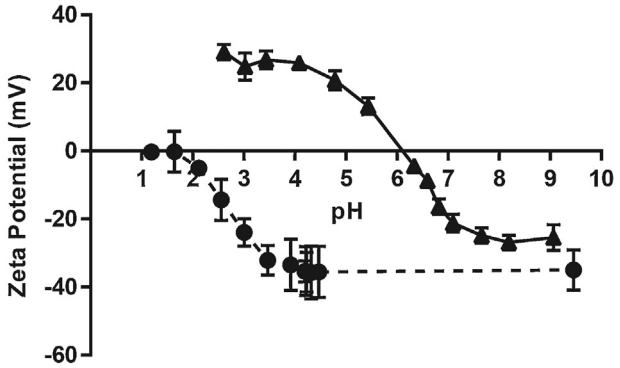

Fig. 1. Zeta potential as a function of pH for alginate (dashed, ●) and FSP (full, ▲). Both components were dissolved in 0.1 M NaCl and titrated with dilute HCl.

3. Results and discussion

3.1. Determination of FSP-pI and alginate-pK_a

To determine the optimal pH for electrostatic SA between positively charged FSP and negatively charged alginate, the pH dependence of the net charge of FSP and alginate was investigated. Fig. 1 shows the zeta potential as a function of pH for both components. Notice that for FSP the zeta potential curve crosses zero at pH 6.1. This point matches the mid-point of the sigmoidal titration curve, and can accordingly be taken as the mean value of the FSP-p*I*. In the case of alginate, the zeta potential curve also describes a sigmoidal shape with a maximum inflexion centered at a pH value of ~2.9, which thus can be taken as the pK_a of alginate. Therefore, in the pH range ~2.5–6.0 the net charge of FSP was positive charged while alginate was negative, and pH 3.8 was chosen for NCX formation.

3.2. Determination of optimal FSP:alginate ratio for successful NCX formation

To determine the optimal FSP:alginate ratio for the formation of stable NCXs, a screening was carried out, where FSP (concentrations between 0.35 and 1.36 mg/mL) were mixed with alginate (concentrations between 0.44 and 1.06 mg/mL). The formation of NCXs was recognized by a characteristic opalescence which was easily judged by the naked eye. An overview of the results from the screening tests is shown schematically in Fig. 2A. Mixing alginate solutions (0.69–0.97 mg/mL) with FSP solutions (0.55–0.69 mg/mL) resulted in spontaneous formation of stable NCXs. The NCXs were characterized with respect to size and PDI (data not shown), which eliminated the combinations marked dark grey in Fig. 2A, as the size and PDI of the NCXs large and polydisperse. The remaining candidates were further characterized with respect to particle size, PDI and zeta potential. Surprisingly, it was found that all candidates gave rise to NCXs having similar properties. Therefore a representative candidate formulation was chosen (FSP:alginate mass ratio 0.69:0.97) for further characterization. Fig. 2B shows the particle size distribution of the NCXs from the selected candidate, together with a table summarizing particle size, PDI and zeta potential. The main population had a mean *Z*-average diameter of 293 ± 5 nm. A small peak corresponding to micron sized particles was also detectable. This peak may arise due to protein aggregates that were not removed during the purification; however since it was a proportionally small population, the contribution to the overall physical and biological properties was regarded negligible. The

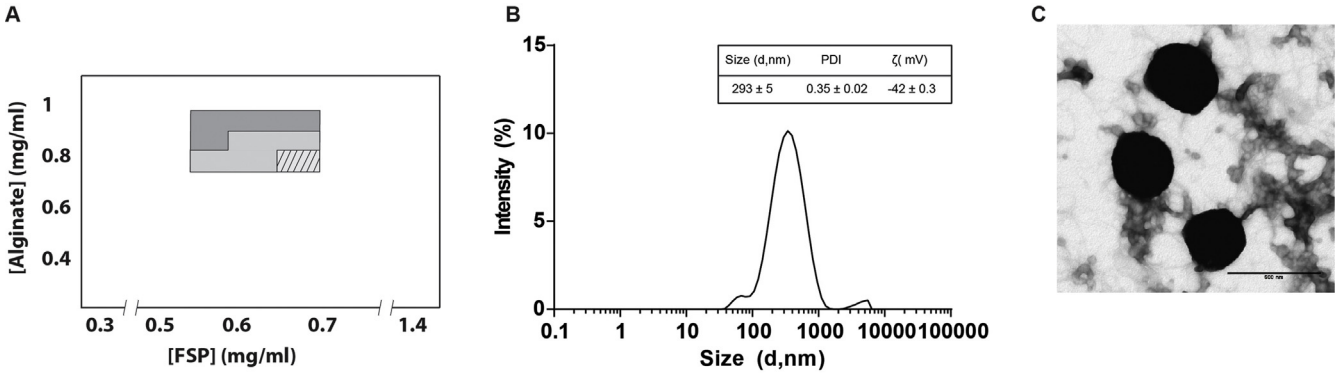

Fig. 2. A) Phase diagram showing an overview of the screening for alginate and FSP NCXs, obtained by mixing both components at varying concentrations (water, pH 3.8, room temperature). White: no formation of NCXs; dark grey: formation of unfavorable NCXs, light grey: formation of favorable NCXs, light grey hatched: chosen candidate. B) Size distribution of NCXs from the chosen candidate. The measurements were carried out at room temperature ($n = 3$). The inset shows an overview of size, PDI and zeta potential. C) TEM image of NCXs. Scale bar: 500 nm.

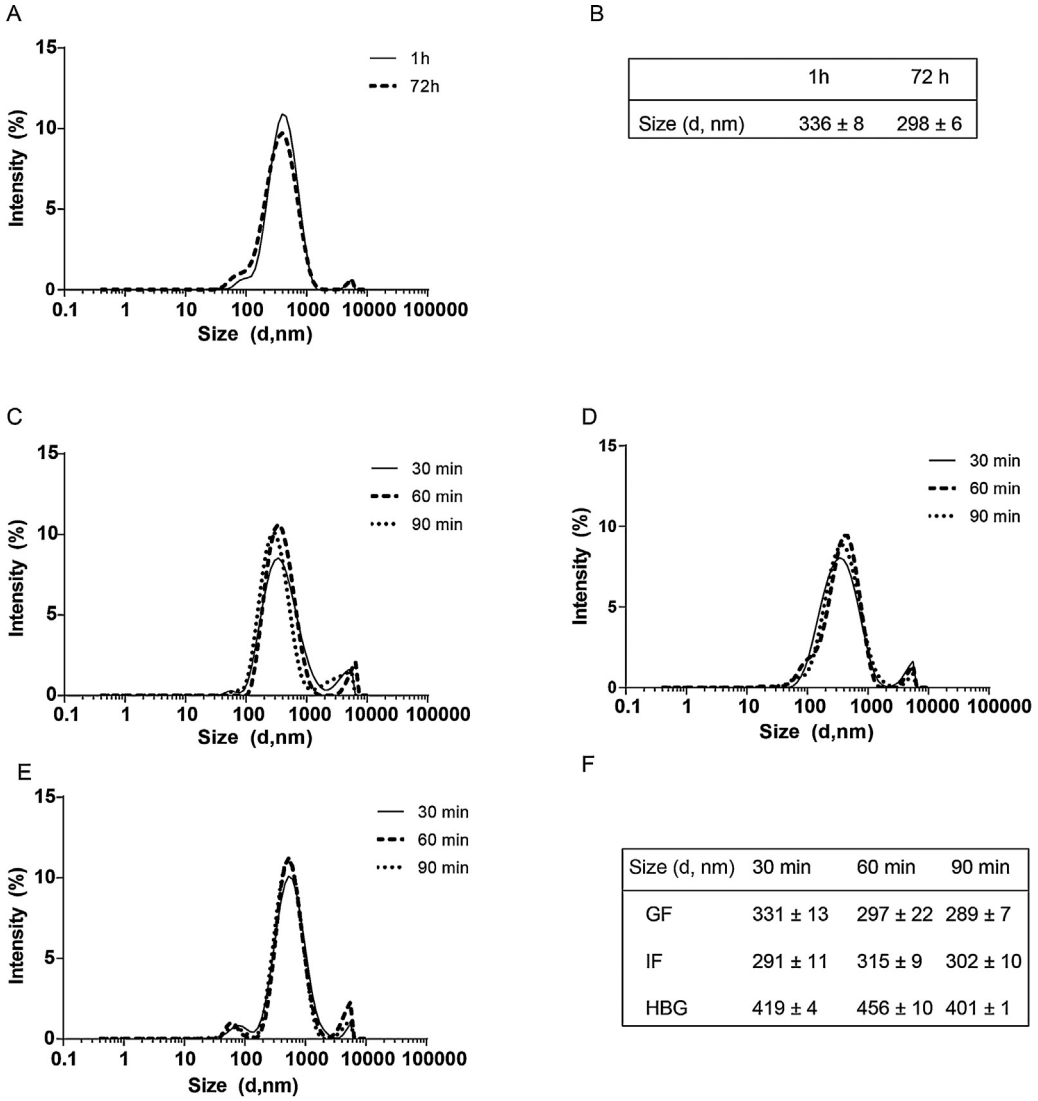

Fig. 3. A) Size distribution of NCXs after incubation in water for 1 and 72 h at room temperature. B) Table summarizing the *z*-average particle size of NCXs described in A), mean ± SD, $n = 3$. C–E) Size distribution of NCXs after incubation during 30 , 60 and 90 min in C) GF (pH 1.2), D) IF (pH 6.8) and E) HBG (pH 7.0), respectively, and F) table summarizing the *z*-average particle size of NCXs described in C–E. Mean ± SD, $n = 3$.

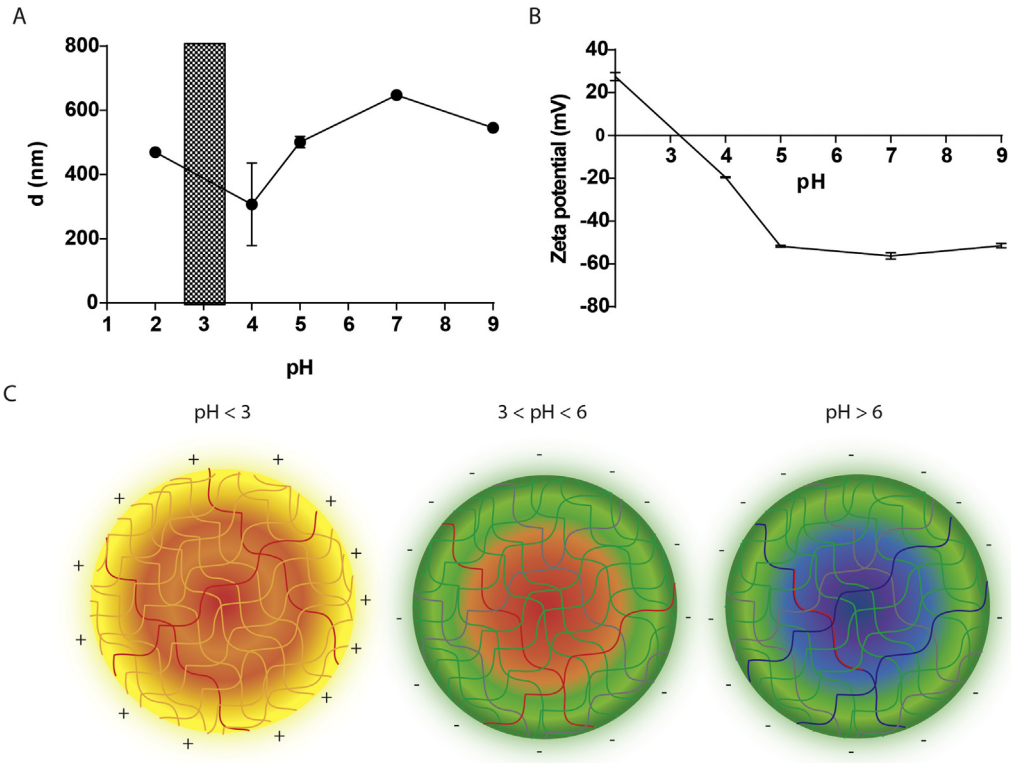

Fig. 4. (A) *Z*-average diameter and (B) zeta potential of FSP–Alg NCXs subjected to different pH, and (C) hypothesized particle structures at three different pH domains (protein; neg.: blue, neut.: grey, pos.: red, alginate; neg.: green, neut.: yellow). (For interpretation of the references to color in this figure legend, the reader is referred to the web version of the article.)

size distribution was large (PDI ≈ 0.35); however, given the very complex mixture of proteins, and that no selection for particular NCXs sizes was attempted a large size distribution was expected. The size of the NCXs was confirmed by TEM (Fig. 2C), which also confirmed a spherical shape. The zeta potential was −42 ± 0.3 mV, which indicated that at the processing conditions the shell of the NCXs was dominated by alginate.

To investigate the yield of production and the composition of the nanoparticles, the proportional amount of FSP and alginate complexed into NCXs were analyzed. Upon NCX formation 56 ± 3% of the original amount of FSP and 82 ± 2% of the initial amount of alginate were incorporated. Hence, the actual FSP:alginate mass ratio in the NCXs was 0.4:0.8, which explains the pronounced negative zeta potential of the NCXs.

3.3. Particle stability

3.3.1. NCXs stability in water during 72 h

The stability of FSP-Alg NCXs after 1 and 72 h incubation in water was investigated by measuring changes in particle sizes over time (Fig. 3A). A small decrease in particle size was observed after 72 h in water. The alternated chemical environment, compared to the processing conditions, may have caused the FSP and alginate to rearrange inside the NCXs, which in this case led to a small decrease in particle size. The limited changes observed suggested that the NCXs in general were stable.

3.3.2. NCXs stability in selected buffer systems

NCX stability in GF (pH 1.2), IF (pH 6.8), and HBG (pH 7.0) were investigated by studying changes in particle size and PDI of the NCXs after incubation for 30, 60 and 90 min in the different solvents. In GF (Fig. 3C) and IF (Fig. 3D), the size of the NCXs

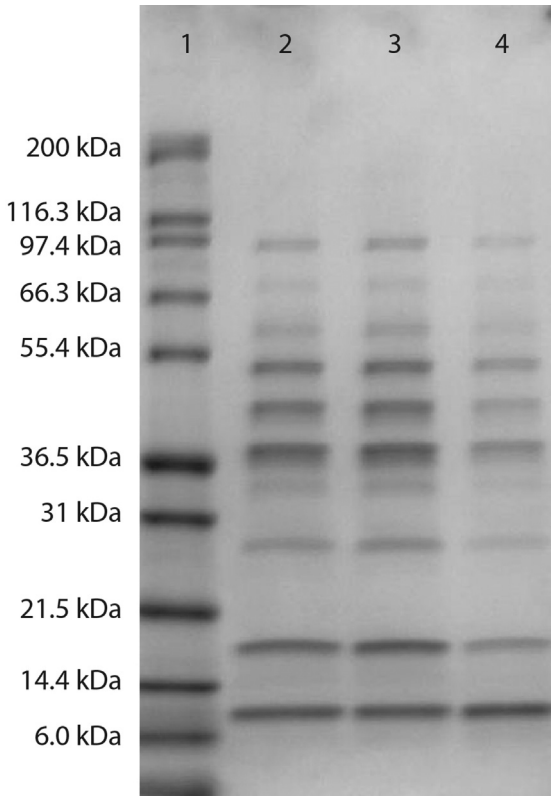

Fig. 5. SDS–PAGE of protein composition in lane 1: marker, lane 2: FSP, lane 3: lane NCXs: 4: Supernatant after NCX formation.

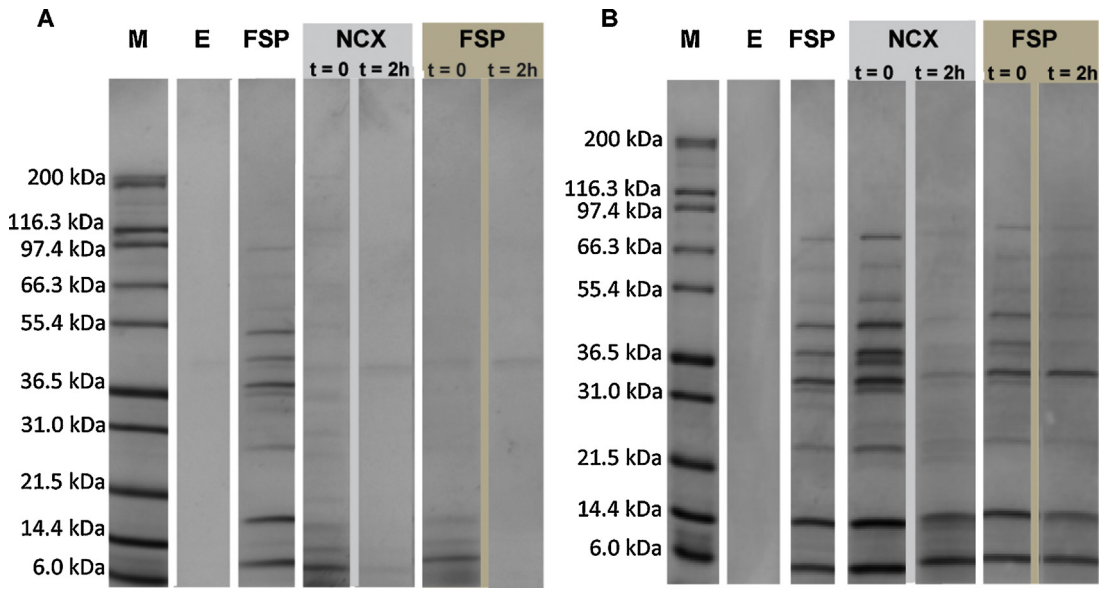

Fig. 6. SDS–PAGE of FSP and NCX degradation products in SGF (A) and SIF (B). M: Marker; E: SGF/SIF. $t = 0$ samples were drawn immediately after the NCXs/FSP was transferred to the enzyme-containing solutions.

remained constant throughout 90 min. In HBG (Fig. 3E) the size of the NCXs was increased after 30 min, compared to the other buffer systems, which indicate that reorganization inside the particles took place. However neither the particle size nor the PDI changed during 90 min, suggesting that the NCXs were stable in HBG. All together the results indicated that the NCXs were stable in the timespan of the experiments in the various physiologically relevant environments.

3.3.3. NCXs stability at different pH values

The stability of NCXs originally formed at pH 3.8, and subsequently incubated for 10 min in different pH environments, was evaluated by particle size and zeta potential measurements (Fig. 4A and B). Fig. 4C shows a model of the hypothesized structure of the NCXs at three pH domains; pH < 3.0, 3.0 < pH < 6.0 and pH > 6.0. Between pH 3 and 6, alginate and FSP were fully oppositely charged, causing the particles to remain stable. Fig. 4B shows that the zeta potential in this pH range was negative, indicating that the shell was dominated by the negatively charged alginate, and hence the majority of the protein may be in the core of the NCXs. At pH ~ 3.0 the particles aggregated (size data point not shown), most likely due to neutralization at the NCX surface. At pH 2, the zeta potential was positive. This may be caused by protonation of protein side chains peeping out through the alginate layer, resulting in a positive zeta potential. The positive surface caused the NCXs to repel each other, thus avoiding aggregation. Above pH 6 both alginate and FSP were negatively charged. The reason to particle stability even above the favorable pH range (pH 3–6), may be due to slow kinetics of FSP deprotonation within the NCXs, causing some residual side chains to remain protonated, even at high pH values. The slow deprotonation rate suggests that the NCXs are composed of a dense network of alginate and FSP.

3.4. Protein composition of NCXs

The protein composition of FSP, NCXs and the supernatant after particle formation was investigated with SDS–PAGE (Fig. 5). The band patterns for the three samples were all similar, indicating that the NCXs consisted of a mixture of all FSP proteins, rather than specific proteins of either high or low molecular weight.

3.5. Degradability of NCXs by proteolytic enzymes

The enzymatic degradation of FSP and NCXs was studied in SGF and SIF by SDS–PAGE. The protein compositions for FSP and NCXs, after exposure to pepsin for a few seconds, are seen in Fig. 6A. Changes in the band patterns for both FSP and NCXs, compared to the band pattern for FSP, indicated that degradation of the proteins was initiated immediately after contact with pepsin. After 2 h, only trace amounts of proteins were left for both NCXs and in FSP. In SIF (Fig. 6B), the degradation was slower. The majority of the proteins were still present after a brief contact with pancreatin, but after 2 h the majority of the proteins were degraded, and only proteins, or protein degradation products, with molecular weight around 6, 14 and 36 kDa, respectively, were not degraded by pancreatin in the timespan of the experiment.

3.5.1. Cytotoxicity of NCXs

Cytotoxicity of NCXs, alginate and FSP were evaluated by the MTS assay in HeLa and U2OS cell lines (Fig. 7A and B) using the MTS assay. Individually, alginate and FSP did not compromise cell viability; however, when combined into NCXs, as the concentration of NCXs increased, cytotoxicity was induced, and at 300 μg/mL the viability was decreased to approximately 50%. This behavior was evident in both cell lines. Vaitkuvienė et al. have previously shown that glycerol has an effect on cell viability [25]. In the present study glycerol was used in the purification of the NCXs. To investigate if glycerol had a similar effect on cytotoxicity on HeLa and U2OS cells, the cytotoxicity of isolated FSP-Alg NCXs (in glycerol) were compared to the cytotoxicity of non-isolated NCXs (Fig. 7A). For the non-isolated NCXs (without glycerol), the dose needed for inducing cytotoxicity was displaced (e.g. at 150 μg/mL no toxicity was observed in the absence of glycerol, while a 20% reduction on cell viability was observed at the same dose of isolated NCXs in glycerol). The decrease in cell viability may thus partly be induced by glycerol. However, even without glycerol the viability was decreased at high NCX concentrations. Most likely there was no uptake of FSP or alginate as separate compounds by the cells, but when complexed into NCXs, uptake took place. At high NCX concentrations there may not have been enough capacity to hydrolyze the components, which thus resulted in decreased viability.

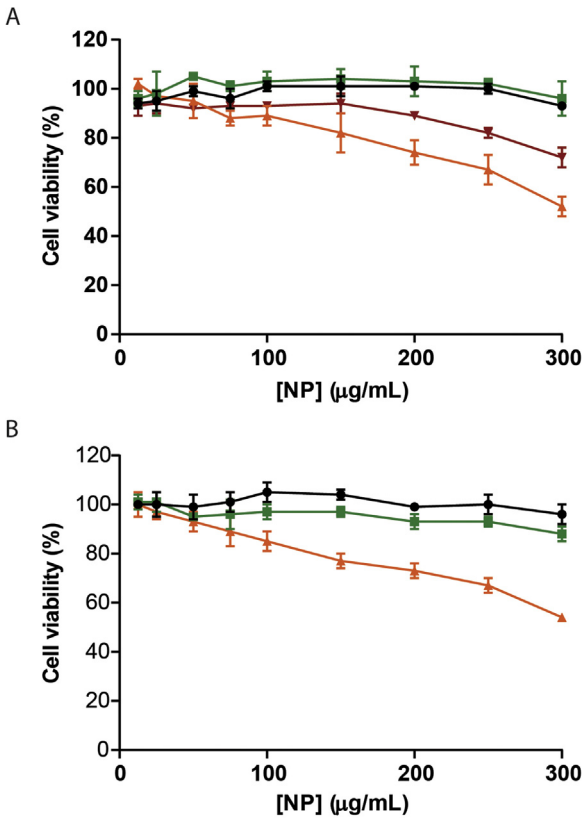

Fig. 7. Cytotoxicity test of NCXs on HeLa cell line (A) and U2OS cell line (B). FSP (●), alginate (■), NCXs (▲), NCXs without glycerol (▼).

4. Conclusion

NCXs were made from FSP and alginate by bulk mixing, utilizing electrostatic SA interactions between the two components at pH 3.8. Screening different combinations of alginate and FSP solutions revealed optimal conditions for NCX formation, but it also showed that the NCX formation entail great stability with respect to variations in processing concentrations, as changes in FSP and alginate processing concentrations, within a certain concentration range, did not affect particle properties. The zeta potential of the NCXs at the processing conditions was -42 ± 0.3 mV, and therefore the shell of the NCXs was hypothesized to be dominated by alginate, whereas FSP mainly was present in the core. The NCXs were stable during 72 h in water and during 90 min in GF, IF, and HBG, besides at different pH value, however changing the pH value from optimal conditions did affect the electrostatic interactions holding the particles together. The remained stability of the particles in the timespan of all experiments indicated that the NCXs in general were stable and composed of a dense network of alginate and FSP. As separate compounds alginate and FSP did not compromise cell viability, and only at high NCX concentrations cell viability in HeLa and U2OS cell lines were affected. The ease, by which the NCXs were formed, together with the distinct stability of the particles, makes the use of NCXs in, for instance biomedical, food or biotechnological applications, appealing.

Acknowledgments

This study was funded by the Danish Strategic Research Council (DSF -10-93456, FENAMI Project). The authors would also like to acknowledge Thomas Andresen, DTU nanotech for using cell laboratory facilities. Moreover the authors would like to thank DTU environment for access to the Zetasizer.

References

[1] J.M. Moss, M.P. Van Damme, W.H. Murphy, B.N. Preston, Arch. Biochem. Biophys. 348 (1997) 49–55.
[2] M. Bayarri, N. Oulahal, P. Degraeve, A. Gharsallaoui, J. Food Eng. 131 (2014) 18–25.
[3] I. Morfin, E. Buhler, F. Cousin, I. Grillo, F. Boué, Biomacromolecules 12 (2011) 859–870.
[4] T. Harnsilawat, R. Pongsawatmanit, D. Mcclements, Food Hydrocoll. 20 (2006) 577–585.
[5] I. Schmidt, F. Cousin, C. Huchon, F. Boué, M.a.V. Axelos, Biomacromolecules 10 (2009) 1346–1357.
[6] S.M.H. Hosseini, Z. Emam-Djomeh, S.H. Razavi, A.A. Moosavi-Movahedi, A.A. Saboury, M.S. Atri, et al., Food Hydrocoll. 32 (2013) 235–244.
[7] S.a. Fioramonti, A.a. Perez, E.E. Aríngoli, A.C. Rubiolo, L.G. Santiago, Food Hydrocoll. 35 (2014) 129–136.
[8] Y. Zhao, F. Li, M.T. Carvajal, M.T. Harris, J. Colloid Interface Sci. 332 (2009) 345–353.
[9] J.P. Fuenzalida, F.M. Goycoolea, Curr. Protein Pept. Sci. 16 (2015) 89–99.
[10] L. Chen, M. Subirade, Biomaterials 27 (2006) 4646–4654.
[11] S. Zhang, Z. Zhang, B. Vardhanabhuti, Food Funct. 5 (2014) 1829–1838.
[12] R. Huang, W. Qi, L. Feng, R. Su, Z. He, Soft Matter. 7 (2011) 6222–6230.
[13] S.L. Turgeon, C. Schmitt, C. Sanchez, Curr. Opin. Colloid Interface Sci. 12 (2007) 166–178.
[14] S.W.A. Himaya, D.-H. Ngo, B. Ryu, S.-K. Kim, Food Chem. 132 (2012) 1872–1882.
[15] G. Pilon, J. Ruzzin, L.-E. Rioux, C. Lavigne, P.J. White, L. Frøyland, et al., Metabolism 60 (2011) 1122–1130.
[16] H.S. Ewart, D. Dennis, M. Potvin, C. Tiller, L. Fang, R. Zhang, et al., Eur. Food Res. Technol. 229 (2009) 561–569.
[17] E.C.Y. Li-Chan, S. Hunag, C. Jao, K. Ho, K. Hsu, J. Agric. Food Chem. 60 (2012) 973–978.
[18] K. Stephansen, I.S. Chronakis, F. Jessen, Colloids Surf. B. Biointerfaces 122C (2014) 158–165.
[19] K.B. Moore, C.D. Saudek, Am. J. Ther. 15 (2008) 484–491.
[20] M. Lehrke, N. Marx, Curr. Opin. Lipidol. 23 (2012) 569–575.
[21] V. Ouellet, S.J. Weisnagel, J. Marois, J. Bergeron, P. Julien, R. Gougeon, et al., J. Nutr. 138 (2008) 2386–2391.
[22] V. Ouellet, J. Marois, S.J. Weisnagel, H. Jacques, Diabetes Care 30 (2007) 2816–2821.
[23] U.K. Laemmli, Nature 227 (1970) 680–685.
[24] N. Blumenkrantz, G. Asboe-Hansen, Anal. Biochem. 54 (1973) 484–489.
[25] A. Vaitkuvienė, V. Kašėta, G. Ramanauskaitė, G. Biziulevičienė, Acta Medica Litu. 16 (2009) 92–97.

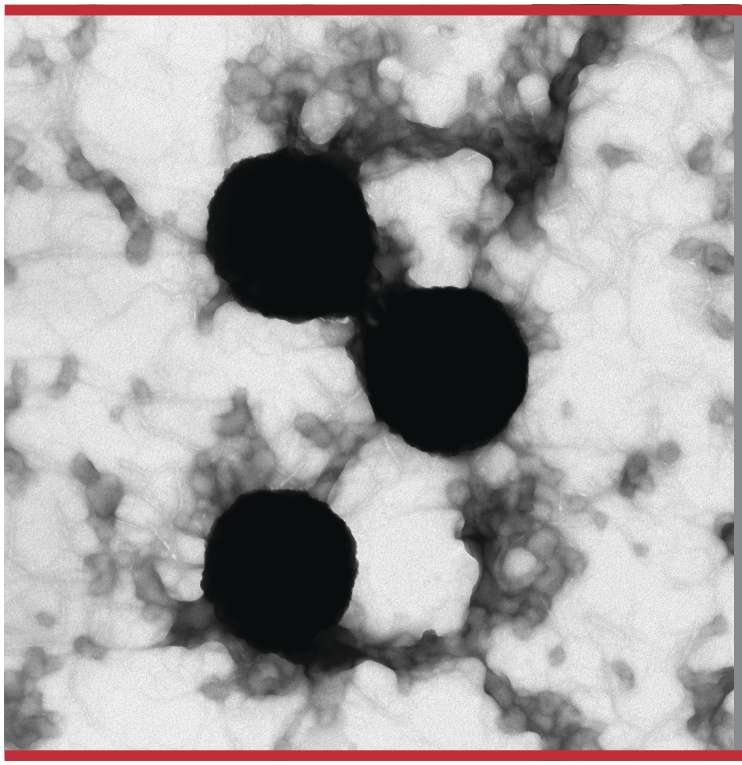

Published by:
DTU Food
National Food Institute
Technical University of Denmark
Søltofts Plads, building 221
DK-2800 Kgs. Lyngby

DTU Food
National Food Institute